NKS-272
ISBN 978-87-7893-345-4

Adsorption and revaporisation studies on iodine oxide aerosols deposited on containment surface materials in LWR

S. Tietze[1], M.R.StJ. Foreman[1], C. Ekberg[1]

T. Kärkelä[2], A. Auvinen[2], U. Tapper[2], S. Lamminmäki[2], J. Jokiniemi[2,3]

[1]Chalmers University of Technology, Göteborg, Sweden
[2]VTT Technical Research Centre of Finland, Espoo, Finland
[3]University of Eastern Finland, Kuopio, Finland

December 2012

Abstract

During a hypothetical severe nuclear accident, the radiation field will be very high in the nuclear reactor containment building. As a result gaseous radiolysis products will be formed. Elemental iodine can react in the gaseous phase with ozone to form solid iodine oxide aerosol particles (iodine oxide).

Within the AIAS (Adsorption of Iodine oxide Aerosols on Surfaces) project the interactions of iodine oxide (IOx) aerosols with common containment surface materials were investigated. Common surface materials in Swedish and Finnish LWRs are Teknopox Aqua V A paint films and metal surfaces such as Cu, Zn, Al and SS, as well as Pt and Pd surfaces from hydrogen recombiners. Non-radioactive and ^{131}I labelled iodine oxide aerosols were produced with the EXSI CONT facility from elemental iodine and ozone at VTT Technical Research Centre of Finland. The iodine oxide deposits were analysed with microscopic and spectroscopic measurement techniques to identify the kind of iodine oxide formed and if a chemical conversion on the different surface materials occurs.

The revaporisation behaviour of the deposited iodine oxide aerosol particles from the different surface materials was studied under the influence of heat, humidity and gamma irradiation at Chalmers University of Technology, Sweden. Studies on the effects of humidity were performed using the FOMICAG facility, while heat and irradiation experiments were performed in a thermostated heating block and with a gammacell 22 having a dose rate of 14 kGy/h. The revaporisation losses were measured using a HPGe detector. The revaporisated ^{131}I species from the surfaces were chemically tested for elemental iodine formation. The parameter dominating the degradation of the produced iodine oxide aerosols was humidity.

Cu and Zn surfaces were found to react with iodine from the iodine oxide aerosols to form iodides, while no metal iodides were detected for Al and SS samples. Most of the iodine oxide aerosols are assumed to be degraded or washed off by containment sprays and steam in the containment. Paint film ingredients were shown to chemically react with the aerosol particles. Pt and Pd surfaces were shown to only weakly physisorb the iodine oxide aerosols which reveals that these aerosols will have a minor effect on the catalytic functionality of the hydrogen recombiners during a severe nuclear accident.

Key words

Severe nuclear accidents, LWR, volatile iodine source term, iodine oxide aerosols, adsorption, revaporisation, containment

NKS-272
ISBN 978-87-7893-345-4

Electronic report, December 2012
NKS Secretariat
P.O. Box 49
DK - 4000 Roskilde, Denmark
Phone +45 4677 4041
www.nks.org
e-mail nks@nks.org

Adsorption and revaporisation studies of iodine oxide aerosols deposited on containment surface materials in LWRs

Final Report from the NKS-R AIAS activity

(Contract: AFT/NKS-R(11)98/1)

S. Tietze[1], M.R.StJ. Foreman[1], C. Ekberg[1]
T. Kärkelä[2], A. Auvinen[2], U. Tapper[2], S. Lamminmäki[2], J. Jokiniemi[2,3]

[1]Chalmers University of Technology, SE-41296 Göteborg, Sweden
[2]VTT Technical Research Centre of Finland, FI-02044 Espoo, Finland
[3]University of Eastern Finland, FI-70211 Kuopio, Finland

July 2012

Report's title **Adsorption and revaporisation studies of iodine oxide aerosols deposited on containment surface materials in LWR**	
Customer, contact person, address NKS-R, Karoliina Ekström, FORTUM, P.O. Box 100, FI-00048 Espoo, Finland (maternity leave) Deputy: NKS-R, Kaisu Leino, Fortum	Order reference AFT/NKS-R(11)98/1

Project name **AIAS – Adsorption of Iodine Oxide Aerosols on Surfaces**	Project number/Short name AIAS
Author(s) S.Tietze, T.Kärkelä M.Foreman, C.Ekberg, A.Auvinen, U.Tapper, S.Lamminmäki, J. Jokiniemi	Pages 85
Keywords Severe nuclear accidents, volatile iodine source term, iodine oxide aerosols, adsorption, revaporisation, containment	Report identification code

Summary

The interactions of iodine oxide aerosols with common surface materials in light water reactor containments (LWR) during a severe nuclear accident are not fully understood. Aerosol particles containing iodine deposited on various surfaces may act as a source for volatile elemental iodine. The elemental iodine rereleased into the containment atmosphere contributes to the volatile iodine source term. The object of the study was to examine iodine oxide (IOx) particles deposited on a range of surfaces and the revaporisation behaviour of ^{131}I from these deposits under the conditions of a severe nuclear accident. The aerosols were deposited on Teknopox Aqua V A epoxy paint, stainless steel (SS 316), copper, zinc, aluminium, platinum and palladium surfaces.

It is likely, that iodine oxide particles, produced in the EXSI CONT facility by the reaction of ozone and gaseous elemental iodine were mainly in the form of I_2O_4 and I_4O_9 when the reaction temperature of elemental iodine and ozone was below 100 °C. The aerosol particles for the deposition were synthesised at 120°C. At this temperature, the particles are likely to contain I_2O_5 since both the other oxides decompose to I_2O_5. When I_2O_4 and I_4O_9 particles react with water elemental iodine (I_2) and iodic acid (HIO_3) are formed. After exposure to humid air, I_2O_5 is rapidly converted to a partially hydrated form $I_2O_5 \cdot HIO_3$, which is also defined as HI_3O_8. On the other hand, the same product is formed when HIO_3 is partially dehydrated.

By using Raman and XPS analysis no chemical bond between iodine oxides and stainless steel, paint or Al surfaces was found. According to the Raman spectrum the form of iodine seemed to be partially hydrated $I_2O_5 \cdot HIO_3$ on painted and SS surfaces. On copper and zinc samples the peaks of solid HIO_3 were detected in the Raman spectra. The results of the XPS analyses also suggest reactions between iodine oxide aerosols and the surface occurred for both copper and zinc surfaces. The probable reaction products would be CuI and ZnI_2. In addition, for all samples the peaks of molecular iodine (I_2) were detected in the Raman spectra, which is likely to be due to the decomposition of I_2O_4 and I_4O_9 particles on the surfaces.

The main factors influencing the iodine chemistry during a severe nuclear accident are temperature, humidity and gamma irradiation. These parameters were found to influence the revaporisation behaviour of ^{131}I from iodine oxide deposits significantly. Humidity in the air was found to be the major parameter for the decomposition of iodine oxide aerosols generated at a temperature of 120 °C.

Metal samples tend to form weaker bonds with the aerosol compounds than epoxy paint which contains organic ingredients that can chemically react with the iodine of the particles.

The typical containment paint film which was studied is a 100 µm thick layer in which mass transfer effects inside the film can affect the iodine chemistry. Pre-irradiation and pre-heating have been shown to have an effect on the ability of the paint to chemisorb iodine. It is assumed that the paint solvents, which are reactive towards iodine, were revaporised during 2 years of heating at 100 °C. Irradiation can cleave carbon-carbon bonds and thus remove functional groups which may be required for chemical absorption.

The aerosols deposited on Pt and Pd were easily revaporised by humidity, heating and by a low dose of gamma rays. Thus it can be expected that the functionality of the hydrogen recombiners will not be seriously affected by these aerosols. It is rather unlikely that metal surfaces and painted surfaces can function as iodine sinks (iodine traps) for the iodine in the form of these iodine aerosols during a severe accident, because the aerosols already revaporised at room temperature, under dry non-irradiation conditions.

Steam and containment sprays are likely to wash the iodine oxide deposits from most of the materials studied or even prevent the sorption on the containment surface materials in a severe accident scenario when the particles are in contact with humidity before sorption can occur.

Confidentiality	Public

Göteborg, 31.07.2012

Christian Ekberg,
Professor,
Project Leader

Contact address

Chalmers University of Technology, Kemivägen 4, SE-41296 Göteborg, Sweden

VTT Technical Research Centre of Finland, Biologinkuja 7, FI-02044 VTT, Espoo, Finland

Preface

Iodine oxide aerosols were deposited on surfaces of materials commonly found inside the containments of the Light Water Reactors (LWRs) used in Swedish and Finnish nuclear power plants. The surface materials investigated were Teknopox Aqua V A epoxy paint films, as well as Al, Cu, Zn, stainless steel (SS 316), Pt and Pd surfaces.

The properties of non-radioactive iodine oxide aerosol were investigated at VTT Technical Research Centre of Finland using microscopic and spectroscopic analysis techniques (SEM-EDX, XPS, RAMAN).

Radioactive (^{131}I) labelled iodine oxide aerosols were produced at VTT in order to study the revaporisation behaviour of absorbed iodine oxide aerosols under severe accident containment conditions. The effects of gamma radiation, humidity and temperature were studied. Studies on the revaporisation behaviour of the iodine oxide aerosols were performed at the Nuclear Chemistry department of the Chalmers University of Technology in Göteborg, Sweden.

The work was funded by NKS and SAFIR2014.

NKS conveys its gratitude to all organizations and persons who by means of financial support or contributions in kind have made the work presented in this report possible.

Table of contents

1 Introduction

During a severe nuclear accident in a nuclear power plant (NPP), gaseous iodine will be released from damaged fuel and transported into the gas phase of the containment building. There it can react with air radiolysis products, such as ozone. As a result, iodine oxide aerosol particles can be formed [1]. These particles are small in diameter and can either remain in the gas phase of the containment or be deposited on the various surfaces of the containment.

In a typical containment for a Swedish or Finnish light water reactor the majority of surfaces are Teknopox Aqua V A epoxy paint, stainless steel, aluminium, copper and zinc surfaces. Palladium and platinum surfaces were also investigated as the aerosols might poison (deactivate) the active surfaces inside the hydrogen recombiners. The deposited particles may also react with the surface, change its properties and form new iodine species. The deposited aerosol particles on the surfaces of both catalytic and structural materials may act as new sources of elemental iodine which could be rereleased into the gas phase of the containment and contribute to the volatile iodine source term [2]. Therefore, it is important to investigate the behaviour and properties of iodine oxide aerosols.

2 Goals

The object of this investigation was to obtain an insight into the chemical form of, and potential for revaporisation of, iodine oxide particles deposited on typical surfaces found inside a containment. Teknopox Aqua V A paint films, stainless steel, aluminium, copper, zinc, palladium and platinum surfaces were all studied under severe nuclear accident conditions (steam, heat, gamma irradiation). The deposited particles and the original surfaces were analysed with microscopic and spectroscopic methods including Raman, XPS and SEM-EDX to obtain speciation data for the iodine on the surfaces.

The revaporisation behaviour of the iodine oxide deposits in a LWR containment under humid conditions were studied in a model of a BWR containment (FOMICAG facility) using NaI detectors. The revaporisation in dry areas of the containment was simulated using a thermostated heating block and a gamma cell with a dose rate of 14 kGy/h. The change of ^{131}I activity from the iodine oxide deposits on the surfaces under dry conditions were measured using an HPGe detector.

3 Background

The formation of iodine oxide aerosol particles from gaseous elemental iodine and ozone has been reported in the literature [1, 3]. In these experiments, ozone has been generated by passing air or O_2 through a corona discharge.

The oxidation of iodine occurs in several steps. Vikis *et al.* [1] found two feasible reaction routes in the temperature range of 293-370 K:

$$I_2 + O_3 \rightarrow IO + I + O_2 \quad (1)$$
$$I_2 + O_3 \rightarrow IO + IO_2 \quad (2)$$

By successive oxidation of the I, IO and IO_2 primary products, the final product I_4O_9 is formed with ozone:

$$I + O_3 \rightarrow IO + O_2 \quad (3)$$
$$IO + O_3 \rightarrow IO_2 + O_2, \text{ etc.} \quad (4)$$

The appearance of the solid I_4O_9 formed did not change when it was stored for several days in a dry atmosphere. When exposed to ambient air, the samples changed from yellow to brown within a few hours. The oxide (I_4O_9) has been reported to be dark yellow in colour in the CRC Handbook of Chemistry and Physics [4].

It is reported that when the sample was heated up to ~400 K (*approx.* 130 °C), I_4O_9 decomposed and I_2O_5 was formed. The sample underwent a mass loss when heated further to ~570 K and the weight loss continued when the temperature was further increased [1].

HIO_3 (iodic acid) can be formed from I_2O_5 (or I_4O_9) when these substances are exposed to water or humid air according to equation [5]:

$$I_2O_5 + H_2O \rightarrow 2\ HIO_3 \quad (5)$$

Dehydration (heating) of HIO_3 regenerates I_2O_5 [5]:

$$3HIO_3 \rightarrow I_2O_5 \cdot HIO_3 + H_2O \quad (6)$$

Many oxides of nonmetals are acid anhydrides, for example dinitrogen tetraoxide is a mixed acid anhydride for nitrous and nitric acid. As a result this formation of iodic acid by the treatment of iodine oxides with water and the formation of iodine oxides by the dehydration of iodic acid is unsurprising.

The properties of selected solid iodine-oxide compounds are presented in Table 1 [4]. The colour of solid iodine(IV) oxide (I_2O_4) and the mixed valence state iodine oxide (I_4O_9) particles are yellow and dark yellow. The decomposition temperature of these iodine oxides is rather low (≤ 100 °C). Both I_2O_4 and I_4O_9 decompose to I_2O_5 and I_2 upon heating. In water, both species decompose to HIO_3 and I_2. Solid elemental iodine is blue-black in colour and it is purple as a gas. HIO_3 is a white solid, but it is very soluble in water. Dehydration of HIO_3 leads to a formation of white crystalline I_2O_5, which has a high melting point of approximately 300 °C.

Table 1: The properties of solid iodine compounds [4].

Compound	Appearance in the solid state	Melting or decomposition temperature	Solubility in water	Other comments
I_2, iodine	blue-black crystals	113.7 °C	slightly soluble	purple gas
I_2O_4, iodine tetraoxide	yellow solid	100 °C (Decomp.)	decomp. to $HIO_3 + I_2$	-
I_2O_5, iodine pentoxide	white crystal-line solid	~300 °C	soluble	-
I_4O_9, iodine nonaoxide	dark yellow solid	75 °C (Decomp.)	decomp. to $HIO_3 + I_2$	-
HIO_3, iodic acid	white solid	110 °C	very soluble	-

In common with elemental iodine the iodine oxide aerosols can either be absorbed by physisorption or chemisorption. While the metal samples are solids which mainly consist of one element, the Teknopox Aqua V A is a complex matrix of organic and inorganic ingredients. Epoxy paints are made of a resin and a hardener. Both compounds contain organic solvents. Much of this paint solvent can be evaporated from epoxy paint films [14]. The iodine oxides are strong oxidants which can react with the paint ingredients forming new organic species. Thus the outcome of the reaction of the iodine oxide particles with the paint surface could depend on the age of the paint film and other conditions in the containment. The interactions of iodine and methyl iodide with the paint have already been studied at Chalmers. It was found that both physisorption and chemisorption occurs with those species. Similar phenomena were expected when the iodine oxide aerosols came into contact with paint.

4 Experimental

4.1 Production of iodine oxide aerosols

Iodine oxide particles were produced from gaseous elemental iodine. Gaseous iodine was produced in a separate flask at the inlet of the deposition facility (EXSI-CONT facility). To 20 ml of an aqueous mixture of potassium triiodide (KI_3) (50 mM) and potassium iodide (70 mM) which contained ^{131}I (20 MBq) was added a few drops of concentrated sulfuric acid. The resulting mixture was gently heated with a heating plate. Sulfuric acid oxidises the hydrogen iodide formed *in situ* into elemental iodine.

The iodine production flask was connected to the EXSI CONT facility [6]. The iodine vapour and ozone generated by an ozone generator were transferred into the facility via a gas flow (0.1 l/min). The inlet was maintained at 50 °C to prevent condensation of the vapour on the cold facility line. The ozone and iodine mixture were mixed by an additional air flow (2.9 l/min, NTP). The total flow rate was 6 l/min (NTP). All gas flows were controlled with mass flow controllers (Brooks 5851S). The facility was heated to a temperature of 120°C to generate iodine oxide particles. The samples to be exposed were placed in a sample holder (a low pressure impactor) at the end of the exposure line.

Some aerosol samples were produced at 50 °C, 100 °C and 150 °C and collected on a filter paper. A Scanning Electron Microscopy (SEM) image of iodine oxide aerosol particles, produced at 120 °C and collected from the gas phase, is presented in Figure 1 [6]. Energy dispersive x-ray (EDX) analysis showed that the particles contained iodine and oxygen [6].

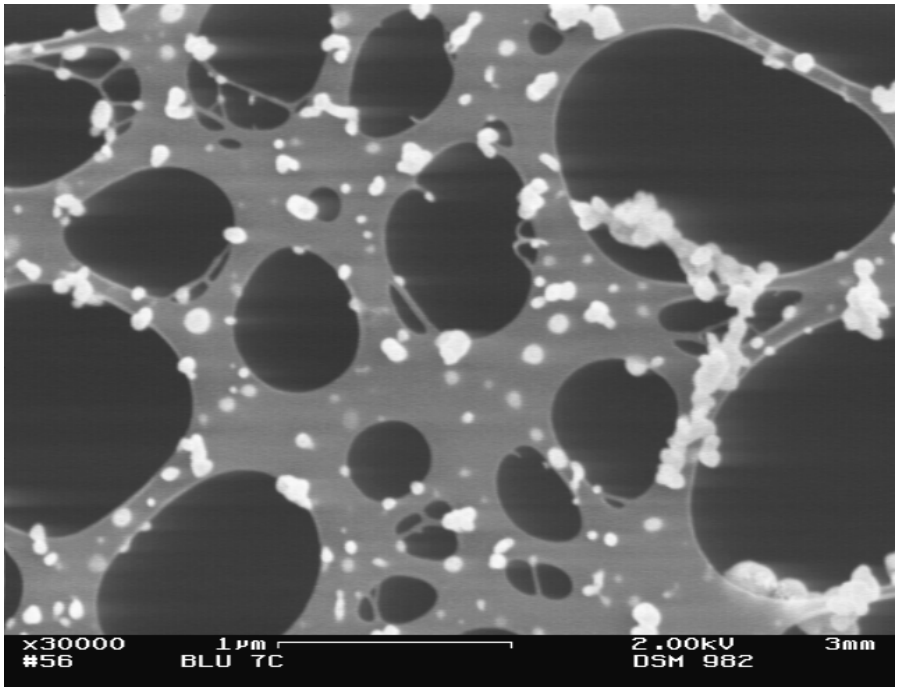

Figure 1: A SEM micrograph of iodine oxide aerosol particles produced at 120 °C [6].

4.2 Exposure of the surface materials to iodine oxide aerosols

Iodine oxide particles were deposited on various surface samples (size of a sample 15 mm x 15 mm x 1 mm) with a custom made impactor. In order to deposit the particles, the total flow rate needed to be increased to *approx.* 100 l/min (NTP). Therefore, a porous tube diluter was attached in line before the impactor in the facility.

Teknopox Aqua V A epoxy paint films (100 µm) were applied to glass slides. Some samples had been aged with heat and irradiation and some samples cured under laboratory conditions (22.7 °C).

4.3 Preparation of samples for SEM-EDX analysis

The details of the analysed samples are presented in Table 2. The total number of samples was 9. The first set of samples were produced in June 2011. The iodine oxide particles were deposited on Teknopox Aqua V A paint (cured for 1 month under laboratory conditions), stainless steel (SS 316), copper and aluminium surfaces. The paint (TEKNOPOX Aqua V A) was the same as that used in some Finnish and Swedish NPP containments. While some epoxy plastics based on building blocks other than bisphenol A have been reported, for example epoxy plastics based on aliphatic ester diepoxides[16] and plant oil (hemp[17] and soybean) have been reported, the majority of epoxys are based on bisphenols such as bisphenol A. When reading the literature on epoxys it is important to understand that other substances[18] are often added to an epoxy which can give the misleading impression that the epoxy is based on a non bisphenol building block.

The samples were stored in a dry vacuum before their analysis. The iodine oxide particles produced at 50 °C, 100 °C and 150 °C were collected on a Teflon™ filter (Millipore Mitex®). The samples were stored in a desiccator over silica gel, at 5°C.

The second set of iodine oxide samples was produced in November 2011. The iodine oxide particles were deposited on Teknopox Aqua V A paint (cured for 1 month under laboratory conditions), stainless steel (SS 316), copper and zinc surfaces. The samples were stored in a dry container, filled with silica gel, at 5 °C.

Table 2. Sample list for SEM-EDX, XPS and Raman measurements.

Sample	Substrate of iodine oxide deposition	Iodine oxide formation T [°C]	Production date	Storage before the analysis	Analysis Techniques
1	Paint	120	06/2011	vacuum, 20 °C, 4 months	SEM, EDX
2	stainless steel (316)	120	06/2011	vacuum, 20 °C, 4 months	SEM, EDX
3	Copper	120	06/2011	vacuum, 20 °C, 4 months	SEM, EDX
4	Aluminium	120	06/2011	vacuum, 20 °C, 4 months	SEM, EDX
5	filter (Mitex®)	100	06/2011	silica gel, 5 °C, 26 weeks	RAMAN
6	Paint	120	11/2011	silica gel, 5 °C, 3+4 weeks	XPS, RAMAN[a]
7	stainless steel (316)	120	11/2011	silica gel, 5 °C, 3+4 weeks	XPS, RAMAN[a]
8	Copper	120	11/2011	silica gel, 5 °C, 3+4 weeks	XPS, RAMAN[a]
9	Zinc	120	11/2011	silica gel, 5 °C, 3+4 weeks	XPS, RAMAN[a]

[a] **Raman analysis of samples was performed 4 weeks after the XPS analysis.**

4.4 Analysis of the iodine oxide deposits with surface analysis techniques

The iodine oxide particle deposits on the samples were analysed with several surface analysis techniques: visual observation, Raman spectroscopy, X-ray photoelectron spectroscopy (XPS) and Scanning Electron Microscopy (SEM) coupled with Energy Dispersive X-ray analysis (EDX).

In order to determine the chemical form of the deposited iodine, Raman spectroscopy was conducted for samples 5, 6, 7, 8 and 9 (see Table 2) at the University of Eastern Finland (Kuopio) by Dr Anna Lähde. The spectrometer used was a Senterra 200LX (Bruker Optics GmbH, Ettlingen, Germany). The wavelength of the laser (for excitation) was 785 nm (red laser) and its power was 10 mW. The part of the spectra studied ranged either from 82 to 1538 cm^{-1} with 3 cm^{-1} resolution or from 127 to 3800 cm^{-1} with 9 cm^{-1} resolution. The samples were analysed at 2 to 3 different locations on the iodine oxide deposit. The filter sample was analysed 26 weeks after preparation of the sample. The analysis of surface samples was completed after 7 weeks of storage.

X-ray photoelectron spectroscopy (XPS) was applied to determine the elemental composition on the surface of the samples 6, 7, 8 and 9 (see Table 2). Since the binding energy of the electrons also depends on the chemical state, some indication of the iodine chemistry could be found based on this analysis. The XPS analysis was conducted at Aalto University (Espoo) by Dr Leena-Sisko Johansson and Dr Joseph M Campbell. The samples were investigated with XPS, using a Kratos Analytical AXIS 165 electron spectrometer with monochromatic Al Kα irradiation at 100 W (X-ray tube voltage 12.5 kV, anode current 8 mA) and charge neutralization. The samples were pre-evacuated in the instrument pre-chamber overnight, in order to stabilize the vacuum conditions. The analysis area in all experiments was less than 1 mm^2, the analysis depth was less than 10 nm and the electron take-off angle was 90°. The analysis was conducted at 3 to 4 different locations per sample. The XPS analysis was conducted after 3 weeks of storage.

The SEM analysis of the samples 1, 2, 3 and 4 (see Table 2) was conducted at VTT (Espoo) by Dr Unto Tapper in order to study the morphology of the deposit layer. The model of the SEM was a LEO 982 Gemini and it was equipped with an EDX spectroscope (NORAN Voyage). The painted samples were coated with platinum in order to prevent the accumulation of electrical charges on the surface during the SEM analysis. The EDX spot analysis and EDX mapping of the same samples was carried out to determine the elemental composition of the samples. The ratio of oxygen and iodine was calculated from the atom concentration using the data from the spot analysis. The intensities of oxygen and iodine in the EDX analysis were detected by measuring the X-ray emission line energies of K-α and L-α respectively. The SEM-EDX analysis was conducted after storing the samples at 20°C in a dry vacuum for 4 months.

4.5 Study of the ^{131}I distribution on the substrate by radioactive means

Samples with deposited iodine oxide particles which bear the radioactive label (^{131}I) were examined using a high purity germanium (HPGe) detector and autoradiography. Measurements with the HPGe detector allow the total amount of ^{131}I sorbed on the surfaces to be determined. The autoradiograph enables the distribution of ^{131}I activity on the entire surface to be mapped in addition to allowing an estimate to be made of the activity.

The samples produced at VTT were packed separately in plastic boxes containing silica gel drying packages. The plastic container is able to absorb volatilised ^{131}I from the sample surface and the silica gel maintains the humidity at a low level. Iodine oxide deposits are hygroscopic, the hydroscopic nature of these deposits can be observed through the rapid colour change of the upper layer when the solid is exposed to humid air (laboratory conditions). The freshly produced samples which have been stored in a cold and dry environment are white. Exposure to the humidity in air causes the upper layer to change colour to yellow-brownish, due to the formation of iodine (see Figure 2). After arrival of the samples at Chalmers, the used silica gel was exchanged for fresh silica gel and the samples were stored at 10 °C until the experiments were conducted. Samples

which had not been used for experiments were measured daily to determine the revaporisation rate of iodine under the storage conditions. For these measurements of the start activity the samples were measured using the HPGe detector for 20 min each. The activity of the samples had not been measured after production or when leaving VTT. Thus the activity after production is unknown. The start activity mentioned in the results is the activity of the samples after arrival at Chalmers and immediately before starting the experiment.

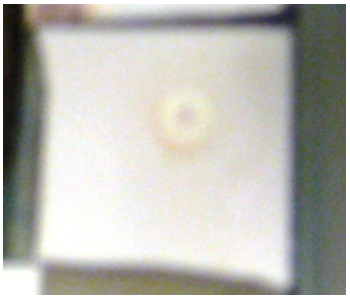

Figure 2A: Teknopox Aqua V A paint sample immediately after opening the exposure chamber.

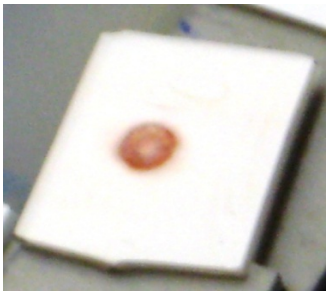

Figure 2B: Teknopox Aqua V A paint sample after *approx.* 1 min exposure to air.

4.6 The revaporisation behaviour of iodine oxide aerosols

The factors that influence the iodine chemistry during a severe accident in a boiling water reactor are the temperature, humidity and the intensity of the radiation field. To investigate the effects of these, three main experiments regarding the desorption behaviour of ^{131}I deposited as iodine oxide particles in the gaseous phase have been performed:

1. Desorption in humid air in a temperature range between room temperature and 250 °C gas phase temperature.
2. Desorption in dry parts of the containment at 150 °C
3. Desorption under dry conditions under the influence of a continuous gamma radiation field with a dose rate of 14 kGy/h. The gamma cell sample chamber temperature was 50 °C.

The desorption behaviour of iodine oxide particles in contact with water was used as a model for a hot steam water film on the painted surfaces in real reactor scenarios. This has been simulated by immersing samples into distilled water.

4.7 Measurement of the revaporisation of ^{131}I from iodine oxide deposits

The revaporisation losses from the sample surfaces was investigated using a HPGe detector. The ^{131}I activity was measured using its gamma emission at 365 keV. The vials holding the paint samples included a spiral of copper wire in the reaction chamber during the experiments. Copper metal is known to be reactive towards elemental iodine but it is almost inert to organic iodides such as methyl iodide.[19] The epoxy paint used was Teknopox Aqua V A paint which has been examined extensively at Chalmers within the PhD work of Sabrina Tietze. It is known that the paint contains ingredients which are reactive towards iodine species. Thus it was expected that under the presence of irradiation and heat that iodine from the decomposition of the iodine oxides could be converted into organic iodines. Observations of the deposited samples showed that the Iodine oxide layer was not a mono-

layer on the sample surfaces. Thus most of the iodine oxide will be physisorbed onto a layer containing iodine and thus might not undergo chemical reactions with the substrate. A volatilisation was then mainly expected to be in the form of inorganic iodine species.

4.8 Desorption studies of iodine oxide aerosols in humid air

The desorption behaviour of surfaces exposed to iodine oxide in humid air has been studied using the **FOMICAG** facility (= **F**acility set-up for **O**n-line **M**easurements of the **I**odine **C**oncentration in an **A**queous and a **G**as phase) at Chalmers (see Figure 3) [15].

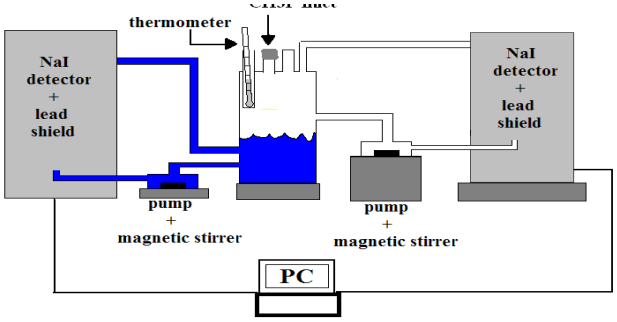

Figure 3: Schematic of the FOMICAG set-up (Chalmers, [15])

The experimental set-up is a lab-scale model of a BWR containment with the relative proportions of the Swedish BWR Oskarshamn 3 ((aq)/(g) = 0.71/0.29) [15]. The centre of the facility is a vessel representing a water pool with lid through which samples can be introduced to the gas phase and aqueous system. The vessel is connected with pipes to one aqueous and one gaseous phase loop. The phases are circulated by two centrifugal pumps to ensure mass transfer, and a magnetic stirrer in the central vessel. The system is heated by a heating plate located under the central vessel and heating tapes placed around all surfaces. To reduce heat losses to the environment the tapes are covered with insulation material. The temperature of the aqueous phase is monitored with a thermometer inserted through one of the openings in the lid and thermo couples are placed on the lid and on the lid surfaces. In each of the loops, gaseous and aqueous, a NaI detector is placed and the change of the ^{131}I concentration in aqueous and gaseous phase is measured on-line.

For the experiments, the vessel was filled up to one-third with double distilled water. The gas phase was normal air. The samples have been placed into the gas or aqueous phase through one of the openings in the lid with a glass hook. The temperature has been raised in a ramp between room temperature (22.7 °C) and 250 °C.

4.9 Desorption studies of iodine oxide aerosols in dry air

The desorption of iodine oxide aerosols under the storage conditions (10 °C, dry air) has been investigated using the samples between their arrival at Chalmers and their use in other experiments, using a HPGe detector.

The thermal desorption behaviour of the iodine oxide particles was investigated by heating the samples separately in vials (20 ml) which were filled with air. The vials also contained copper spirals. Copper is known to be reactive towards elemental iodine. Thus by measuring the copper wire it was possible to detect any release of elemental iodine from the painted surface. The vials were heated in a thermostated aluminium block. At intervals the samples and copper wires were examined using a HPGe detector.

The desorption effects at 50 °C had been monitored by exposing the samples to gamma irradiation in a gamma source with a sample chamber temperature of 50 °C. The temperature of the gamma irradiation chamber was due to the decay heat of the ^{60}Co sources used in the irradiator. Furthermore the desorption behaviour of ^{131}I has been investigated at 150 °C because this is the reference temperature in severe accident research for BWR reactors. In BWR reactors venting of the containment is initiated when the average containment temperature reaches 150 °C and exceeds a pressure of 5-6 bars.

4.10 Desorption studies of iodine oxide aerosol particles under the influence of gamma irradiation

The desorption behaviour of ^{131}I from deposited iodine oxide aerosol particles caused by gamma irradiation (dose rate of 14 kGy/h) has been investigated by irradiating the samples separately in air filled vials (20 ml). The sample chamber temperature in the gamma cell during the irradiation was *approx.* 50 °C. In common with the heat treated samples, the irradiated samples were examined using a HPGe spectrometer. The samples had been pre-heated for *approx.* 24 h at the irradiation cell temperature to evaluate the temperature effect.

The ability of metal samples (Cu, Al, Zn, SS, Pd, Pt), as well as fresh and artificially aged films of the epoxy paint Teknopox Aqua V A to bind ^{131}I from iodine oxide aerosols chemically to the substrate, has been compared. The paint films were either fresh (1 month aging before exposure to the aerosols), samples aged for 18 months (21.5 ± 0.5 °C), samples aged for 2 years at 100 °C and samples that had been exposed to γ-radiation for 1 day, 3 days and 9 days (14 kGy/h and a temperature of 50 °C).

4.11 Desorption studies of iodine oxide aerosols on water covered surfaces

The desorption behaviour of ^{131}I from deposited iodine oxide aerosols on surfaces covered with a water film has been simulated by inserting the samples into double distilled water. Iodine oxide aerosols are known to be water soluble.

5 Results

5.1 Visual observations of the non-radioactive deposits

After the deposition of iodine oxide particles on the samples, the samples were removed from the impactor. The deposit was originally pale yellow (see Figure 4). The details of samples 6, 7 and 8 are presented in Table 2. The other samples were: aluminium, B Teknopox Aqua V A paint cured for 1 month, C Teknopox Aqua V A paint cured for 18 months and D paint TEKNOPOX Aqua V A paint aged 2 years at 100°C. The analysis of samples A, B, C and D is not presented in this report.

The colour of particles turned to brown/purple after a few minutes in ambient air (see Figures 5 and 6) as the particles reacted with the humidity of the air. This reaction was much faster than Vikis *et al.* [1] reported. Probably the sizes of our particles were smaller than those used in the study of Vikis *et. al*. Therefore, the increased surface area to volume ratio would have increased the rate. The samples were stored in a dry plastic container. After a few days, the particles in the deposit spots on the paint were darkening, even though they were being stored under dry conditions (see Figure 7a). However, the deposition spots on all metal surfaces remained light in colour during these dry storage conditions. It seems that the reaction of iodine oxide particles with the paint is different to that of the particles with the

metal surfaces. Figure 7b shows the samples after five weeks of storage. The details of the samples are presented in Table 2.

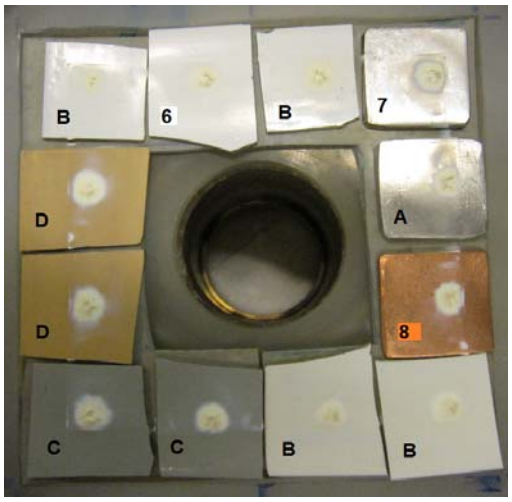

Figure 4: The iodine oxide particles deposited on various paint and metal surfaces. The pale yellow colour of particles is noticeable.

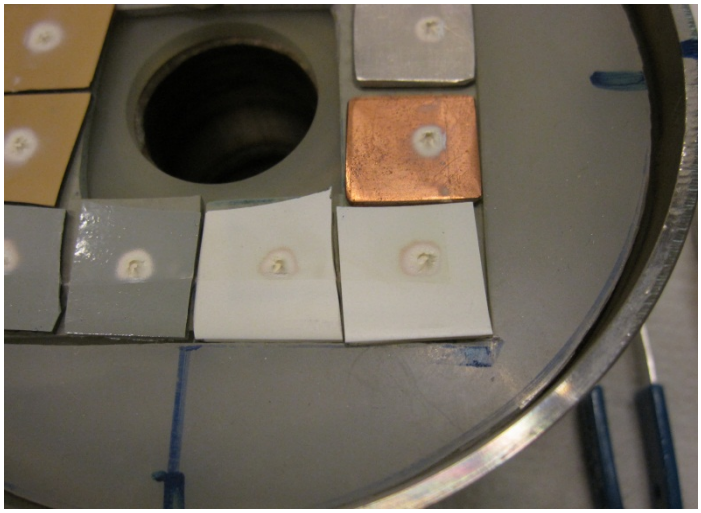

Figure 5: The iodine oxide particle deposits after a few minutes. A brownish colour can be seen on the edges of the deposition spots.

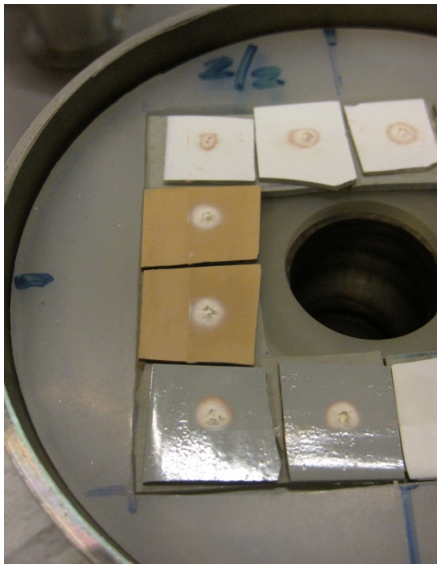

Figure 6: The iodine oxide deposits after ~5 minutes. The deposition spots are turning darker.

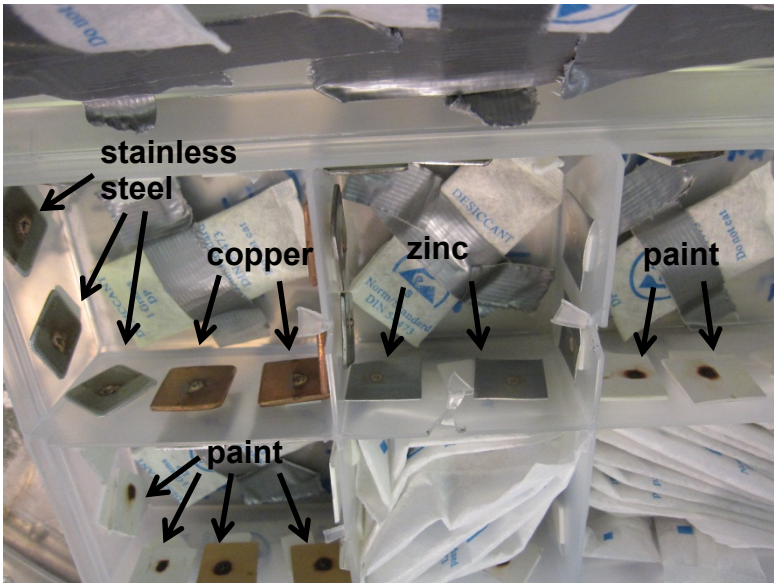

Figure 7a: The iodine oxide deposition samples after a few days, packed in a dry casing. The deposition spots on the painted surfaces are dark. Some lighter colours can be seen in the deposition spots on all the metal surfaces.

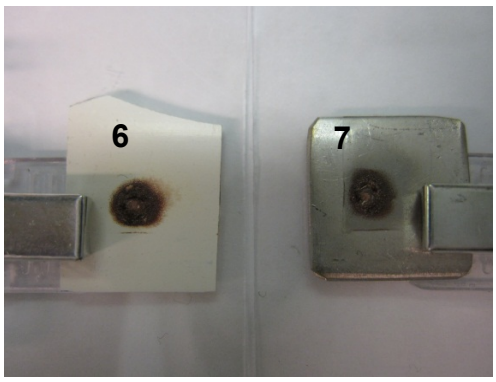

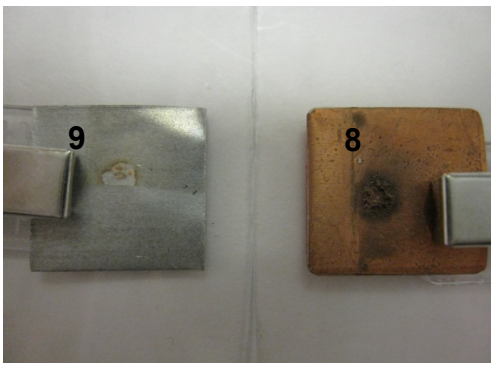

Figure 7b: The deposition spots on paint (6), stainless steel (7), zinc (9) and copper (8) after five weeks. The amount of iodine oxide particles on the zinc is low and the colour of the deposition has remained light/yellow.

5.2 Results from Raman analysis

The particles collected on the Teflon™ filter (Mitex®) (sample 5) were brown yellow when the filter was taken out of the exposure chamber (see Figure 8).

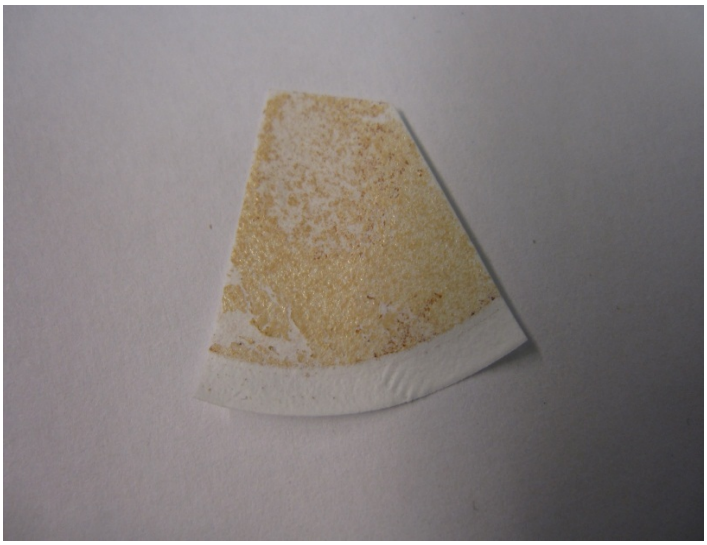

Figure 8: Iodine oxide particles collected directly from gas phase on filter (Mitex®). Particles were produced at 100°C and showed a yellow colour.

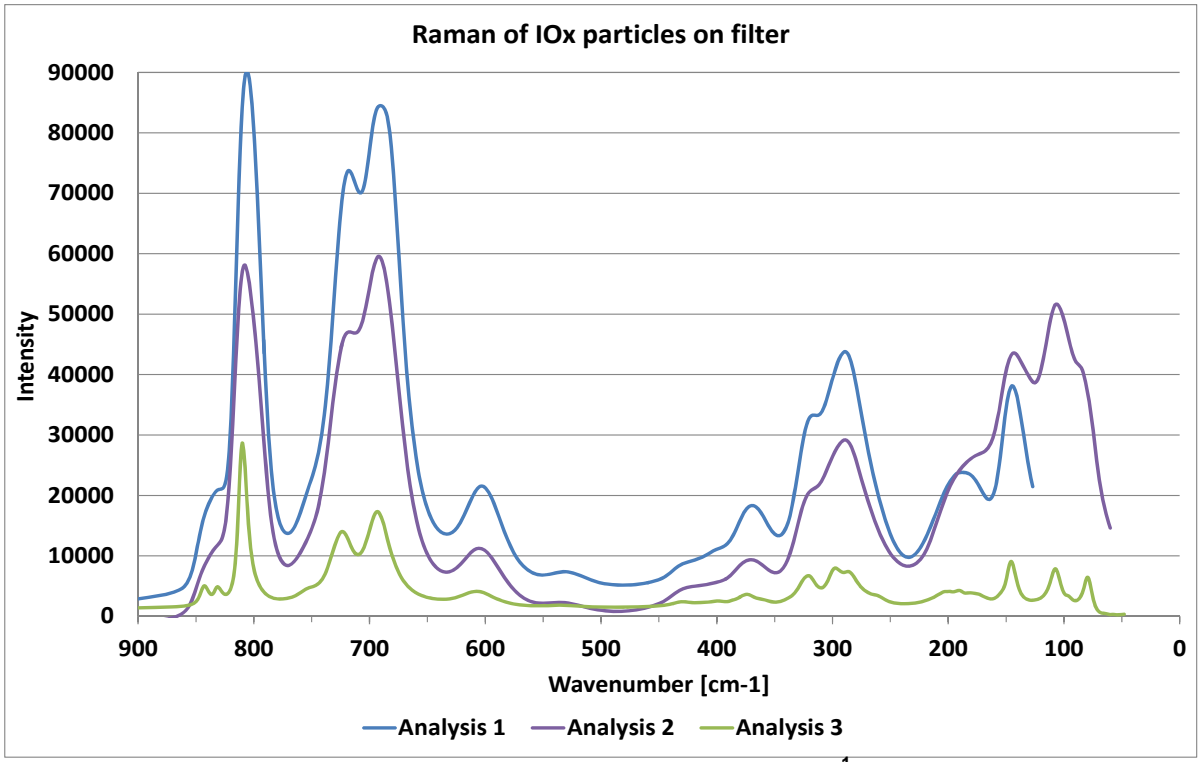

Figure 9: Raman spectra (wave numbers 0-900 cm^{-1}) of iodine oxide particles collected on a Teflon™ filter. Particles were produced at 100°C. The sample was analysed in three locations

The Raman spectrum of iodine oxide particles on the filter (Analysis 3) corresponded to the Raman spectrum of solid I_2O_5, (Figure I2). The two other spectra (Analysis 1 and 2) correspond to the Raman spectrum of solid I_2O_5 with iodine molecules (I_2) adsorbed on it (Figure I2). The spectral data of these spectra are presented in Appendix I, Table I1 and Appendix J, Table J1. The colour of solid I_2O_5 is reported to be white. However, the colour of the particles on the filter were yellow (see Figure 8).

Iodine(IV) oxide (I_2O_4) is a yellow compound and a probable reaction product of ozone and gaseous elemental iodine. It decomposes when heated to form iodine(V) oxide and elemental iodine:

$$5\ I_2O_4 \rightarrow 4\ I_2O_5 + I_2 \qquad (7)$$

The band of I_2 molecules, at *approx.* 192 cm^{-1} [7] (or 180 cm^{-1} and 189 cm^{-1} [8]), is clearly visible in the Raman analyses 1 and 2. Therefore, the iodine oxide particles on the filter sample were originally most likely I_2O_4 or a mixture of I_2O_4 and I_2O_5.

The measured Raman spectra (wave numbers 0 - 900 cm^{-1} and 500 – 825 cm^{-1}) of iodine oxide particles deposited on paint (sample 6), stainless steel (sample 7), copper (sample 8) and zinc (sample 9) surfaces, are presented in Figures 10, 11 and 12.

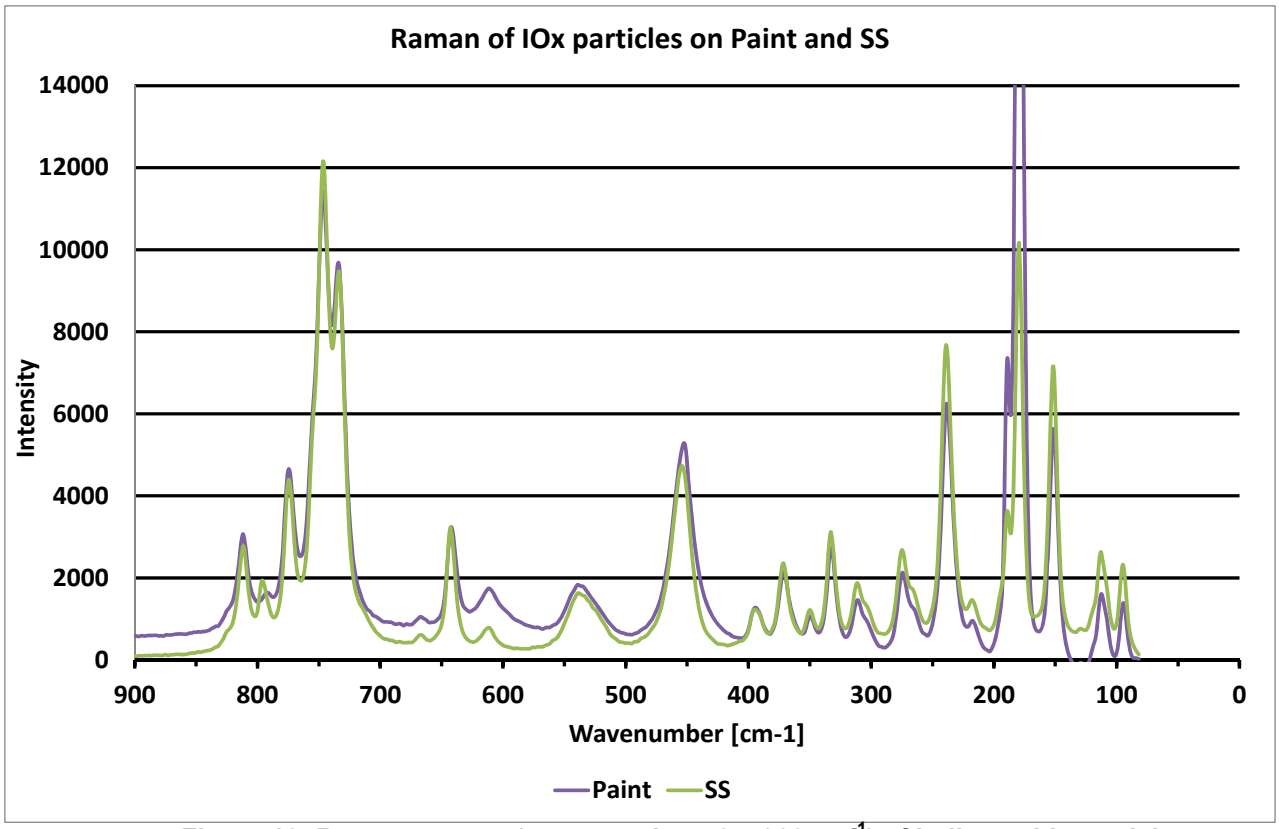

Figure 10: Raman spectra (wave numbers 0 – 900 cm^{-1}) of iodine oxide particles deposited on paint and stainless steel surfaces.

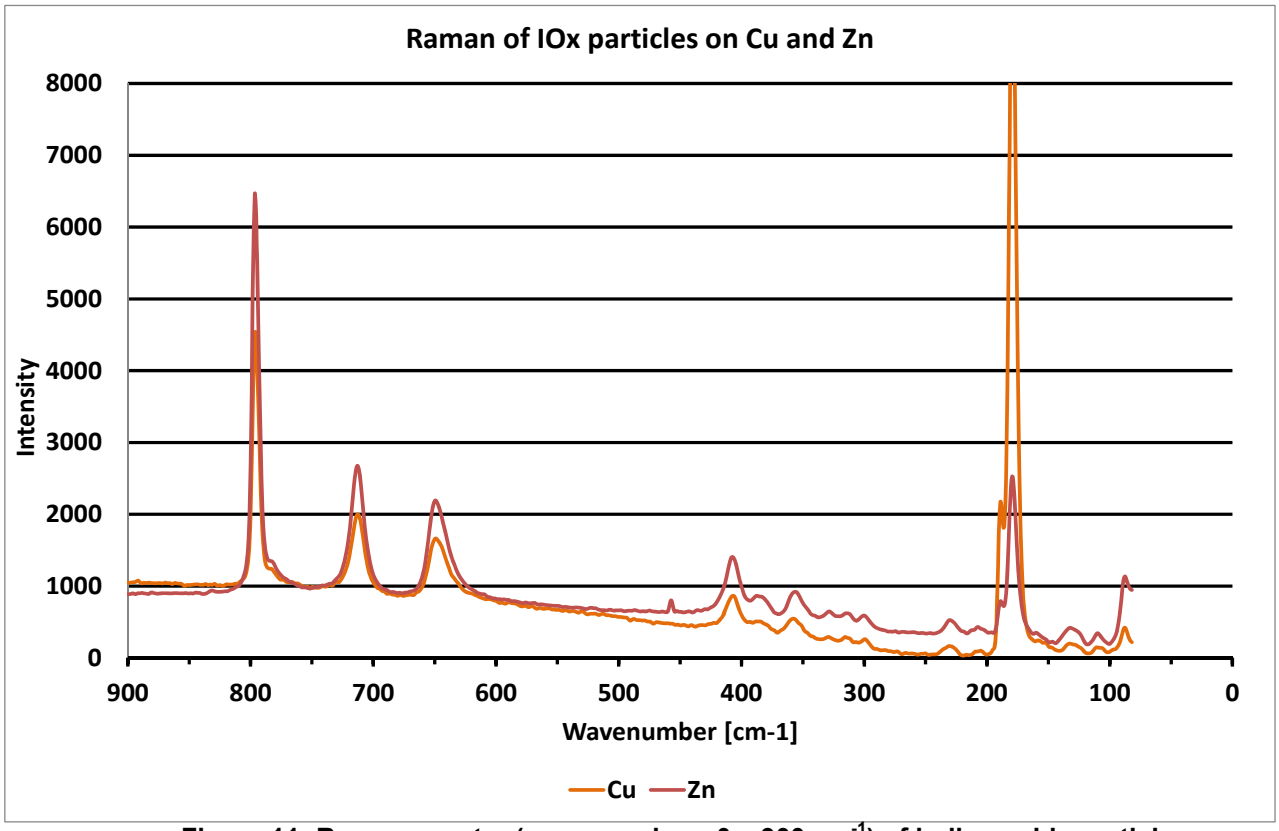

Figure 11: Raman spectra (wave numbers 0 – 900 cm^{-1}) of iodine oxide particles deposited on Cu and Zn surfaces.

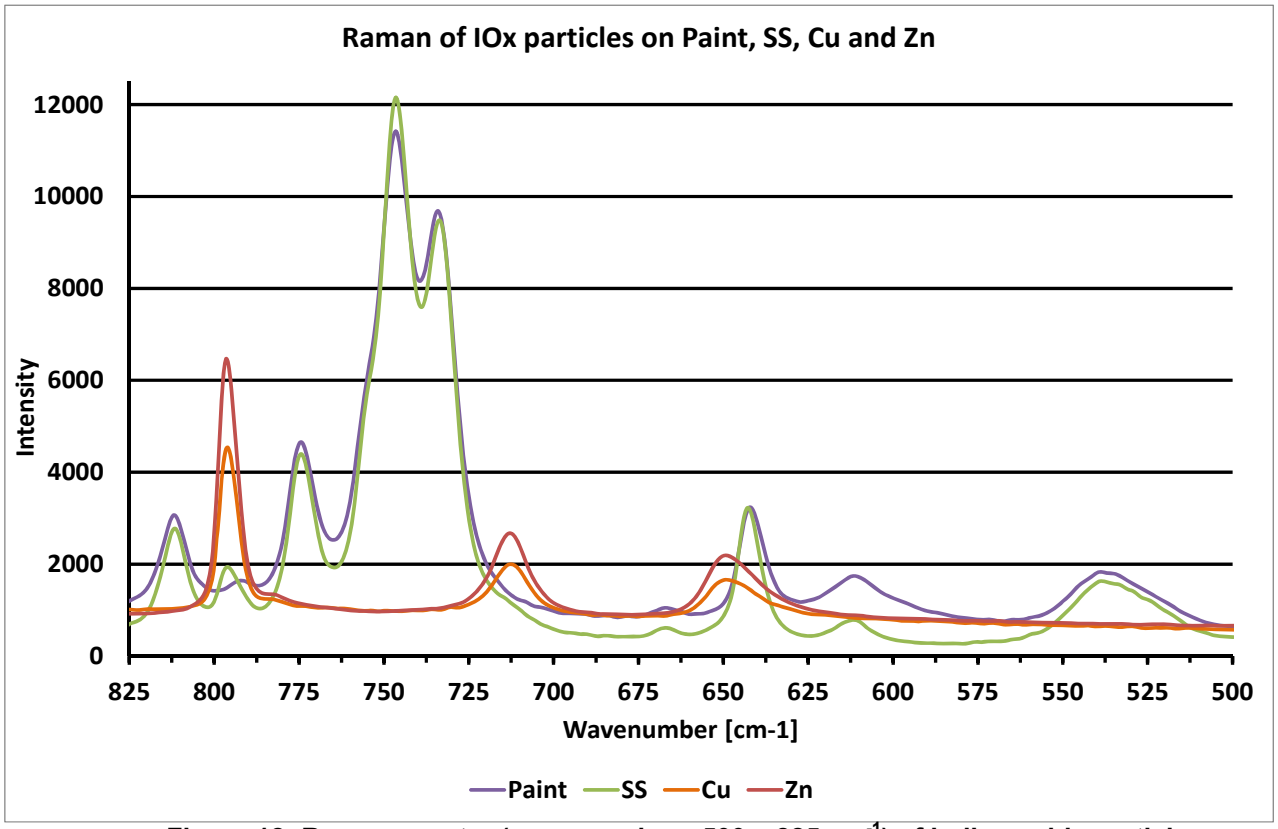

Figure 12: Raman spectra (wave numbers 500 – 825 cm^{-1}) of iodine oxide particles deposited on paint, stainless steel, Cu and Zn surfaces.

The Raman spectra of iodine oxide particles on paint and stainless steel surfaces are similar. They correspond to the spectrum of partially dehydrated solid HIO_3 which was defined as HI_3O_8 or $I_2O_5 \bullet HIO_3$ which is presented in Appendix I, Figure I6. It is noteworthy that HI_3O_8 has been observed in the solid state,[20] in common with oleum (disulfuric acid) it is a compound where the high valent atoms are each surrounded by a polyhedron of oxygen atoms (and in the case of iodine a stereochemically active lone pair). In both the iodine and sulfur compounds some of the oxygen atoms are bridging between the halogen or chalcogen atoms. The fully hydrated iodic acid has been characterised by neutron diffraction in the solid state.[21]

The spectra of iodine oxide particles on copper and zinc are similar to each other but they differ from the Raman spectra of particles on paint and stainless steel surfaces. The spectra does not correspond either with the spectra of I_2O_4, I_2O_5 or aqueous HIO_3 presented in Appendix I. However, the Raman spectra of particles on copper and zinc surfaces resembles the spectrum of solid HIO_3 presented in Appendix I, Figure I4. A quite strong peak in the spectra of copper and zinc samples was seen at ~400 cm^{-1}, this peak is not present in the spectrum of solid HIO_3.

The peaks of elemental iodine at wave numbers of approx. 180 cm^{-1} and 189 cm^{-1} [8] are also visible on paint, stainless steel, copper and zinc surfaces. The spectral data of the spectra are presented in Appendix I, Table I1 and Appendix J, Table J2.

5.3 Results from XPS analysis

The XPS spectra of the binding energy of electrons in the centre of the iodine oxide depositions on paint, stainless steel, copper and zinc samples are presented in Figure 13. The binding energy was high on the paint, stainless steel and copper surfaces. This means that iodine was oxidised. It is most likely that the layer of iodine oxide particles was thick at the centre of the deposition, and the outer layer of the particles had not reacted with the surface. A small fraction of iodine was in a low oxidation state on the surfaces, which is evident as a shoulder in the spectra at a smaller energy (peaks at approx. 621 eV). However, iodine was not oxidised (or it had a very low oxidation state) on the zinc surface. It seems that iodine oxides reacted with zinc throughout the entire layer.

The XPS spectra of the iodine binding energy on the edge of the iodine oxide deposition on the same samples are presented in Figure 14. The peaks of iodine were similar on the paint and stainless steel surfaces as in the centre of the deposition. The binding energy of iodine was high on both surfaces which means that iodine was mostly oxidised. Probably, paint and stainless steel surfaces had very little effect on the outer layer of iodine oxide particles on the samples. A small fraction of iodine was also in low oxidation state on both surfaces. On the copper surface iodine had both high and low binding energy peaks, indicating that a significant fraction of iodine was in a low oxidation state at the edge of the deposition. On the zinc surface all iodine was in a low oxidation state, as mentioned previously.

The complete binding energy spectra of the centre and at the edge of the deposition are presented in Appendixes A and B, respectively. The corresponding elemental concentrations are presented in Appendix C.

No significant differences in the oxygen binding energy between the edge and the centre of the deposition on the zinc samples were detected. On paint and stainless steel samples the oxygen binding energy was slightly higher in the centre of the deposition. On the copper sample the increase in oxygen binding energy in the centre was more notable. These results

indicate that iodine was not oxidized on the zinc surface. On the other surfaces the fraction of iodine oxides was slightly higher in the centre of the deposition.

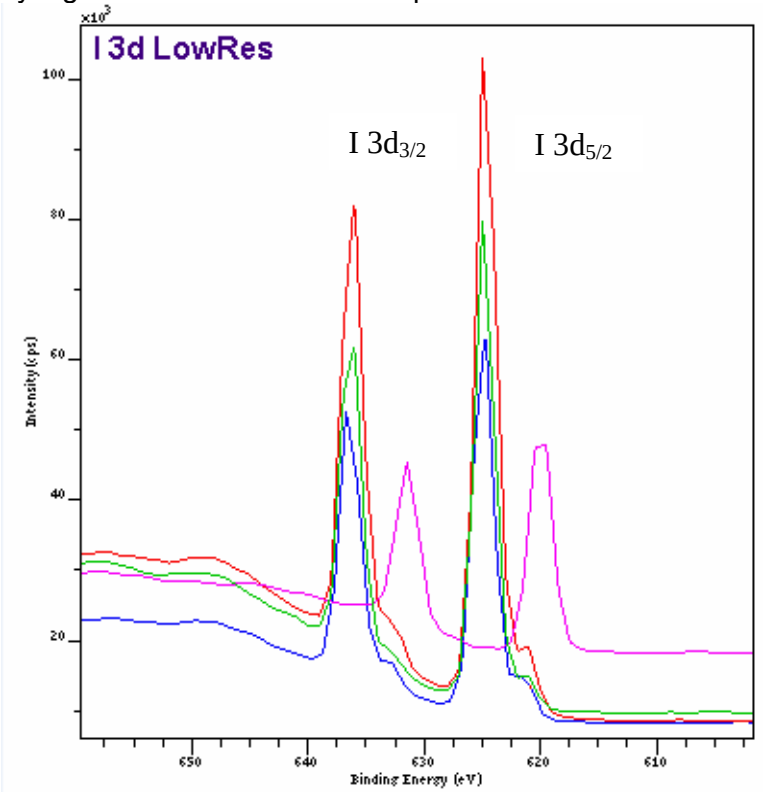

Figure 13: XPS spectrum (binding energy) of the deposit (spin orbits I $3d_{5/2}$ and I $3d_{3/2}$) on paint (green), stainless steel (blue), copper (red) and zinc (magenta) surfaces. The analysis was conducted in the centre of the deposition area with a thick deposit layer.

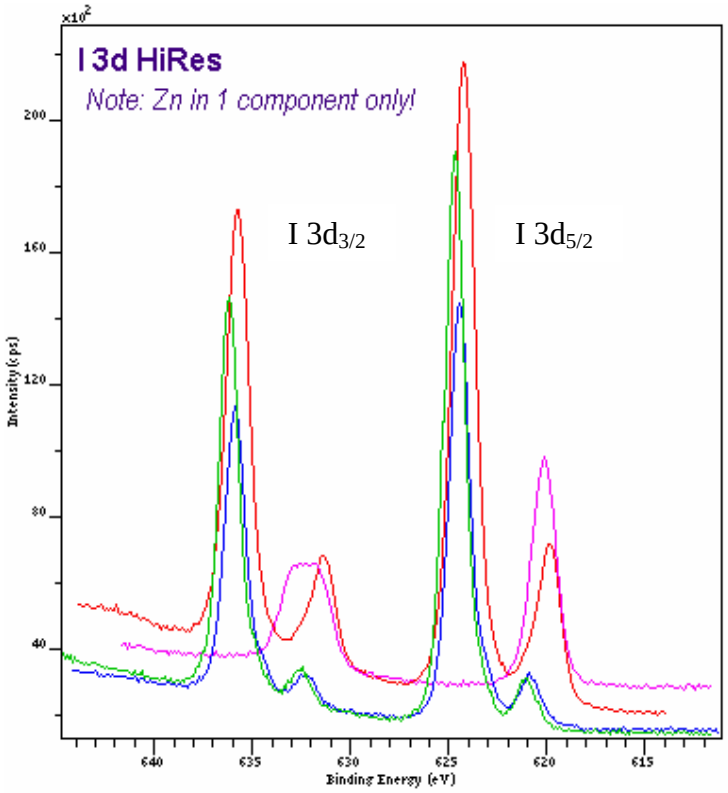

Figure 14: XPS spectrum (binding energy) of the deposit (spin orbits I $3d_{5/2}$ and I $3d_{3/2}$) on paint (green), stainless steel (blue), copper (red) and zinc (magenta)

surfaces. The analysis was conducted on the edge of the deposition area with a thin deposit layer.

The elemental concentrations presented in appendix C clearly show that zinc has reacted all through the deposit layer as its concentration is almost constant across the sample. This may relate to the fact that zinc has simple redox chemistry and forms a single water soluble iodide. In contrast copper only forms a single water insoluble iodide (CuI), and it is known that thin films of copper iodide are semiconductors. A small amount of copper can also be found in the centre of the deposition indicating that the iodine oxide deposit has partially reacted with the copper surface. The inorganic components of steel (iron and chromium) and paint (magnesium) can only be found at the edge of the deposit. It is noteworthy that nickel both forms a hydrated iodide (nickel(II) iodide hexahydrate)[22] and an anhydrous iodide.[23] When the hydrated form of a nickel halide is heated to form the anhydrous form it can be very difficult to redissolve the dehydrated nickel compound in water again because of the change of the crystal structure. The effect is more pronounced in the case of chromium(III) chloride and chromium(III) bromide where the fact that the metal atoms in anhydrous metal salts have octahedral coordination environments and have d3 electronic configurations combined to cause these dehydrated halides to be, for many intents and purposes, insoluble in water whereas the hydrated forms of these chromium(III) halides are very quick to dissolve in water.

An accurate speciation of iodine oxides is not possible from the XPS results alone as the spectrometer used in the analysis has a resolution of *approx.* 1 eV. The difference in the iodine binding energy between different iodine oxide species can be as small as 0.1 eV, see Table 3. The non-oxidised iodine compound on copper and zinc surfaces may be CuI (619.0 eV) and ZnI_2 (619.8 eV), respectively. The binding energy of elemental iodine is 619.9 eV. It is thus possible that elemental iodine is responsible for the small shoulders seen in spectra from painted and stainless steel surfaces.

According to XPS analysis, the samples also contained rather high fractions of carbon (C) and silicon (Si) impurities. Some surface contamination has most likely taken place during the handling and storage of the samples in the laboratory, or these elements could be present due to the use of silicone pump oils in vacuum pumps.

Table 3: Binding energies of I $3d_{5/2}$ and O 1s [9].

I $3d_{5/2}$ binding energy		O 1s binding energy	
	eV		**eV**
I_2	619.9	metal oxides	approx. 528-531
I_2O_5	623.3	CuO	529.6
HIO_3	623.1	Cu_2O	530.3
H_5IO_6	623.0		
CuI	619.0		
ZnI_2	619.8		
NiI_2	619.0		

5.4 Results from SEM - EDX analysis

All samples analysed with SEM showed a greater diameter of iodine containing crystals on the surface of the metal and paint samples than the diameter of the deposited iodine oxide particles on the filter (~50 to 100 nm). It is likely that iodine oxide particles underwent further reactions after being absorbed onto the paint and metal surfaces. The crystal growth took place during the 4 months of storage before examination with scanning electron microscopy (SEM).

5.4.1 SEM-EDX analysis of a painted sample exposed to iodine oxide (Teknopox Aqua V A)

The deposit on the painted surface was examined using SEM. A SEM micrograph of a painted reference sample and an iodine oxide deposition sample on a painted surface are presented in Figure 15.

Additional micrographs of iodine depositions are presented in Appendix D1. In the centre of the deposition area, iodine oxide particles seem to have dissolved at some point; this is likely to be due to exposure to humid air. These areas contained pool like regions. On the edge of the deposits a thick layer of a crystalline solid containing iodine was found. These crystals were larger than the particles that had been deposited on the surface. An area that contained very little iodine could be observed between the centre and the edge of the deposit.

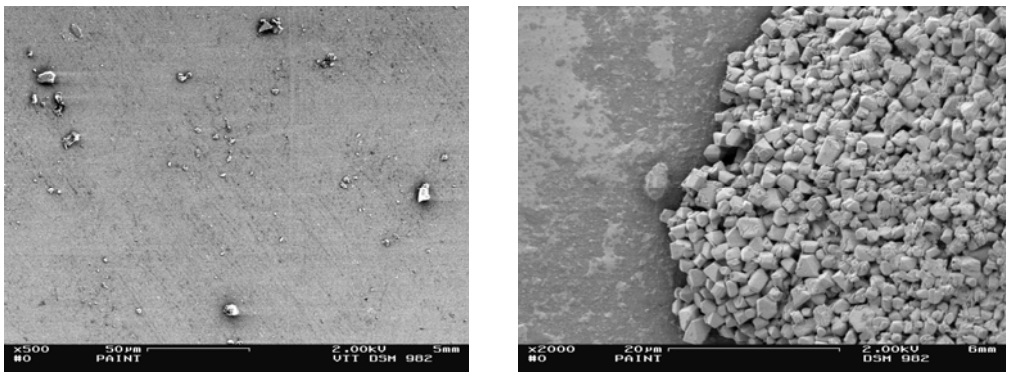

Figure 15: A SEM micrograph of the iodine oxide exposed Teknopox Aqua V A paint sample. A reference sample of a painted surface contained some

particular impurities (on the left). Fairly large crystals containing iodine had formed on the edge of the deposit area on the sample (on the right).

The elemental mapping of the deposit area, presented in Figure 14 and in Appendix D2, confirmed that iodine and oxygen could primarily been found in the same locations. Both elements were visible in the centre and at the edge of the deposit area. Elements present in the paint such as carbon, titanium and sulphur could be seen between these two deposit areas. Signals from aluminium, silicon and magnesium are thought to have been caused by impurities.

Another elemental map of dissolved deposit on the painted surface is presented in Appendix D3. Signals from iodine and oxygen are also found in these figures. Carbon is visible only in areas that do not contain deposited material. The signal to noise ratio for the element maps for the other elements in the paint are too poor for any conclusions to be drawn.

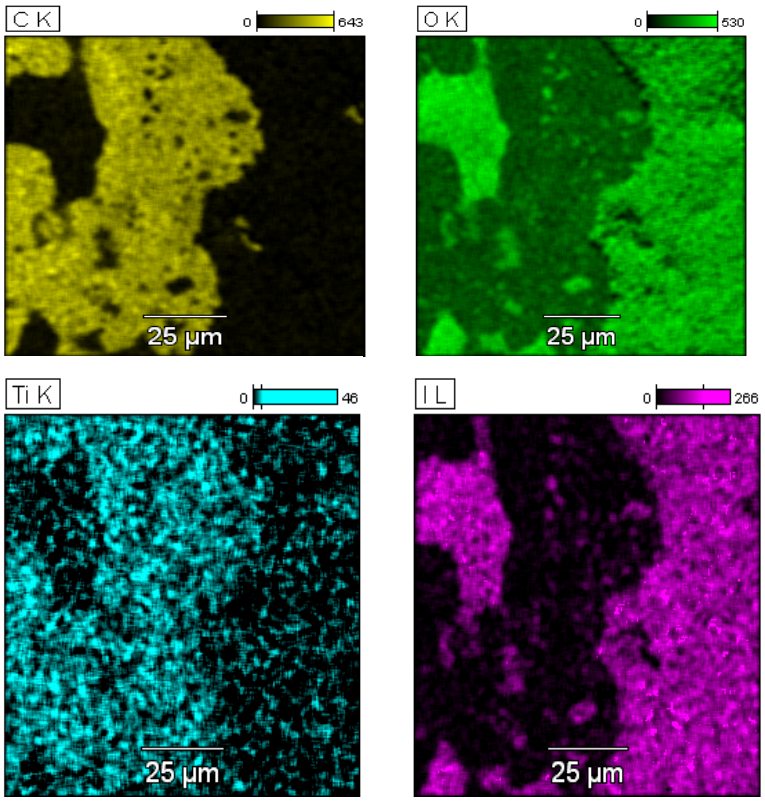

Figure 16: The elemental map of deposit on painted surface acquired with EDX.

EDX spot analysis was performed in the same areas as the EDX maps presented in Appendix D2 (also Figure 16) and D3. The locations of the spot analysis as well as the resulting spectra are presented in Figure 17 and in Appendix D4. An additional EDX spot analysis was also conducted outside of the deposited area of the painted sample. Results from that analysis are presented in Appendix D5. The spot analysis confirmed that primarily iodine and oxygen could be detected on areas that contained deposited aerosols. The ingredients of the paint were visible in areas outside of the deposit. The oxygen to iodine ratio could be calculated from the three spots containing some deposits, see Appendixes H1 and H2. The results are presented in Table 4. It can be said that the oxygen to iodine ratio was remarkably similar in all measured locations despite the difference in the appearance of the deposit. According to EDX spot analysis it cannot be ruled out that the deposit was indeed partially hydrated I2O5•HIO_3 (=HI_3O_8) with some adsorbed elemental iodine as suggested by the Raman spectra.

Table 4: Oxygen to iodine ratio measured with SEM-EDX spot analysis in deposit located on a painted sample.

Reference	O:I ratio	Deposit description
Fig. 15 Spot 1	2.26	Dissolved, centre
Fig. 15 Spot 3	2.10	Crystalline, edge
D4 Spot 2	2.23	Dissolved

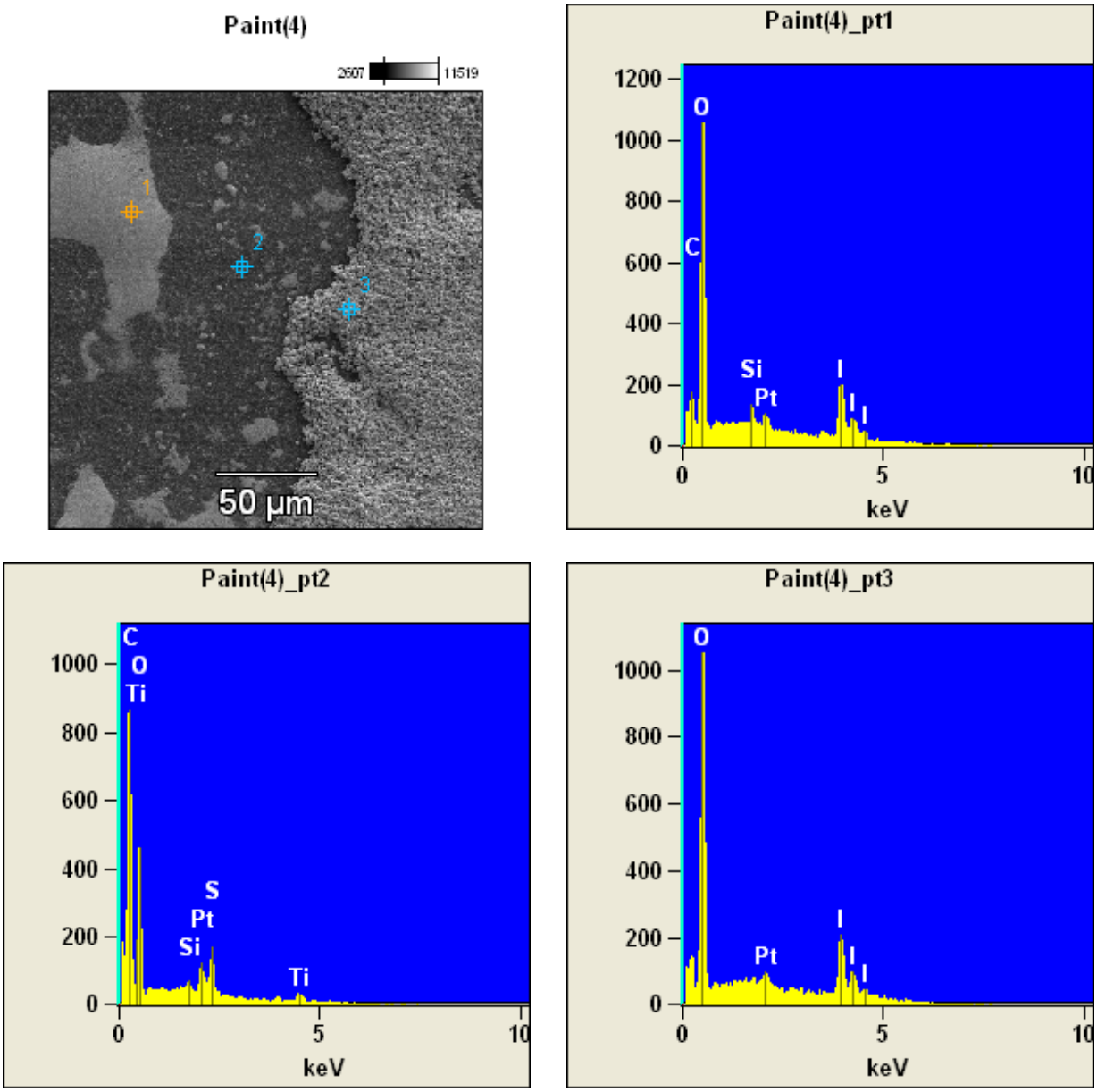

Figure 17: The EDX spectra of three locations on a painted surface. Spot 1 is located on dissolved deposit in the centre of the deposit. Spot 2 is on a section relatively free of deposited iodine. Spot 3 is located on a crystalline deposit at the outer edge of the deposition area.

5.4.2 SEM-EDX analysis of a stainless steel (316) surface exposed to iodine oxide

A SEM micrograph of a stainless steel reference sample and a sample with the iodine oxide deposit are presented in Figures 18A and 18B. A collection of further SEM micrographs of the sample is presented in Appendix E1. The grain boundaries on the surface of the stainless steel sample appeared to be quite broad. While on the painted samples, the iodine oxide particle deposit appeared to have dissolved after deposition on the surface, on the steel sample no evidence of this effect can be seen. It appears that the growth of the crystals containing iodine on the surface depends on the grain size of the stainless steel sample. The size and orientation of crystals on the surface suggested that the deposited iodine oxide particles had also reacted with the humidity of the air.

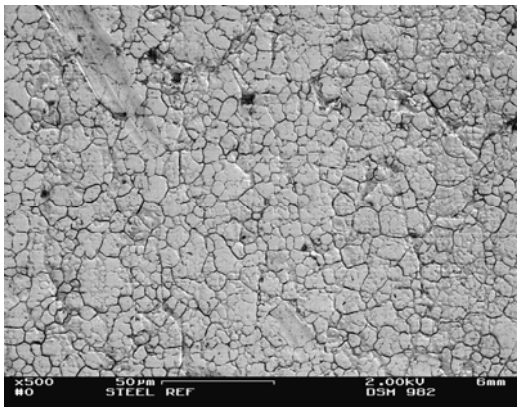

Figure 18A: A SEM micrograph of a stainless steel reference sample. The grain boundaries of the stainless steel appear to be quite broad.

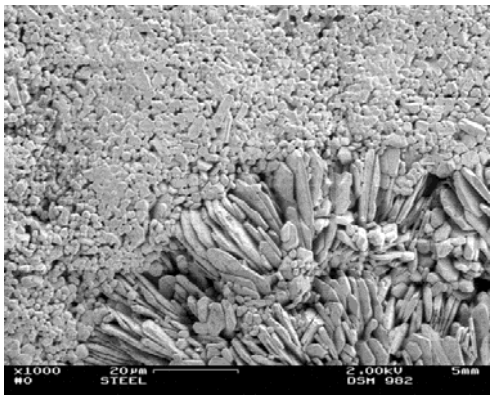

Figure 18B: A crystalline deposit was evident on the surface. The size of the crystals depended on the location.

The EDX map of the deposit area is presented in Figure 19 and in Appendix E2. Iodine is found in the area where the crystals are located. The amount of oxygen found correlates well with the iodine deposit. The constituents of stainless steel (iron, nickel, chromium and molybdenum) were detected in areas free of the iodine oxide crystals.

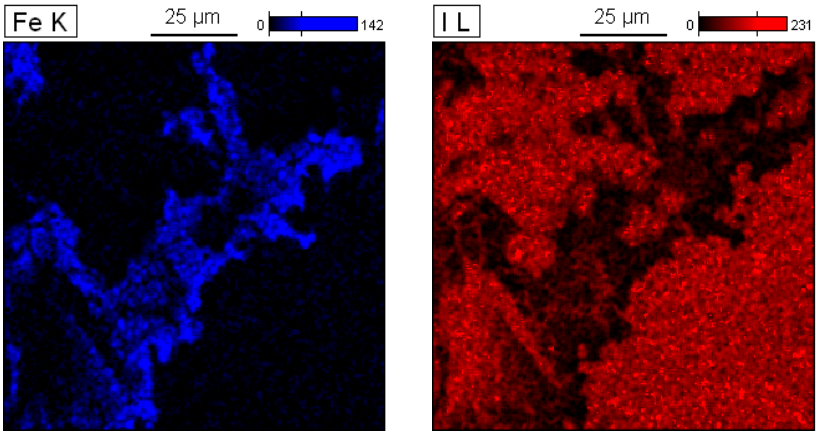

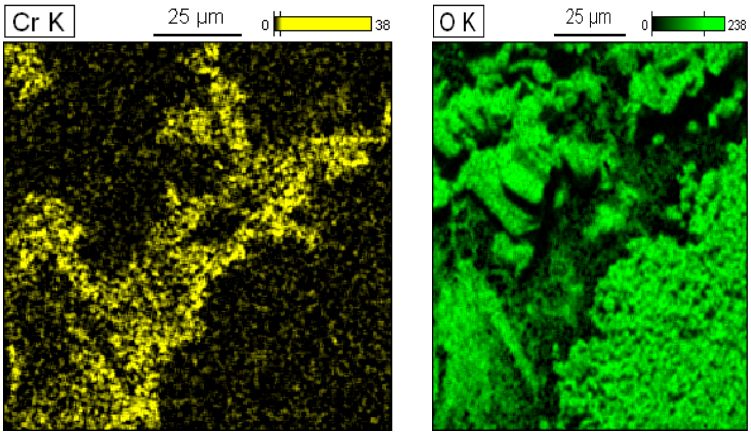

Figure 19: The EDX map of iodine oxide deposition on a stainless steel sample.

Another EDX mapping was done outside of the deposition area. The map presented in Figure 20 and in Appendix E3 revealed that iodine oxide could be found mainly in the chromium rich grain boundaries of the stainless steel.

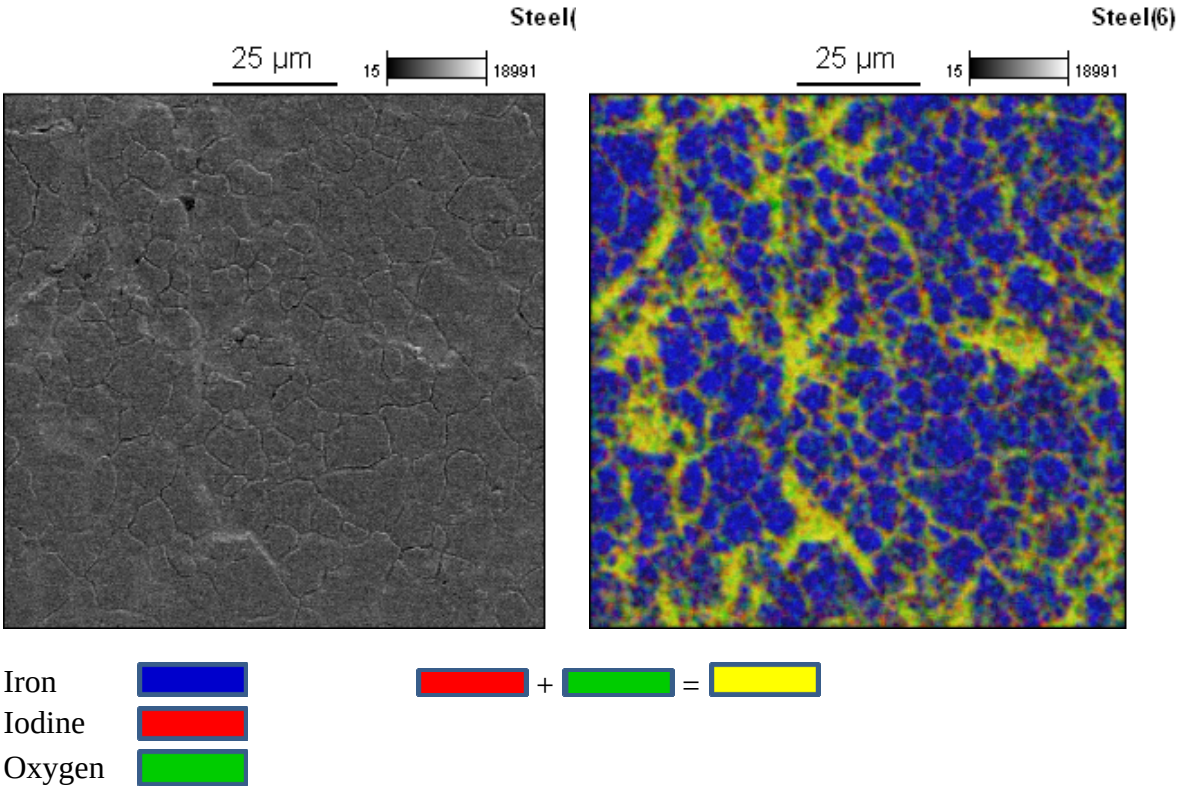

Figure 20: The distribution of iron, iodine and oxygen on the stainless steel surface analysed with EDX. The analysed location is outside of the original particle deposition. Iodine oxide is located mainly in the grain boundaries of the steel.

With the stainless steel sample, EDX spot analysis was conducted on the area with crystalline iodine oxide deposits (Appendixes E4, E5 and E6), on grain boundary deposits (Appendixes E7 and E8) and outside of the deposit area (Appendix E9). Based on the spot

analysis the calculated oxygen to iodine ratios are presented in Table 5, see Appendixes H1 and H2. On or close to the crystalline deposit, the oxygen to iodine ratio varied between 2.02 and 3.19 with one notable exception of 0.88. The average ratio of all analysed spots was 2.5. As with the painted sample, the EDX analyses agreed with the Raman results; that the form of iodine could have been partially hydrated I_2O_5•HIO_3 (=HI_3O_8) with some adsorbed elemental iodine. It should be noted though that both the ratio as well as the appearance of the deposit varied strongly as a function of location. The ratio on grain boundaries varied between 2.8 and 3.16 suggesting that the form of iodine at the boundaries could have been HIO_3.

Table 5: The oxygen to iodine ratios measured with SEM-EDX spot analysis in a deposit of iodine oxide on a stainless steel sample.

Reference	O:I ratio	Deposit description
E4 Spot 1	2.96	Close to crystalline deposit
E4 Spot 2	2.23	On crystalline deposit
E4 Spot 3	3.13	Close to crystalline deposit
E4 Spot 4	2.56	Close to crystalline deposit
E4 Spot 5	2.39	On crystalline deposit
E5 Spot 1	2.02	On crystalline deposit
E5 Spot 2	0.88	Close to crystalline deposit
E6 Spot 1	2.85	On crystalline deposit
E6 Spot 2	3.19	On crystalline deposit
E7 Spot 1	3.16	On grain boundary
E7 Spot 2	2.88	On grain boundary
E8 Spot 2	2.80	On grain boundary

5.4.3 SEM-EDX analysis of a copper surface exposed to iodine oxide

A SEM micrograph of a copper reference sample and an iodine oxide deposit on a copper surface are presented in Figures 21A and 21B. Further SEM micrographs of the copper sample are presented in Appendix F1. Three distinctively different areas could be observed in the SEM images. Especially in the centre of the deposit area, the deposit seemed to be rather thick, uniform and composed of large grain-like structures. Closer to the edge of the deposit, the solid was mainly in the form of small crystals. Large pool-like structures of particles which seem to have dissolved and re-solidified were observed both among the grains as well as on top of the small crystals.

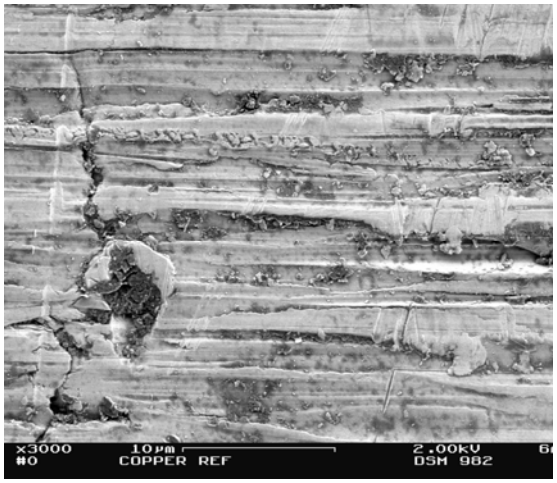

Figure 21A: A SEM micrograph of a copper reference sample.

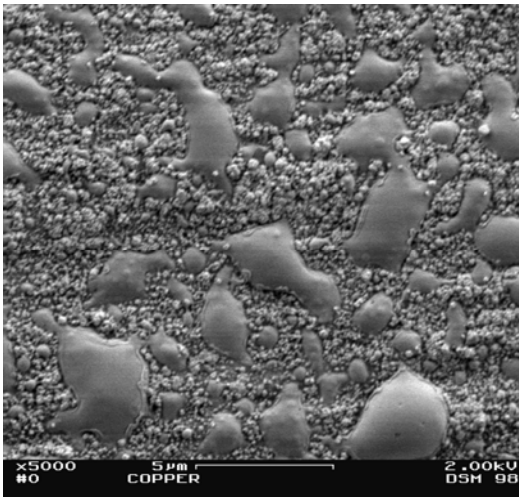

Figure 21B: Iodine oxide particles had reacted on the copper surface and formed crystalline as well as pool like structures.

The elemental map of the crystalline area with the pool-like structures is presented in Figure 22 and in Appendix F2. It can be seen that the iodine is almost uniformly deposited over the whole area. The oxygen seems to be mainly located on the pool-like structures on the surface. These pool like deposits are thick enough to prevent a signal due to the copper surface being observed. In contrast the surfaces of the crystalline areas of the deposit are very rich in both copper and iodine. These results strongly suggest that iodine is present in at least two different chemical forms. Spectra from the EDX spot analysis in this area are presented in Appendix F4. The oxygen to iodine ratio calculated from the spot analysis is presented in Table 6, see Appendixes H1 and H2. It shows that the ratio was close to 3 on the pools and only 0.5 on the crystalline surface. These results are in agreement with the Raman and XPS analysis, which suggested that there would most likely be solid HIO_3 and CuI formed on the surface.

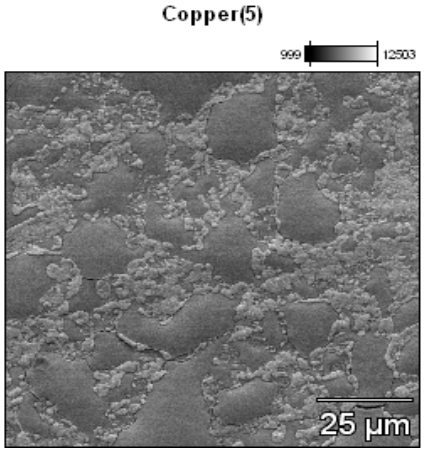

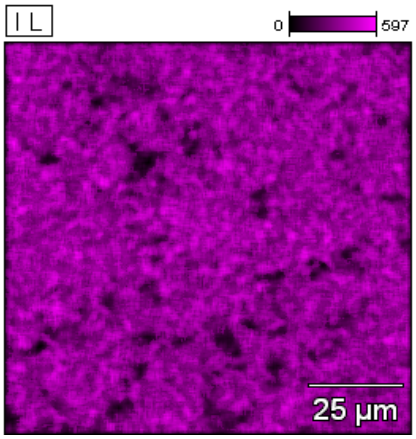

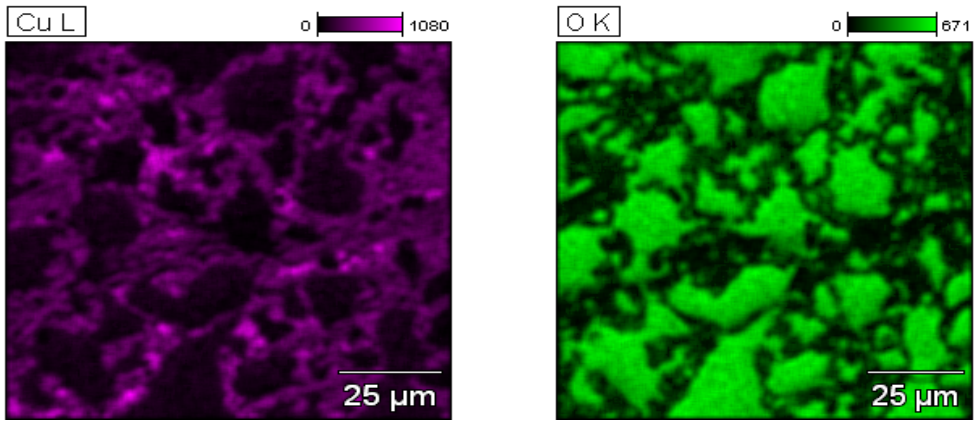

Figure 22: EDX map of iodine deposition on copper sample in the area of crystalline deposit with pool-like structures.

An EDX map of the iodine deposition on a copper surface in an area with a thick, uniform deposit with grain-like structures is presented in Appendix F3. In this area iodine, oxygen and copper seems to be rather evenly distributed all over the analysed area. Spectra from the EDX spot analysis as well as the locations of the analysed spots are presented in Figure 23. Spectra from another EDX spot analysis taken from the area with a seemingly uniform deposit are presented in Appendix F5. On four spots the oxygen to iodine ratio varied between 2.0 and 2.3. One location seemed to be enriched with iodine as the ratio was only 0.7. According to the EDX spot analysis, copper seems to have reacted and mixed with the iodine oxide particle layer. The earlier finding that the deposit would be a mixture of solid HIO_3 and CuI cannot be excluded.

Table 6: The oxygen to iodine ratios measured with SEM-EDX spot analysis of a deposit on a copper surface.

Reference	O:I ratio	Deposit description
F4 Spot 1	2.92	Pool like feature
F4 Spot 2	0.50	On crystalline deposit
Fig. 21 Spot 1	0.69	On grain-like deposit
Fig. 21 Spot 2	2.00	On grain-like deposit
Fig. 21 Spot 3	2.35	On grain-like deposit
F5 Spot 1	2.07	On grain-like deposit
F5 Spot 2	2.22	On grain-like deposit

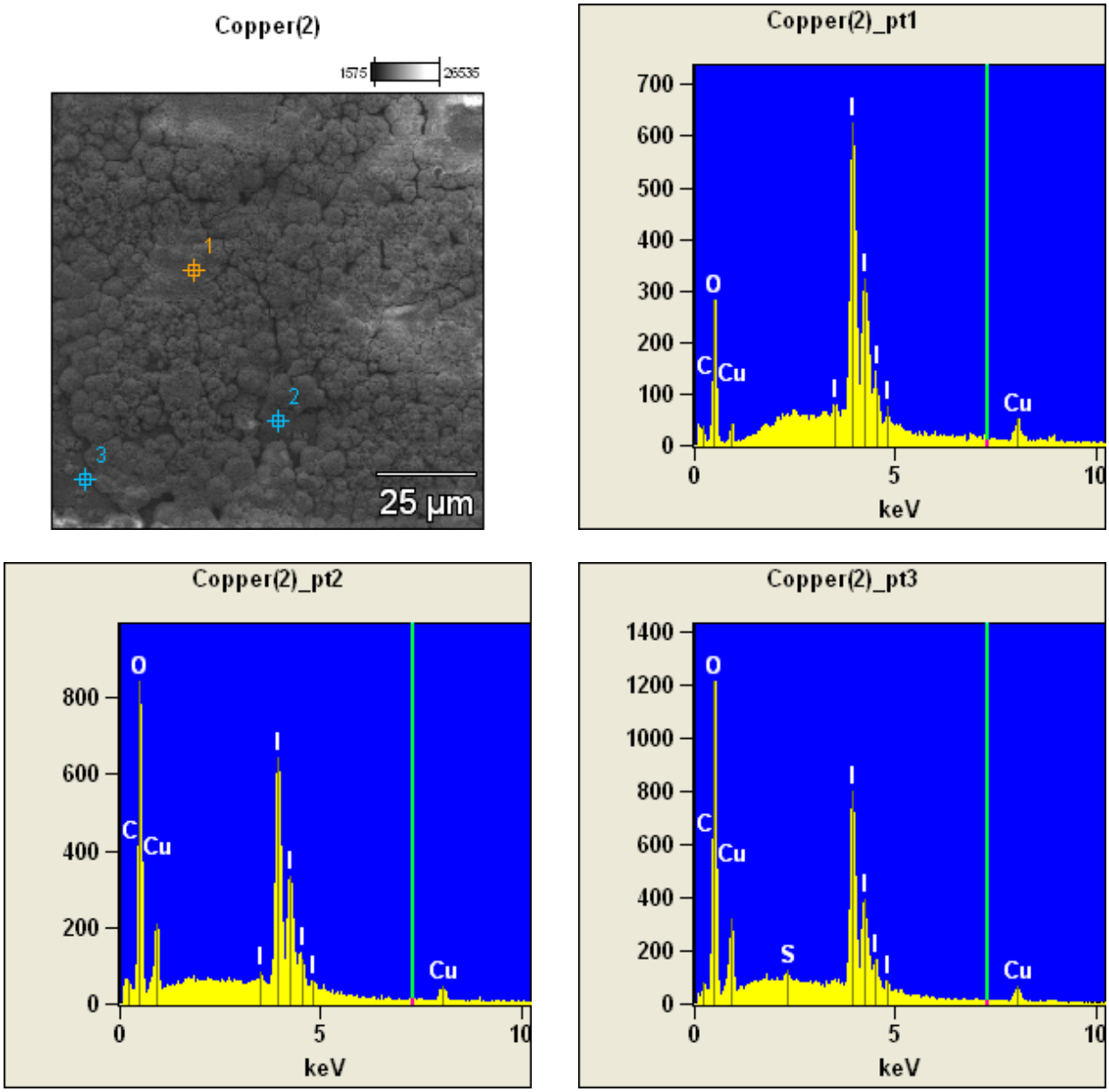

Figure 23: A SEM micrograph of the deposit on a copper surface is presented in a grey field image (top left). Other images present the EDX spectra obtained from the three spot analysis marked in the SEM image.

5.4.4 SEM-EDX analysis of an aluminium surface exposed to iodine oxide

An SEM micrograph of an aluminium reference sample and Iodine oxide deposit on an aluminium surface are presented in Figures 24A and 24B. Further SEM micrographs of the copper sample are presented in Appendix G1. Also in the case of aluminium samples the structure of the deposit seemed to have changed during storage. The crystals on the deposition sample had cubic and leaf-like shapes.

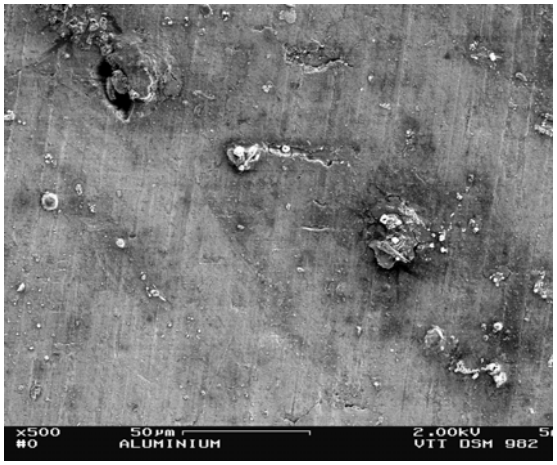

Figure 24A: A SEM micrograph of the aluminium reference sample revealed some impurities on the surface.

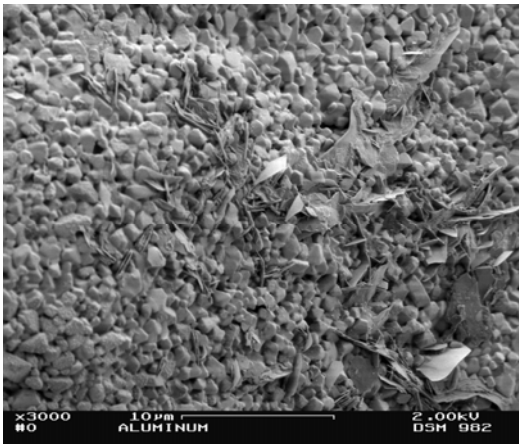

Figure 24B: The deposited iodine oxide particles had formed cubic like and leaf like crystals during storage.

The elemental map of the iodine oxide deposit area is presented in Figure 25 as well as in Appendixes G2 and G3. Evidently, iodine and oxygen are very highly correlated in the maps. The iodine oxide deposit seemed to have spread along the grooves on the aluminium surface. Aluminium is only visible on areas of the surface without any particle deposition. This suggests that aluminium had not reacted with the iodine oxide deposit. Silicon, carbon and magnesium are visible as impurities on the sample. Spectra from the EDX spot analysis in the centre and on the edge of the deposition area are presented in Figure 26 and in Appendix G4. The oxygen to iodine ratios calculated from the spot analysis are presented in Table 7, see Appendixes H1 and H2. It shows that the ratio was about 2.2 in the centre and about 3.6 on the edge.

Based on the EDX results, it is not possible to determine the chemical form of the deposit. However, the iodine oxide ratio in the centre is very close to the values measured for the deposit on the painted surface. On paint the deposit had not reacted with the surface and the chemical species suggested by Raman was partially hydrated $I_2O_5 \bullet HIO_3$ ($=HI_3O_8$) with some elemental iodine. Later performed experiments with ^{131}I labelled deposits confirmed the assumption that ^{131}I from the iodine oxide can move into the paint film and can react with paint ingredients. No chemical reaction products of iodine with the surface material were detected on the aluminium surface.

The oxygen to iodine ratio seemed to be much higher within the grooves, where the deposit had spread on the surface. The same effect was observed at the grain boundaries on the steel surface. The deposit spread on the surface may be in the form of HIO_3. It is important to bear in mind that the reaction of elemental iodine with aluminium metal is catalysed by water.

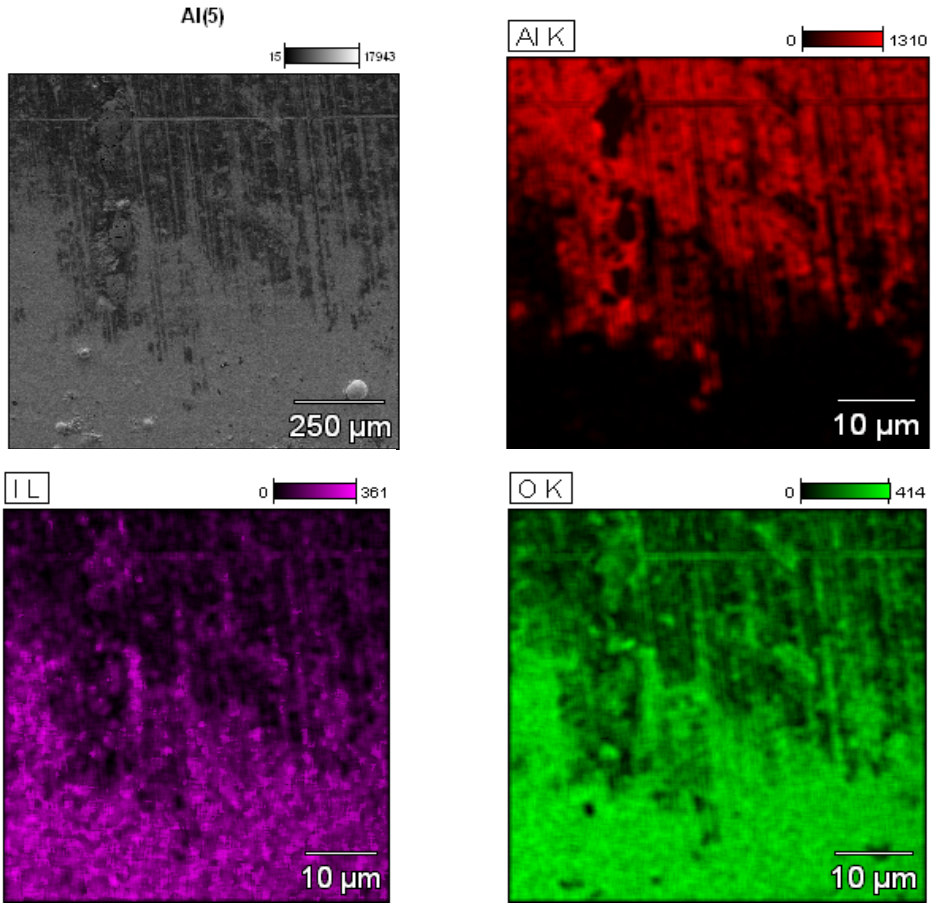

Figure 25: EDX map of the iodine oxide deposit on an aluminium surface close to the edge of the deposition area.

Table 7: The oxygen to iodine ratios measured with SEM-EDX spot analysis in the iodine oxide deposit on an aluminium sample.

Reference	O:I ratio	Deposit description
Fig. 24 Spot 1	2.1	Crystalline deposit at the centre
Fig. 24 Spot 3	2.2	Crystalline deposit at the centre
G4 Spot 2	3.6	Deposit on the edge

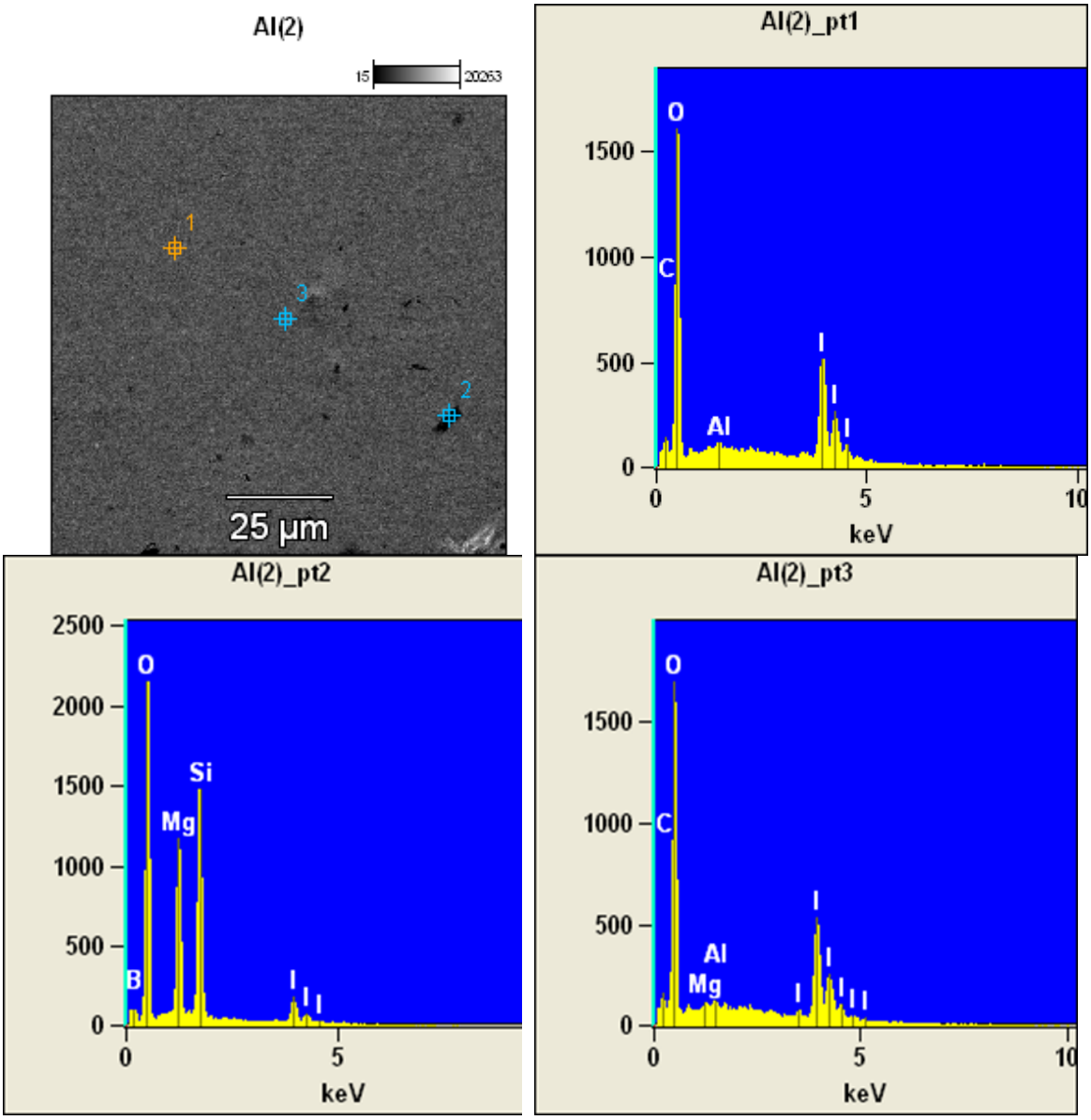

Figure 26: A SEM micrograph of a deposit on an aluminium sample is presented in a grey field image (top left). Other images present the EDX spectra obtained from the three spot analysis marked in the SEM image.

5.5 Examination of the iodine oxide deposits by radiochemical means

The iodine oxide aerosol deposits were originally a white colour and not in the form of a mono-layer (visible by eye). Humidity in the air caused the outer layer to change colour towards brown. This might be due to the formation of elemental iodine (see Figure 27).

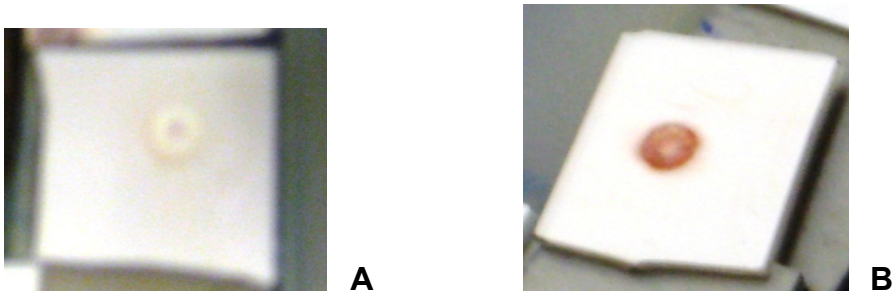

Figure 27: Teknopox Aqua V A paint sample A) immediately after opening the exposure chamber B) After *approx.* 1 min exposure to air

On the metal substrates, the oxidation process was slower for Cu, SS, Pt and Pd (see Figure 28 and Figure 29). Only the outer ring darkened and heating and irradiation caused the deposit to stay white while the deposits on Al and Zn were dark all the time (see Figure 28 and Figure 29).

Figure 28: SS, Pt and Pd samples exposed to gamma irradiation

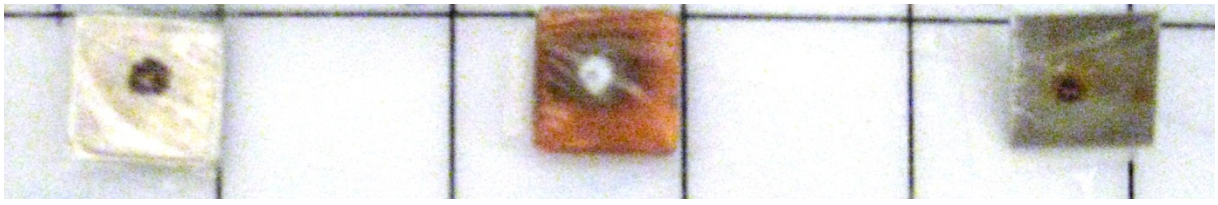

Figure 29: Al, Cu and Zn samples exposed to gamma irradiation

The application method of the particles was supposed to be at a single point. Autoradiography was used to determine how far the activity migrates on the surface of the samples.

For the stored samples, the majority of the activity was at the point where it was applied, most probably mainly still in form of the iodine oxide aerosols. Since the samples had been exposed *approx.* 1 week before the measurement it can be argued that the radioactive iodine

was not able to migrate from one point on the surface to another under the conditions of storage (see Figure 30 and Figure 31).

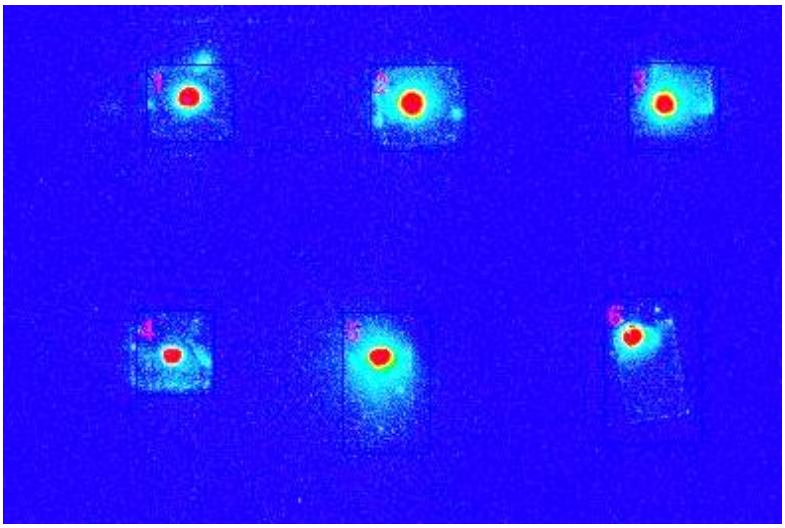

Figure 30: Autoradiography of the metal samples exposed to iodine oxide aerosol. Top row (left to right), copper, aluminium and zinc. Bottom row (left to right) stainless steel, platinum and palladium. (1 Cu, 2 Al, 3 Zn, 4 SS, 5 Pt, 6 Pd)

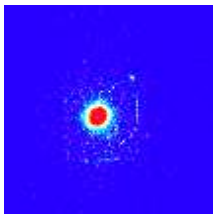

Figure 31: Autoradiography of a paint sample exposed to iodine oxide aerosols

Samples were treated with hot humid air, heat, and later irradiation. Humid air caused the radioactive iodine to escape from the solid deposit and spread downwards (see Figure 32 and Figure 33). The ^{131}I was liberated and was distributed between the gas phase and the aqueous phase of the simulated containment. The paint samples retained a higher percentage of the activity; this is thought to be due to chemical reactions of the paint with the iodine. The paint remained brown in colour. The paint retained its radioactivity even after washing in water and sodium thiosulfate solution (see Figure 34).

Figure 32: Pt sample exposed to hot, humid air (FOMICAG, 250 °C)

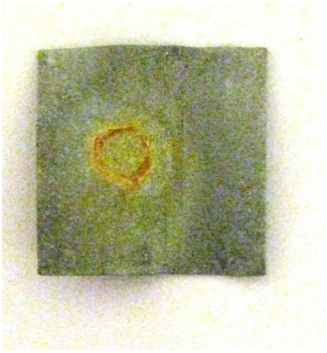

Figure 33: Zn sample after exposure to hot, humid air (FOMICAG, 250 °C)

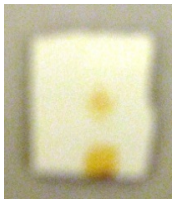

Figure 34: Paint sample after exposure to humid air in the FOMICAG facility (250 °C)

The desorption of the aerosols from the metal substrates was not accompanied with a large amount of migration over the surface or readsorption. The spot size remained constant (see Figure 35).

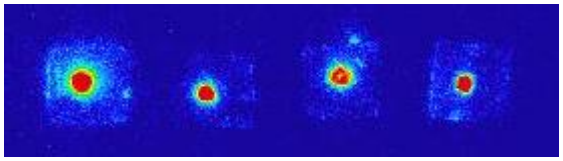

Figure 35: Distribution of ^{131}I on metal substrates after 3360 kGy gamma radiation exposure

In contrast the spot size increased when the paint samples where heated, this can be explained by migration of the radioactive iodine from one part of the paint to another (see Figure 36).

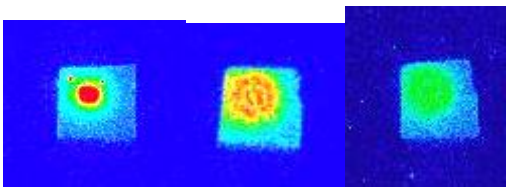

Figure 36: Paint sample after exposure to 150 °C after 1h, 24 h and 10 days

A visual examination of the paint sample (see Figure 37) showed that heat and irradiation changed the colour of the paint. The original deposit was still visible after 10 days and the spread of activity was accompanied by a colour change. It is noteworthy that a paint sample which has not had iodine oxide particles deposited on it changes colour evenly when it is subject to either irradiation or heating.

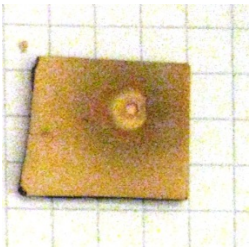

Figure 37: Heat and irradiation treated paint sample exposed to iodine oxide

5.6 Revaporisation of iodine oxide aerosols from different surfaces at room temperature (RT)

Tests on the stability of the iodine oxide aerosols under the storage conditions showed that the outer layers of the thick deposit of iodine oxide released ^{131}I (see Table 8 and Table 9) from all surface materials. The revaporisation occurred on the upper layer of the deposit and not in the form of organic iodines from the paint surfaces, since the release rates from all paint samples are approximately the same (see Table 9). Aging caused by heat and irradiation would reduce the number of functional groups in the paint to react with iodine and thus would lead to a reduced sorption of ^{131}I.

Table 8: Revaporisation at RT from metal surfaces

	Remaining ^{131}I [%]					
t [h]	**Pt**	**Pd**	**Cu**	**Al**	**Zn**	**SS**
0	100.0	100.0	100.0	100.0	100.0	100.0
24	76.1	86.4	79.8	81.9	89.0	-
48	66.4	-	-	-	-	-
72	43.3	-	-	-	-	-

Table 9: Revaporisation at RT from painted surfaces

	Remaining ^{131}I [%]					
t [h]	**non-treated**	**1008 kGy**	**3024 kGy**	**336 kGy**	**18 month cured**	**2 a, 100 °C**
0	100.0	100.0	100.0	100.0	100.0	100.0
24	87.6	89.3	88.1	87.4	88.5	89.9
48	79.5	-	80.7	81.7	79.0	-
72	72.4	-	0.0	77.6	-	-

5.7 Temperature effect on the revaporisation of ^{131}I from iodine oxide aerosol deposits

The effect of gamma irradiation of the metal and paint samples in the desorption of iodine has been investigated by exposing them to gamma rays. However due to the decay heat of the cobalt-60 used in the irradiation system the samples were also heated to 50 °C during the irradiations. To allow the effect of the radiation to be understood the effect of heating to 50 °C was first investigated. Figure 38 and Table 10 shows the loss of ^{131}I over 33 h heating at 50 °C from metal surfaces. Figure 39 and Table 11 shows how much of the released activity was in the form of elemental iodine.

Table 10: Revaporisation of ^{131}I at RT from metal surfaces

	% ^{131}I revaporised					
t [h]	**Al**	**Cu**	**Zn**	**Pd**	**Pt**	**SS**
0	0.0	0.0	0.0	0.0	0.0	0.0
0.25	7.8	10.8	2.5	10.0	28.9	26.8
0.5	14.6	21.5	9.9	19.7	36.7	32.2
1	19.9	27.6	16.4	37.7	47.9	37.5
3	23.8	30.9	18.3	45.9	58.5	40.7
6	28.5	40.6	23.7	66.6	75.9	44.3
24	35.6	44.5	35.4	78.2	78.2	56.6
33	40.5	46.5	36.9	81.5	85.7	57.7

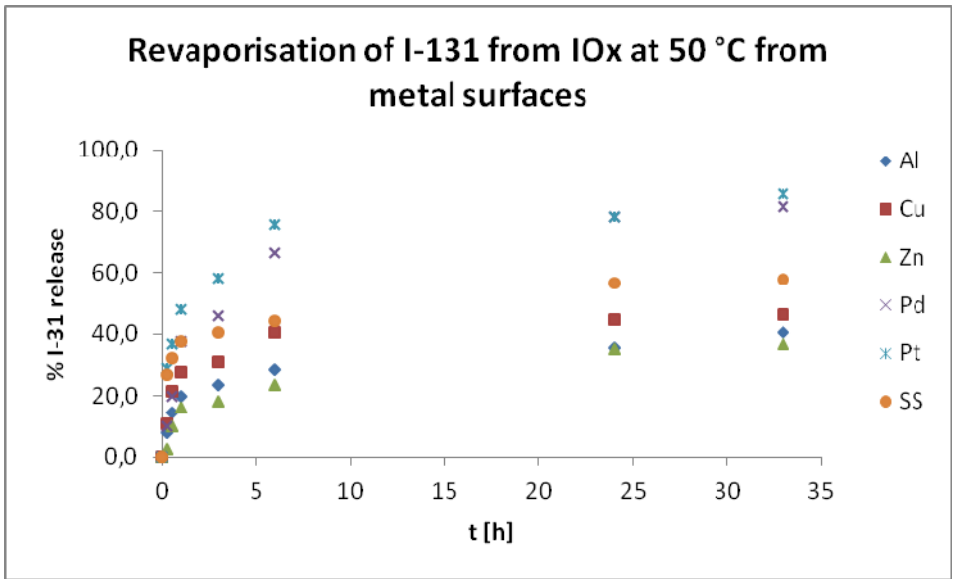

Figure 38: Revaporisation of ^{131}I from metal surfaces exposed to iodine oxide at 50 °C

Table 11: Revaporisation at RT from metal surfaces in the form of elemental iodine

	% I_2 revaporised					
t [h]	**Al**	**Cu**	**Zn**	**Pd**	**Pt**	**SS**
0	0.1	0.1	0.1	0.1	0.1	0.4
0.25	0.1	0.1	0.2	0.1	0.1	0.5
0.5	0.2	0.1	0.3	0.2	0.2	0.6
1	0.3	0.2	0.4	0.2	0.4	0.6
3	0.3	0.2	0.6	0.3	0.5	0.6
6	0.4	0.3	0.7	0.4	0.5	0.6
24	0.4	0.4	0.9	0.5	0.6	0.7
33	0.4	0.5	0.9	0.6	0.7	0.7

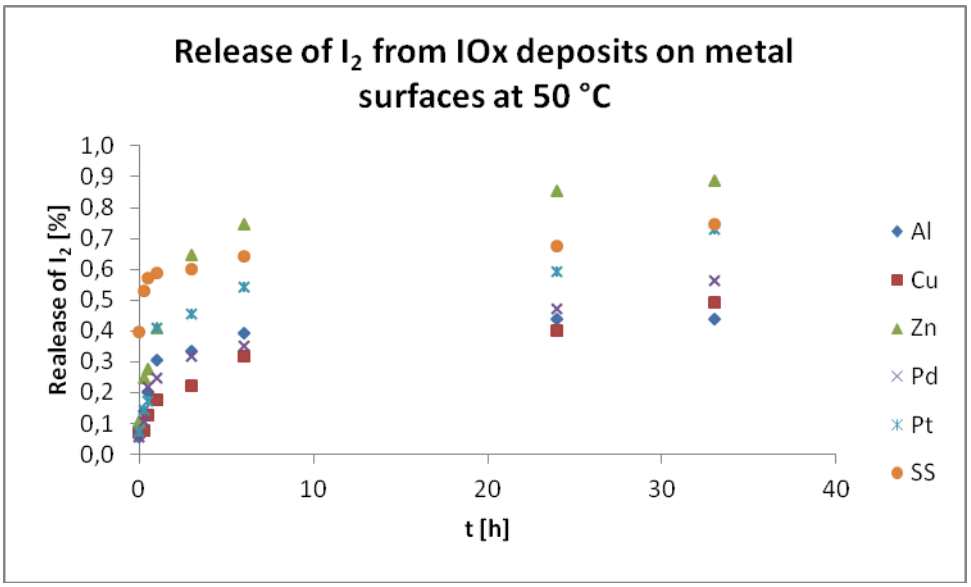

Figure 39: Release of ^{131}I in form of I_2 from IODINE OXIDE aerosols on metal surfaces

Against our expectations the majority of the released activity was not in the form of elemental iodine. The deposited aerosol layer was rather thick which could be the reason why large amounts of ^{131}I were re-released within a short time when the samples are exposed to normal air. The highest loss occurred from the Pd and Pt samples.

The release from painted samples was significantly lower (see Table 12). It showed that the revaporisation from aged samples was higher than from a fresh, non-aged painted surface. The release loss was significantly higher from a sample heated to 100 °C for 2 years than from a fresh one and was similar to the effect of a pre-irradiation damaged paint exposed to 3024 kGy gamma irradiation. This supports the assumption that most iodine binds to the paint solvents in the paint. Most solvents have a higher boiling point than 50 °C and will be evaporated below 300 °C. Gamma irradiation is assumed to break C-C- bonds leading to the loss of functional groups reactive to iodine. The majority of the released species is assumed to be in the form of iodine oxide. The amount of released elemental iodine is still rather low but higher than from the metal surfaces. The oxidation to elemental iodine is higher on the painted surfaces.

Table 12: Iodine oxide revaporisation from painted surfaces at 50 °C

	Iodine oxide revaporisation [%]					
t [h]	non-treated	18m cured	2 a/100 °C	336 kGy	1008 kGy	3024 kGy
0	0	0	0	0	0	0
0.5	3.9	5.7	13.3	17.1	21.1	10.9
1	4.3	6.2	23.7	18.9	21.2	15.6
3	7.8	16.2	38.0	20.8	23.8	20.3
6	10.5	19.8	40.6	25.2	26.6	24.8
18	16.2	22.2	44.5	30.2	32.9	35.1
30	17.3	27.6	49.9	37.5	38.2	45.3

Table 13: I_2 revaporisation from painted surfaces at 50 °C

	I_2 revaporisation [%]					
t [h]	non-treated	18m cured	2 a/100 °C	336 kGy	1008 kGy	3024 kGy
0	0	0	0	0	0	0
0.5	0.85	1.82	3.86	3.27	0.62	1.29
1	0.94	1.77	3.55	3.00	0.66	1.30
3	0.94	1.84	4.31	3.27	0.67	1.93
6	1.15	1.99	4.55	3.39	0.69	2.24
18	1.30	2.59	4.81	3.90	0.77	2.42
30	1.34	2.02	4.84	3.50	1.67	2.75

5.8 Revaporisation of iodine oxide aerosols from painted surfaces at 150 °C

Paint samples were heated to 150 °C to study the revaporisation of iodine at the expected average containment temperature during a severe nuclear accident in a BWR which is experienced before venting of the containment is initiated.

A non-irradiated paint was compared to a 336 kGy and 3024 kGy pre-irradiated paint (see Figure 40). A paint sample damaged by irradiation released more ^{131}I than a fresh, non-irradiated one. The reason could be that after heating a smaller amount of small organic molecules which can react with the iodine are present in the paint. The majority of ^{131}I release occurred within the first 50 h, followed by a slower release rate until 100 h and a significant lower release rate afterwards. It is thought that later in the release experiment, the iodine species which migrated into deeper layers of the paint film (total thickness 100 µm) were released.

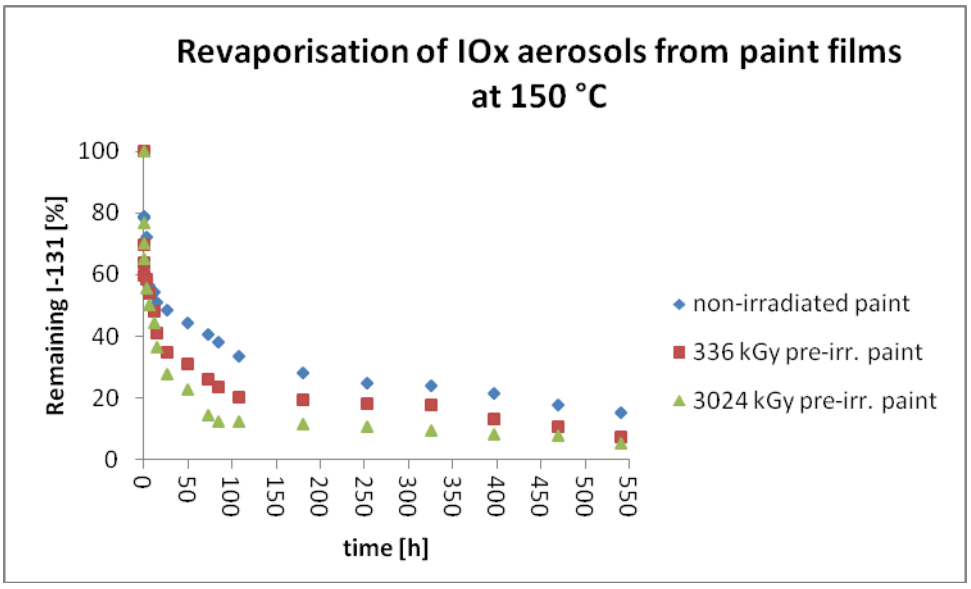

Figure 40: Release of ^{131}I from iodine oxide exposed paint films at 150 °C

The fraction of the iodine released as elemental iodine was rather low (see Figure 41). Most of the physisorbed iodine oxide aerosol is assumed to be released in its original form and not to be reduced into elemental iodine. The slope of the non-irradiated paint curve is not constant (see Figure 40) indicating that a migration or chemical conversion of ^{131}I in the paint film occurs.

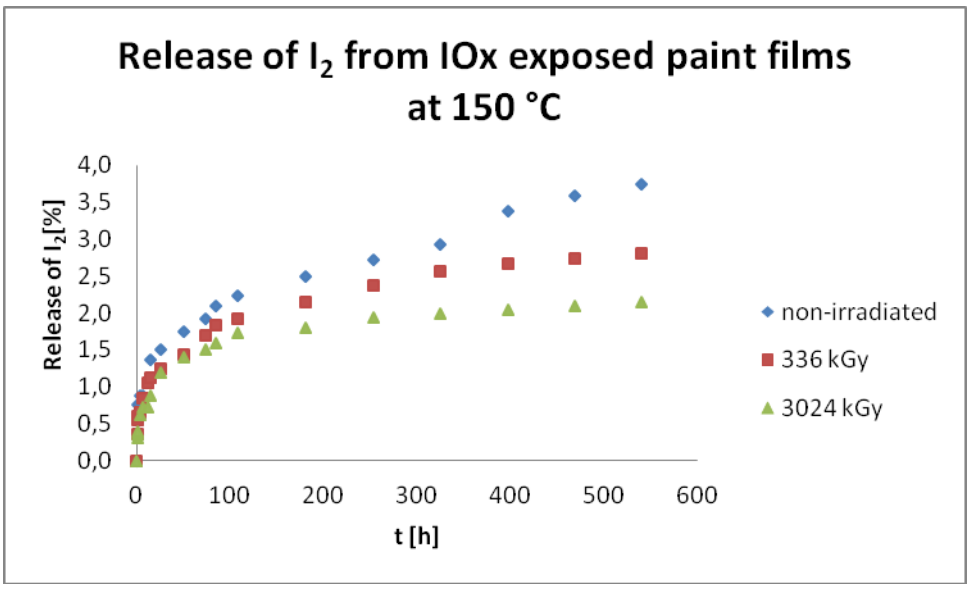

Figure 41: Release of ^{131}I in form of elemental iodine from paint films at 150 °C

5.9 Revaporisation studies of iodine oxide aerosols under the influence of gamma irradiation

The iodine deposits on the metal surfaces (Al, Cu, Zn and SS) which were irradiated with a γ-dose rate of 14 kGy/h all exhibited similar revaporisation behaviour (see Figure 42).

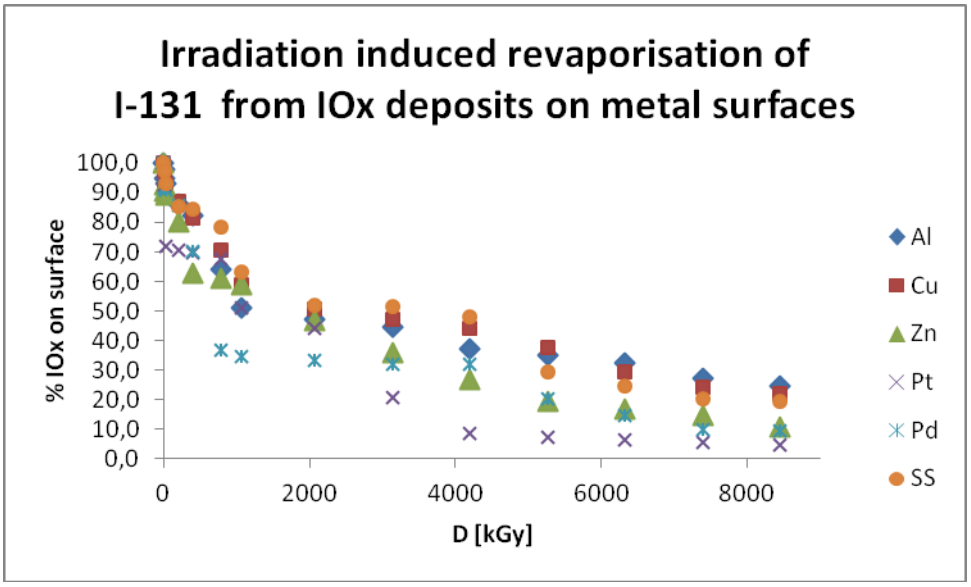

Figure 42: Revaporisation rate of ^{131}I from iodine oxide deposits under γ-irradiation (14 kGy/h; 50 °C)

Zn, Pt and Pd lost more of the ^{131}I activity on the surface suggesting mainly weaker adsorption phenomena on these metals (see Table 15).

Table 15: Revaporisation of iodine oxide aerosols from metal surfaces induced by γ – radiation (50 °C)

	Iodine oxide on surface [%]					
D [kGy]	**Al**	**Cu**	**Zn**	**Pt**	**Pd**	**SS**
0	100.0	100.0	100.0	100.0	100.0	100.0
0.7	98.0	95.1	92.6	92.6	91.7	97.7
7	95.0	93.7	90.5	92.5	91.2	97.7
35	93.0	92.6	89.5	72.0	90.8	93.3
203	86.4	87.1	80.1	70.4	85.7	85.4
392	82.5	81.3	62.7	69.9	70.3	84.4
784	63.9	70.4	60.9	67.7	36.9	78.5
1064	51.0	58.9	58.8	51.3	34.6	63.4
2072	47.3	50.7	46.7	44.3	33.2	52.1
3136	44.3	47.1	36.0	20.6	31.8	51.4
4200	37.3	44.0	26.6	8.4	31.8	48.0
5264	35.2	37.5	19.5	7.0	20.0	29.5
6328	32.3	29.3	16.7	6.4	14.6	24.6
7392	27.3	24.2	14.8	5.3	9.7	20.4
8456	24.4	21.9	10.9	4.7	9.3	19.3

Paint samples of the epoxy paint Teknopox Aqua V A aged under different conditions have been irradiated with a dose rate of 14 kGy/h (see Table 16). After a dose of *approx.* 300 - 600 kGy most of the loosely bond ^{131}I has been released since *approx.* 50 % of the total ^{131}I was released (see Figure 43). After an achieved dose of *approx.* 100 kGy the release rate

went down slightly. The paint started to dry out, turned brown and got brittle indicating significant damage to the paint. The heat treated sample had the highest revaporisation, as well as the most irradiation damaged paint (see Figure 43) indicating that pre-heating caused release of the paint solvents and pre-irradiation maybe the breakdown of the functional groups.

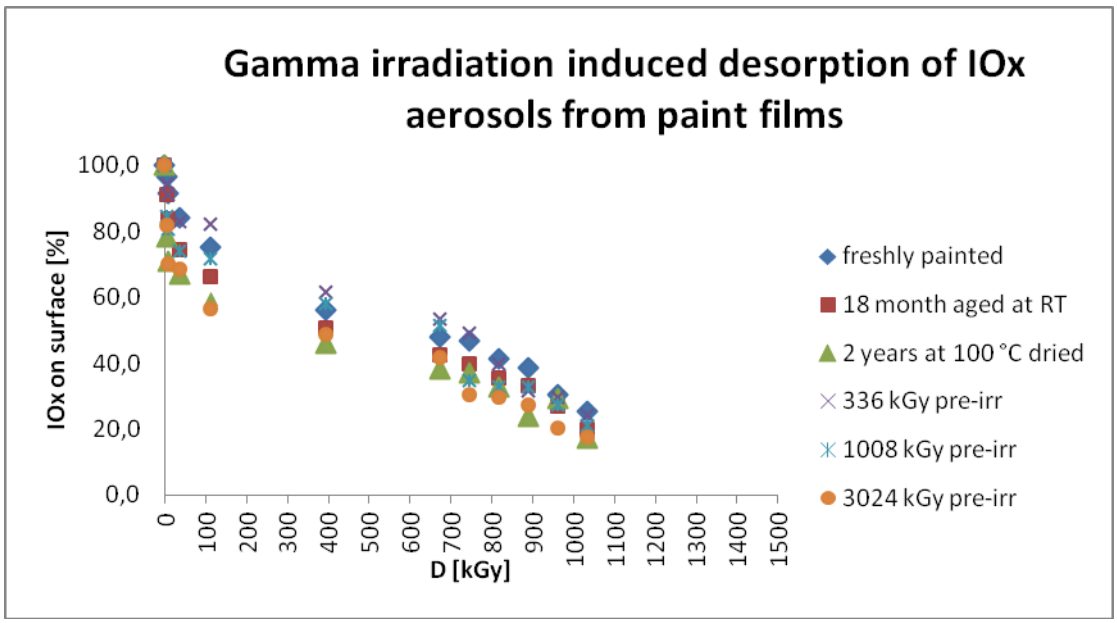

Figure 43: γ – irradiation induced revaporisation of ^{131}I from painted surfaces

Table 16: γ – irradiation induced revaporisation of ^{131}I deposited as iodine oxide particles (50 °C) from painted surfaces

		Gamma irradiation induced I-131 release				
D [kGy]	freshly painted	18 month aged at RT	2 years at 100 °C dried	336 kGy pre-irr	1008 kGy pre-irr	3024 kGy pre-irr
0	100,0	100,0	100,0	100,0	100,0	100,0
3,5	96,6	91,2	78,1	94,1	84,5	81,8
7	91,4	83,6	70,8	91,1	80,7	70,3
35	84,3	74,6	67,0	83,1	74,0	68,5
112	75,1	66,1	59,5	82,2	71,6	56,7
392	56,2	50,8	46,0	61,4	58,1	48,9
672	47,8	42,6	38,3	53,3	51,4	41,9
744	46,7	39,8	37,0	49,1	34,7	30,5
816	41,2	35,5	32,6	39,6	32,6	29,5
888	38,7	33,1	23,9	31,7	32,6	27,2
960	30,5	27,1	29,3	29,7	27,2	20,2
1032	25,2	20,1	17,0	24,3	21,2	17,7

5.10 Revaporisation studies of iodine oxide aerosols from water covered surfaces

Paint and metal samples exposed to the aerosol particles had been immersed in distilled water and the leaching behaviour was studied. *Approx.* 65 % of the ^{131}I activity remained on the copper surface after it had been leached in double distilled water at room temperature

and 58 % remained after heating the aqueous phase to 70 °C. On fresh paint immersed in a water surface, *approx.* 10 % of the activity remained at room temperature and 2 % less after 24 h heating of the sample in a 150 °C thermostated aluminium block. All activity was washed off from SS and Al samples which were heated in contact with water suggesting that the surfaces of these metals did not undergo any chemical reaction with the iodine oxide deposit.

Paint samples undergo chemical reactions with the iodine oxide particles since a yellow/brownish mark remained after washing, heating and irradiation. ^{131}I from the solid deposit moved inside the paint film which can be seen on the sample which was exposed to heat and humidity in the FOMICAG facility (see Figure 31).

5.11 Revaporisation studies of iodine oxide aerosols in contact with humid air (FOMICAG)

Samples were placed in the gas phase part of the FOMICAG facility. The gas phase temperature was increased from room temperature to 250 °C. After exposing the samples for 4-5 days to these conditions all the samples lost the majority of their ^{131}I activity. In the table below the percentage of the iodine which remained on the samples is tabulated.

Table 17: Remaining amount of ^{131}I on hot, humid air exposed sample surfaces

Surface	% ^{131}I
Al	2.3
Cu	6.9
Zn	4.1
SS	0.5
Pt	0.2
Pd	1.9
paint	20.3

The paint films retained most of the activity due to chemisorption while from the SS, Pt and Pd surfaces the deposit washed off easily and at temperatures below 100 °C. The released iodine species were distributed between the gas phase and the water phase.

6 Conclusions

The interactions of iodine oxide aerosols on the surfaces of a LWR NPP containment during a severe accident is poorly documented in the literature. Particles deposited on various surfaces may act as a source of volatile iodine, which may be released back into the containment atmosphere and contribute to the volatile iodine source term. The focus of the study was the examination of the properties of iodine oxide particles on various surfaces and the revaporisation behaviour of these particles under severe accident conditions. Iodine oxide particles were deposited on Teknopox Aqua V A paint films of different aged state and metal surfaces such as stainless steel, copper, aluminium, zinc, palladium and platinum.

It is likely that the iodine oxide particles produced by the reaction of ozone and gaseous elemental iodine, were mainly in the chemical forms of I_2O_4 and I_4O_9 when the reaction temperature was below 100°C. This conclusion is supported by the yellow colour of the particles on the filter sample. The particles for deposition on the surface materials were synthesized at 120°C. At this temperature, the formation of I_2O_5 is more likely especially as both other oxides decompose to I_2O_5. The deposit on the samples also had a lighter colour than those collected on a filter sample. When I_2O_4 and I_4O_9 particles react with humidity they form HIO_3 and I_2. After exposure to humid air, I_2O_5 is rapidly converted to its partially hydrated form $I_2O_5 \bullet HIO_3$, also defined as HI_3O_8. On the other hand, the same product is formed when HIO_3 is partially dehydrated. The observed decomposition reaction was faster than reported in the literature and is assumed to be caused by a smaller diameter of the iodine oxide particles.

With Raman and XPS analysis no chemical reactions of iodine oxides with the stainless steel surface and painted surfaces could be identified. According to the recorded Raman spectra the form of iodine seemed to be partially hydrated $I_2O_5 \bullet HIO_3$ on steel and painted surfaces. In addition, both Raman and XPS analysis found molecular iodine (I_2), which is likely to be formed due to decomposition of I_2O_4 and I_4O_9 particles on the surfaces. According to the recorded SEM micrographs, the deposited iodine oxides seemed to be dissolved in the centre and crystalline at the edge of the painted sample. On the steel sample the deposit appeared crystalline. The diameter of crystals was larger than the diameter of the deposited particles. On the steel sample the iodine was also spread along the grain boundaries. According to the EDX analysis, the oxygen to iodine ratio was higher on the grain boundaries than on the crystalline deposit. The form of iodine detected might be HIO_3. The iodine deposit on the aluminium surface was only studied with SEM-EDX. The deposit seemed to be very similar to that on the steel surface. There was no obvious reaction with the aluminium surface detectable. Also in this case iodine seemed to have spread along the grooves on the aluminium surface. The oxygen to iodine ratio was again higher on the grooves than on the crystalline deposit.

On copper and zinc samples the peaks of solid HIO_3 and molecular iodine were detected in the Raman spectra. The results of the XPS analyses also suggested reactions between the Iodine oxide deposit and the surface on both samples. The probable reaction products could be CuI and ZnI_2. The reaction seemed to be more extensive on the zinc surface, for which no chemical form of iodine could be identified with XPS. The differences between the Raman and XPS results may be caused by the fact that the signal for XPS comes from a layer that is only a few nanometres deeper than the surface. The SEM-EDX analysis of the copper sample suggested that, when the deposit layer was thin, areas with CuI crystals were mixed with areas with HIO_3 formation. As the deposit layers became thicker these two compounds seem to have formed a rather homogeneous grain-like structure.

The main parameters relevant for the revaporisation of an iodine species from iodine oxide deposits during a severe nuclear accident in a light water reactor are: heat, humidity and gamma irradiation exposure. Humidity was shown to be the major factor for the revaporisation of the outer layers of multi-layer deposits.

Metal samples tend to form weaker bonds with the aerosol compounds than epoxy paint surfaces. Paint films both physisorbs the aerosol but its organic ingredients can undergo chemical reactions with the iodine of the particles as well. The paint film is a 100 µm thick matrix where additional mass transfer of iodine species inside the film occurs and affects the iodine chemistry. The absorbed species are likely to either migrate in its original chemical form into the paint or in chemical converted forms when reacting with the paint ingredients. Pre-irradiation and pre-heat treatment was shown to have an effect on the ability of the paint to chemisorb iodine. It is assumed that the paint solvents which are reactive towards iodine were revaporised during 2 years of heating at 100 °C. Irradiation can cause cleavage of chemical bonds in organic substances and thus alter the functional groups.

The aerosols deposited on Pt and Pd were easily revaporised by humidity, low heat and a low gamma dose. Thus it can be expected that the functionality of the hydrogen recombiners will not be affected by these aerosols.

It is rather unlikely that metal surfaces and painted surfaces can function as a relevant iodine sink for the studied iodine oxide aerosols during a severe accident since the aerosols already revaporised at room temperature, under dry non-irradiation conditions.

Steam or containment sprays are likely to wash off the iodine oxide deposits on most of the studied materials or even prevent the sorption on the containment surface materials in a severe accident scenario when the particles are in contact with humidity before sorption can occur.

References

[1] A.C. Vikis, R. Macfarlane, Reaction of iodine with ozone in the gas phase, J. Phys. Chem. 89 (1985) 812-815

[2] B. Clément, L. Cantrel, G. Ducros, F. Funke, L. Herranz, A. Rydl, G. Weber, C. Wren, State of the Art Report on Iodine Chemistry, NEA/CSNI/R(2007)1, 2007.

[3] T. Kärkelä, J. Holm, A. Auvinen, C. Ekberg, H. Glänneskog, U. Tapper, R. Zilliacus, Gas phase oxidation of elemental iodine in containment conditions, 17th International Conference on Nuclear Engineering, ICONE17. Brussels, 12 - 16 July 2009. ASME. Vol. 2 (2009), 719 – 727

[4] D. R. Lide, CRC Handbook of Chemistry and Physics, 86th edition, CRC Press, Boca Raton (FL), 2005.

[5] M. W. Chase, NIST-JANAF thermochemical tables for the iodine oxides, Journal of Physical and Chemical Reference Data, 25(5), 1297–1340, 1996.

[6] T. Kärkelä, J. Holm, A. Auvinen, R. Zilliacus, U. Tapper, Experimental study on iodine chemistry (EXSI) – Containment experiments with elemental iodine, VTT-R-00717-09, 2009.

[7] S. Sunder, J. C. Wren and A. C. Vikis, Raman Spectra of I_4O_9 Formed by the Reaction of Iodine with Ozone, Journal of Raman Spectroscopy, 16, 6, 424-426, 1985

[8] J. Bronić, L. Sekovanić, A. Mužic, T. Biljan, J. Kontrec and B. Subotić**,** Host-Guest Interaction of Iodine with Zeolite A, Acta Chim. Slov., 53, 166–171, 2006.

[9] J. Chastain, R. C. King Jr (Eds.), Handbook of X-ray Photoelectron Spectroscopy, Physical Electronics, Eden Prairie 1995.

[10] O. H. Ellestad, T. Woldbäck, A. Kjekshus, P. Kläboe, K. Selte, Infrared and Raman studies of crystalline I_2O_5, $(IO)_2SO_4$, $(IO)_2SeO_4$ and I_2O_4, Acta Chemica Scandinavica 35, 155-164, 1981.

[11] K. Selte, A. Kjekshus, Iodine oxides Part II. On the system H_2O-I_2O_5, Acta Chemica Scandinavica 22, 3309-3320, 1968.

[12] G. Dählie, A. Kjekshus, Iodine oxides, Part I. On $I_2O_3 \cdot SO_3$, $I_2O_3 \cdot 4SO_3 \cdot H_2O$, $I_2O_3 \cdot SeO_3$ and I_2O_4, Acta Chemica Scandinavica 18, 144-156, 1964.

[13] J. R. Durig, O. D. Bonner, W. H. Breazeale, Raman Studies of Iodic Acid and Sodium Iodate, The Journal of Physical Chemistry, 69, 11, 3886-3892, 1966.

[14] S.Tietze, M. Foreman, C. Ekberg, B. van Dongen, Identification of the chemical inventory of different paint film types applied in nuclear facilities, Journal of Nuclear Materials, submitted manuscript 2012.

[15] H. Glänneskog, Y. Albinson, J.O. Liljenzin, G. Skarnemark, Apparatus for on-line measurements of iodine species concentrations in aqueous and gaseous phases, Journal of Nuclear Instruments & Methods in Physics Research, 498, 517-521, 2003.

[16] N. Gao, W-Q. Liu, S-Q. Ma, C. Tang and Z-L. Yan, Journal of Polymer Research,19,

article number 9923, 2012.

[17] N.W. Manthey, F. Cardona and T. Aravinthan, Journal of Applied Polymer Chemistry, 125, E511 to E517, 2012.

[18] L-J. Qian, L-J. Ye, G-Z. Xu, J. Liu and J-Q. Guo, Polymer Degradation and Stability, 2011, 96, 1118-1124.

[19] P.T. Mctigue and D.J. Young, Australian Journal of Chemistry, 18, 1851, 1965.

[20] Y.D. Feikema and A. Vos, Acta Crystallographica, 20, 769-777, 1966.

[21] K. Stahl, and M. Szafranski, Acta Chemica Scandinavica, 46, 1146-1148, 1992 and K. Stahl and M. Szafranski, Acta Crystallographica C, 48, 1571-1574, 1992.

[22] M. Louer, D. Grandjean and D. Weigel, Journal of Solid State Chemistry, 7, 222-228, 1973.

[23] J.A.A. Ketelaar, Zeitschrift fuer Kristallographie, Kristallgeometrie, Kristallphysik, Kristallchemie, 88, 26-34, 1934.

Appendix

Appendix A. The binding energies of IOx deposits at the deposition spot measured with XPS

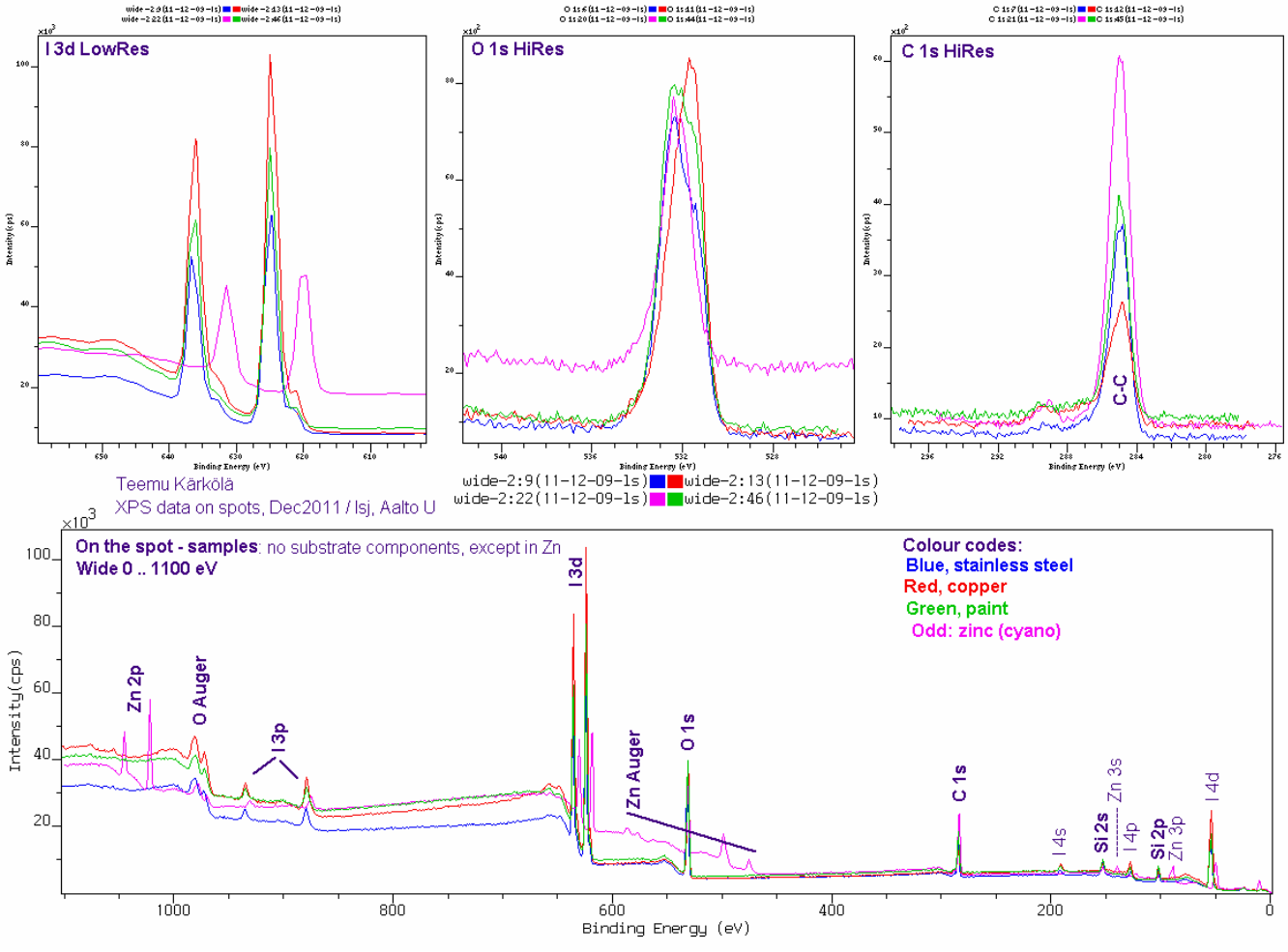

Appendix B. The binding energies of IOx deposits on the edge of the deposition spot measured with XPS.

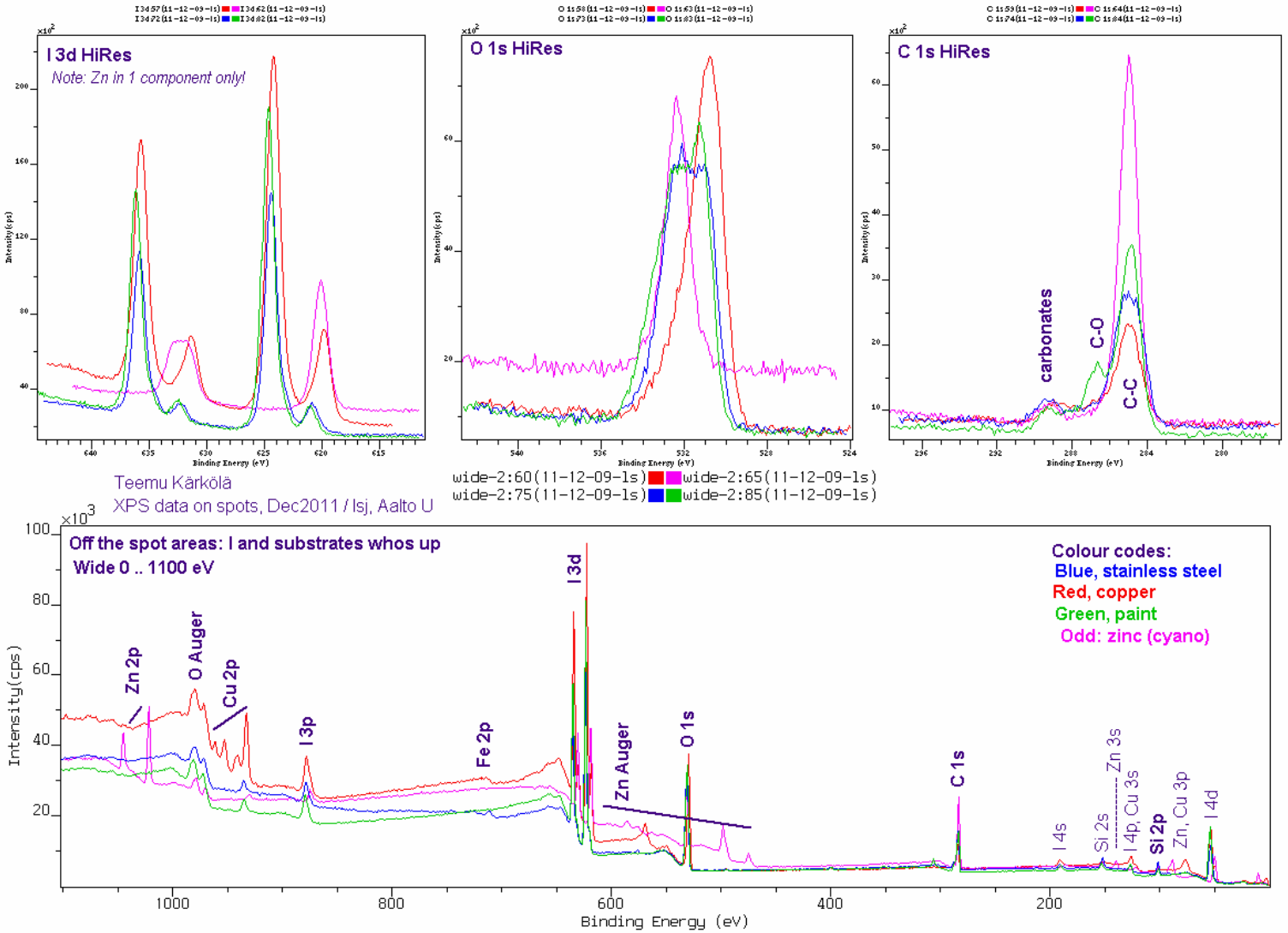

Appendix C. The atomic concentrations of elements on the samples measured with XPS

.

	location	Atomic Concentrations from wides								C 1s HiRes components			
Samples	**#**	**O 1s**	**C 1s**	**I 3d**	**Si 2p**	**N 1s**	**Cr 2p**	**Fe 2p**	**notes**	**C-C**	**C-O**	**C=O**	**COO**
SS	***1 spot***	40.6 %	38.6 %	7.7 %	12.3 %	0.7 %	***0.0 %***	***0.2 %***	No steel in spot	85.7 %	8.5 %	2.4 %	3.4 %
	2 off spot	47.6 %	33.0 %	14.8 %	1.1 %	1.9 %	0.6 %	1.0 %	Iodine everywhere	61.2 %	17.5 %	9.1 %	12.2 %
	3 "fringe"	41.9 %	39.2 %	6.8 %	8.8 %	1.2 %	0.6 %	1.6 %		76.9 %	7.7 %	4.4 %	11.1 %
	4 off spot	41.3 %	39.5 %	5.6 %	7.0 %	1.2 %	1.9 %	3.5 %		75.0 %	9.0 %	5.7 %	10.3 %
	#	**O 1s**	**C 1s**	**I 3d**	**Si 2p**	**N 1s**	**Cu 2p**						
Copper	***1 spot***	47.2 %	29.8 %	14.0 %	7.4 %	0.6 %	***1.1 %***		Low Cu in spot	71.9 %	12.2 %	6.9 %	9.1 %
	2 off spot	39.7 %	42.0 %	9.5 %	0.7 %	1.8 %	6.4 %			62.6 %	17.4 %	7.4 %	12.6 %
	3 off spot	44.8 %	29.3 %	13.7 %	1.6 %	1.7 %	8.9 %			69.9 %	12.7 %	7.6 %	9.8 %
	#	**O 1s**	**C 1s**	**I 3d**	**Si 2p**	**N 1s**	**Mg 2p**						
Paint	***1 spot***	41.9 %	38.0 %	8.0 %	10.4 %	1.1 %	***n.a.***		No substrate in spot	85.6 %	6.8 %	3.8 %	3.9 %
	2 off spot	36.3 %	48.9 %	4.8 %	5.6 %	3.6 %	ca 1%			63.3 %	23.9 %	6.8 %	6.0 %
	4 off spot	40.3 %	44.1 %	8.2 %	5.1 %	1.5 %	ca 1%			64.7 %	21.5 %	6.7 %	7.1 %
	#	**O 1s**	**C 1s**	**I 3d**	**Si 2p**		**Zn 2p**						
zinc	***1 spot***	22.8 %	62.3 %	3.6 %	4.8 %		***6.4 %***		Zinc cntent	91.6 %	3.9 %	0.0 %	4.5 %
	2 off spot	21.6 %	63.0 %	4.2 %	4.2 %		7.0 %		similar everywhere	90.7 %	4.3 %	0.4 %	4.7 %
	3 spot	21.7 %	63.1 %	3.7 %	5.5 %		6.0 %		High carbon everywhere	90.5 %	4.5 %	0.8 %	4.2 %

Appendix D1. SEM-EDX analysis of painted samples.

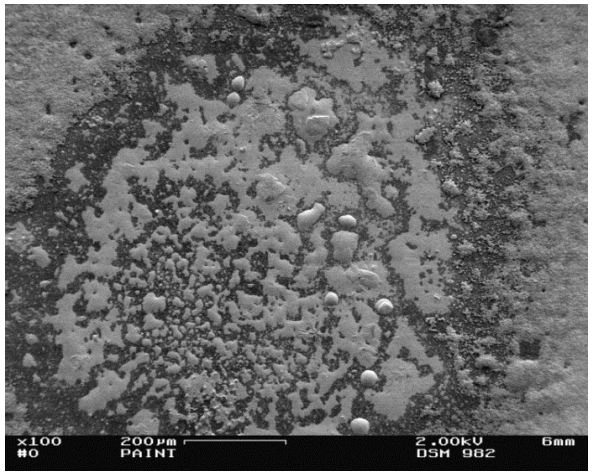

Fig. D1. SEM micrograph of IO_x deposit on painted surface shows areas with clearly different morphologies.

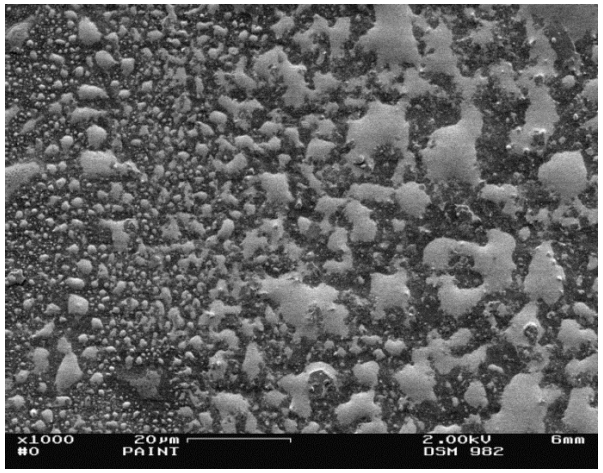

Fig. D2. In the centre of the deposit area IO_x particles seems to have been dissolved.

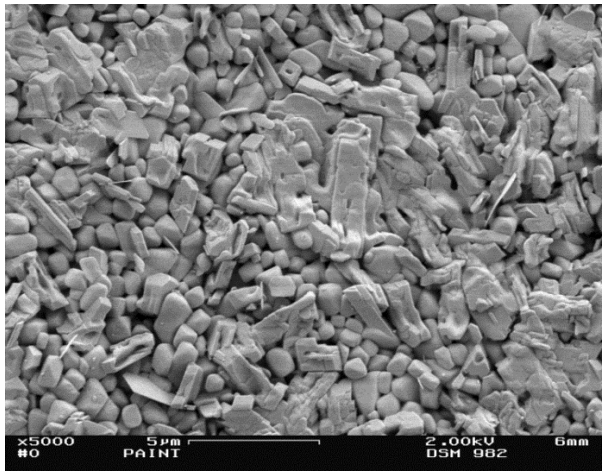

Fig. D3. At the edge of the deposit area iodine compounds have formed a fairly thick layer of large crystals.

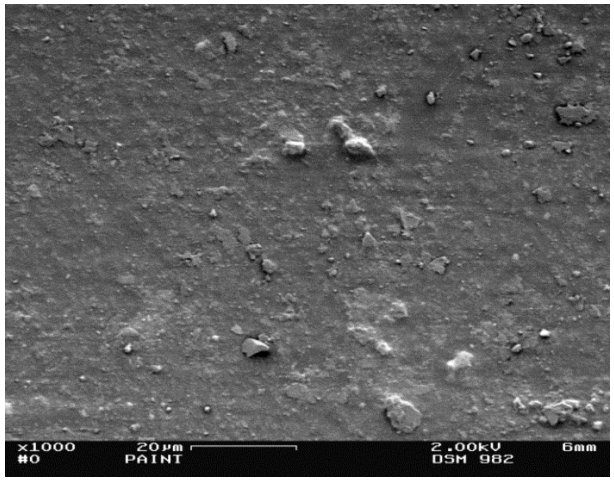

Fig. D4 (left). Painted surface outside of the deposit area shows some particulate impurities.

Appendix D2. EDX map of the IOx deposit on a painted surface

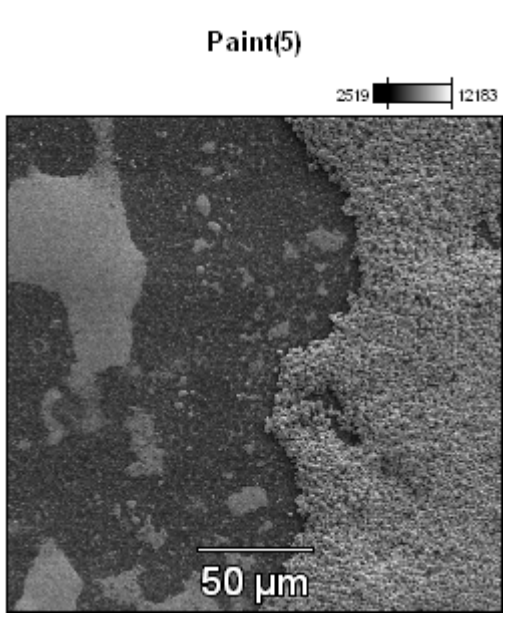

Data Type:	**Net Counts**
Image Resolution:	**1024 by 1024**
Image Pixel Size:	**0.21 µm**
Map Resolution:	**256 by 256**
Map Pixel Size:	**0.85 µm**
Acc. Voltage:	**8.0 kV**
Magnification:	**500**

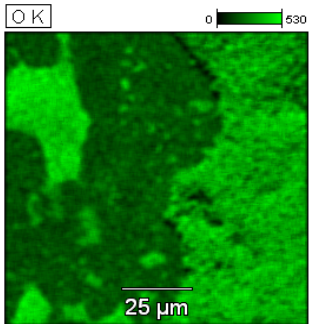

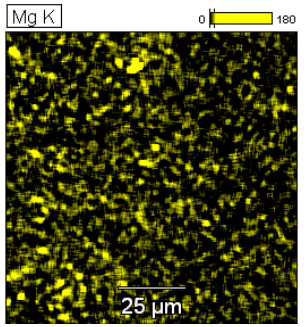

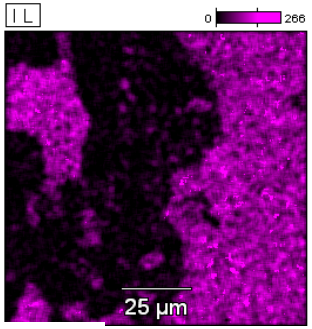

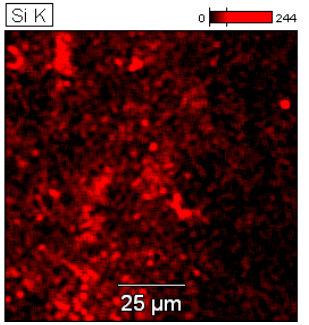

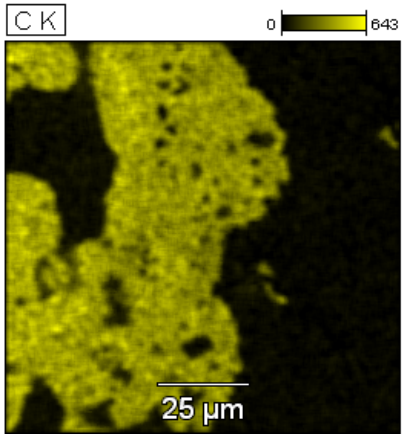

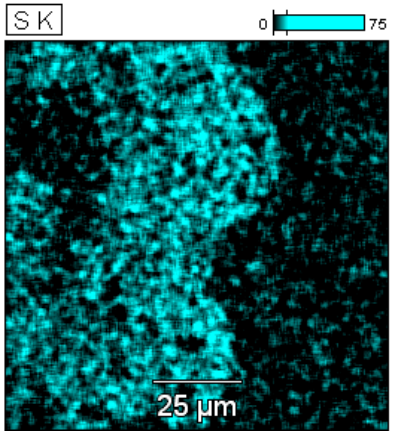

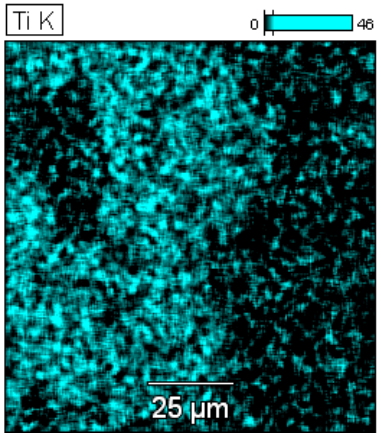

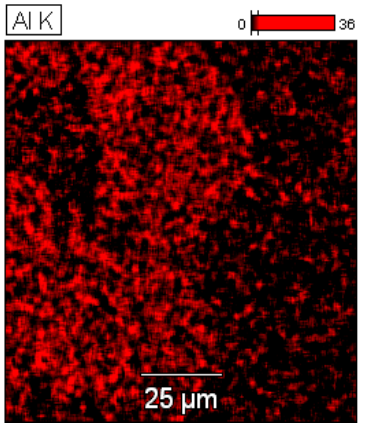

Appendix D3: EDX map of the dissolved deposit on a painted surface

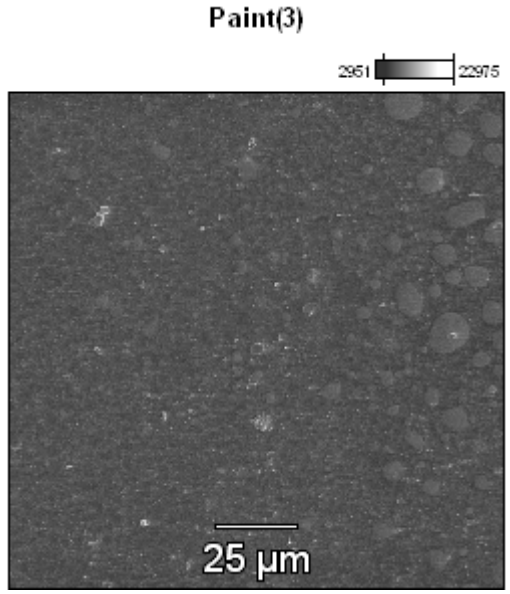

Data Type:	**Net Counts**
Image Resolution:	**1024 by 1024**
Image Pixel Size:	**0.15 µm**
Map Resolution:	**256 by 256**
Map Pixel Size:	**0.61 µm**
Acc. Voltage:	**8.0 kV**
Magnification:	**700**

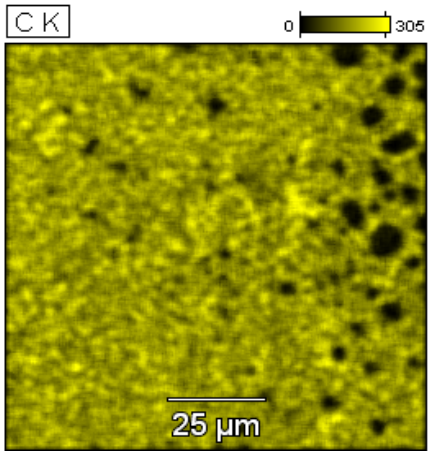

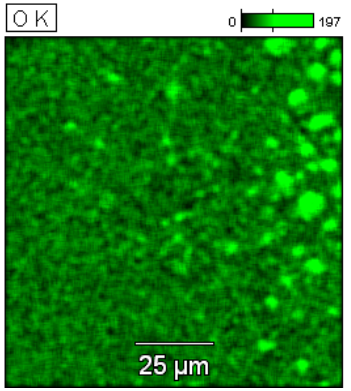

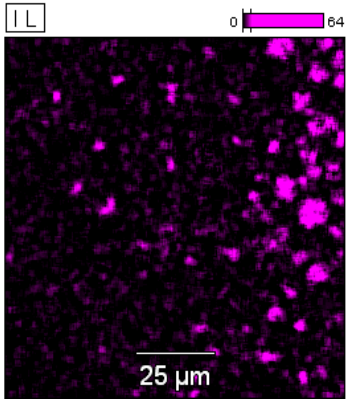

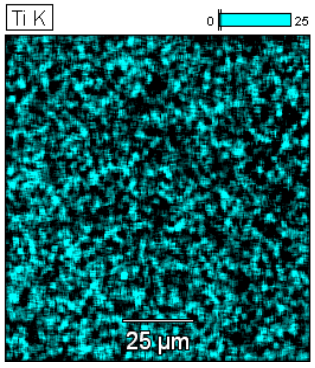

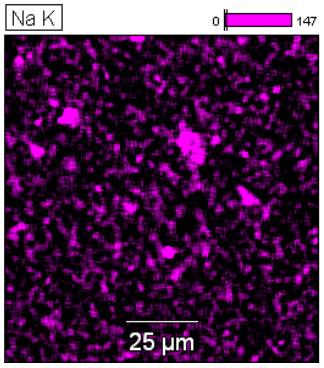

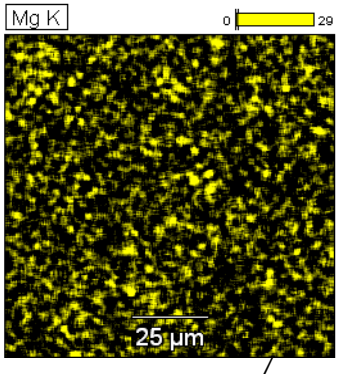

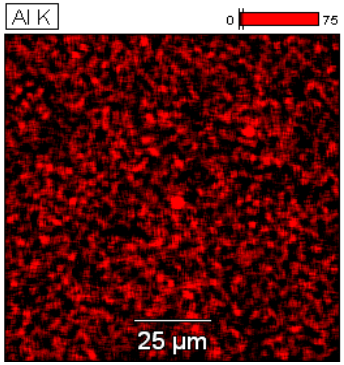

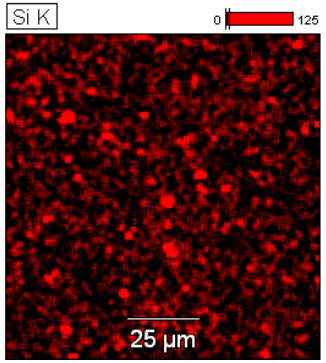

Appendix D4: EDX spectrum of dissolved deposit on paint (Spot 2) and that of painted surface outside of deposit area (Spot 1 and 3)

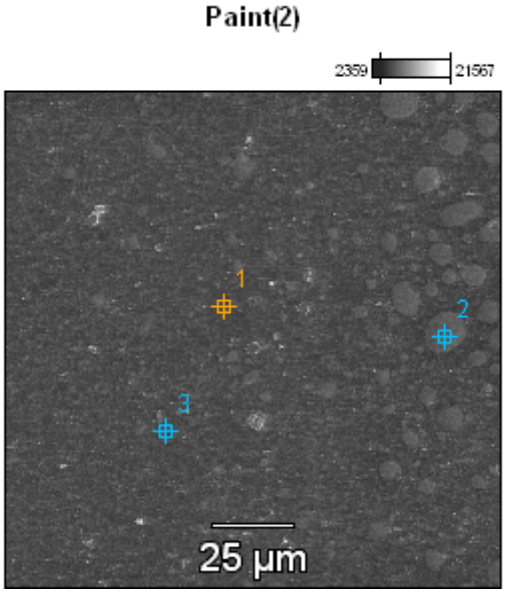

Image Name:	Paint(2)
Image Resolution:	1024 by 1024
Image Pixel Size:	0.15 µm
Acc. Voltage:	8.0 kV
Magnification:	700

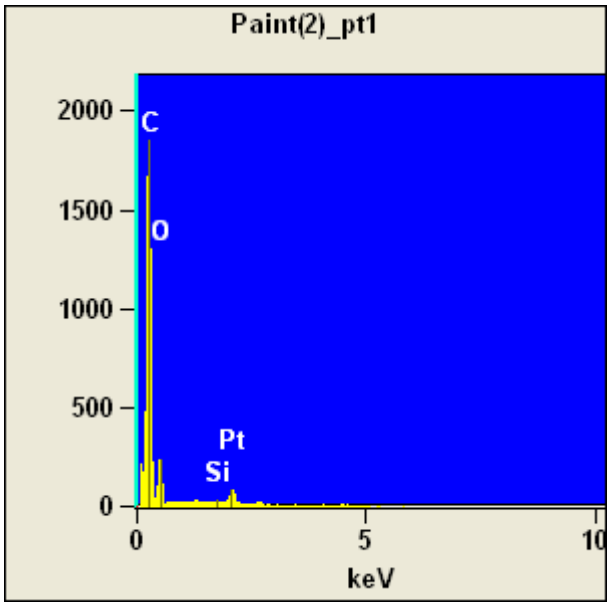

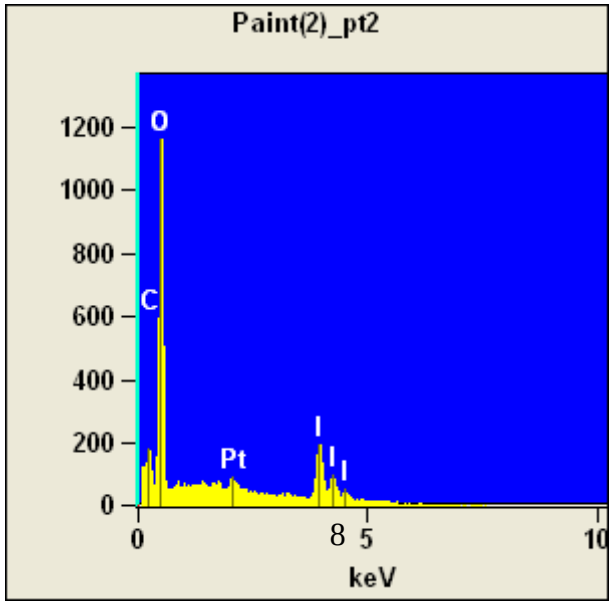

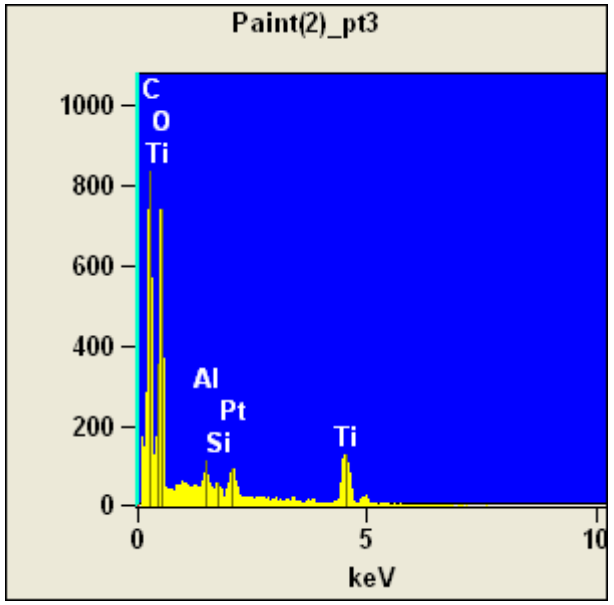

Appendix D5: EDX spectra of two spots measured on a painted surface outside of the deposit area

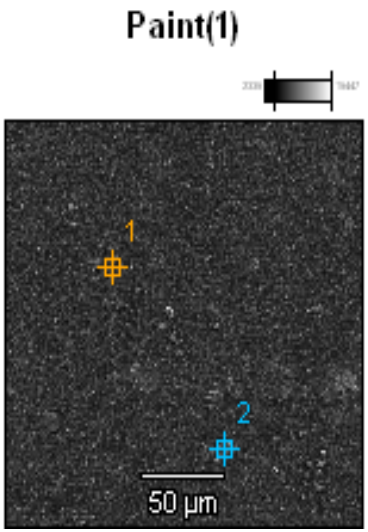

Image Name:	Paint(1)
Image Resolution:	1024 by 1024
Image Pixel Size:	0.21 µm
Acc. Voltage:	8.0 kV
Magnification:	500

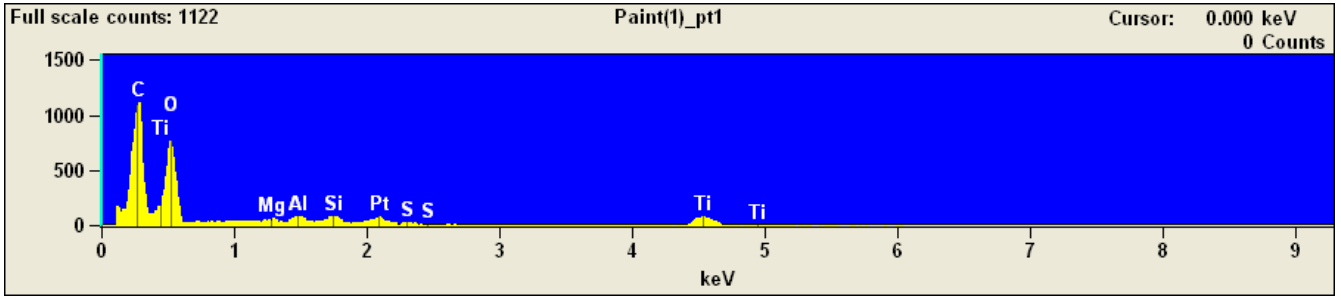

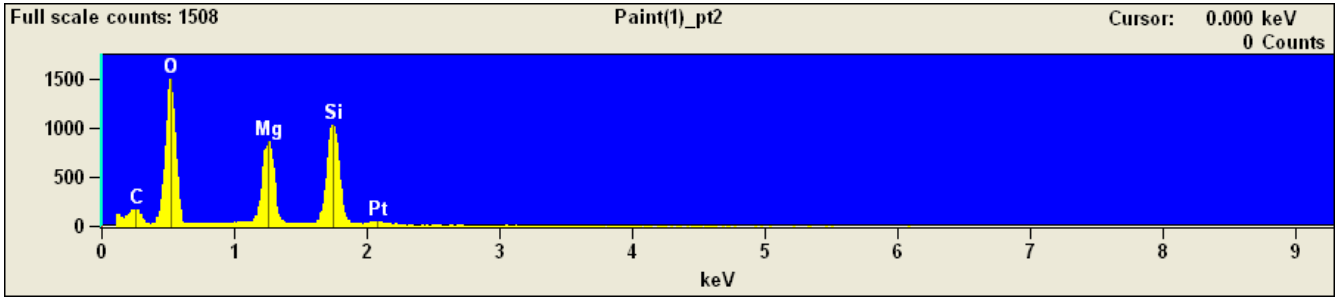

Appendix E1: SEM micrographs of a IOx deposit on stainless steel

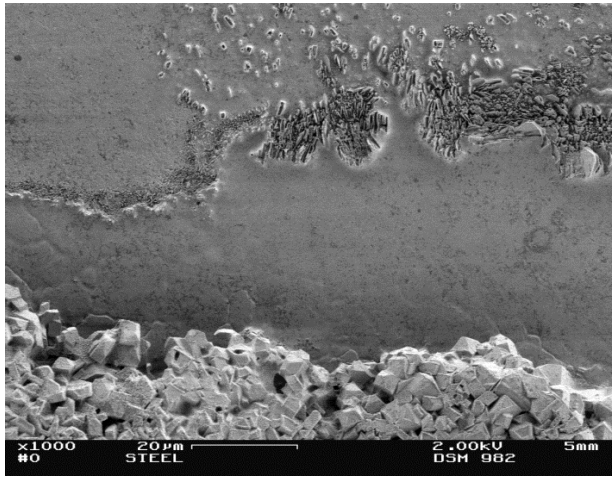

Fig. E1. Solid IO_x crystals are grown on the stainless steel surfaces.

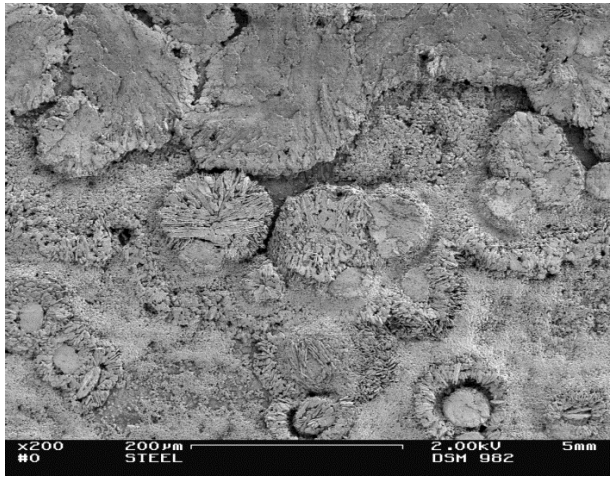

Fig. E2 The outline of grain boundaries is clearly visible under the IO_x crystals.

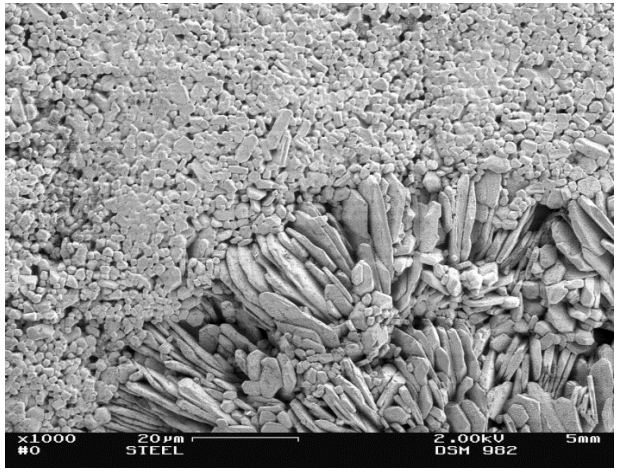

Fig E3. The size of the IO_x crystals varies as a function of location on stainless steel surface.

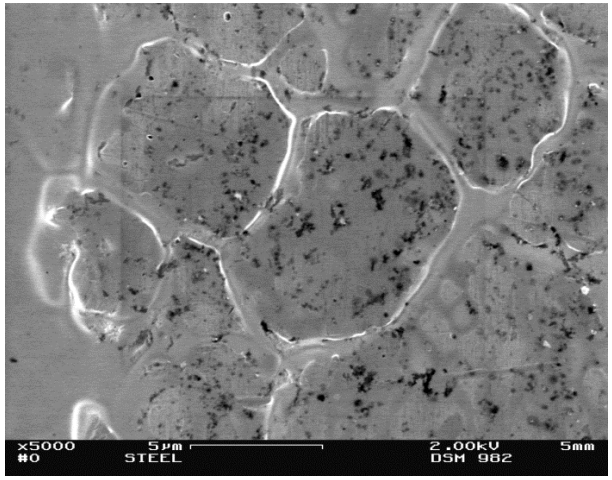

Fig. E4 (left). Grain boundaries on stainless steel outside of the deposition area.

Appendix E2: EDX map of a IOx deposit on stainless steel

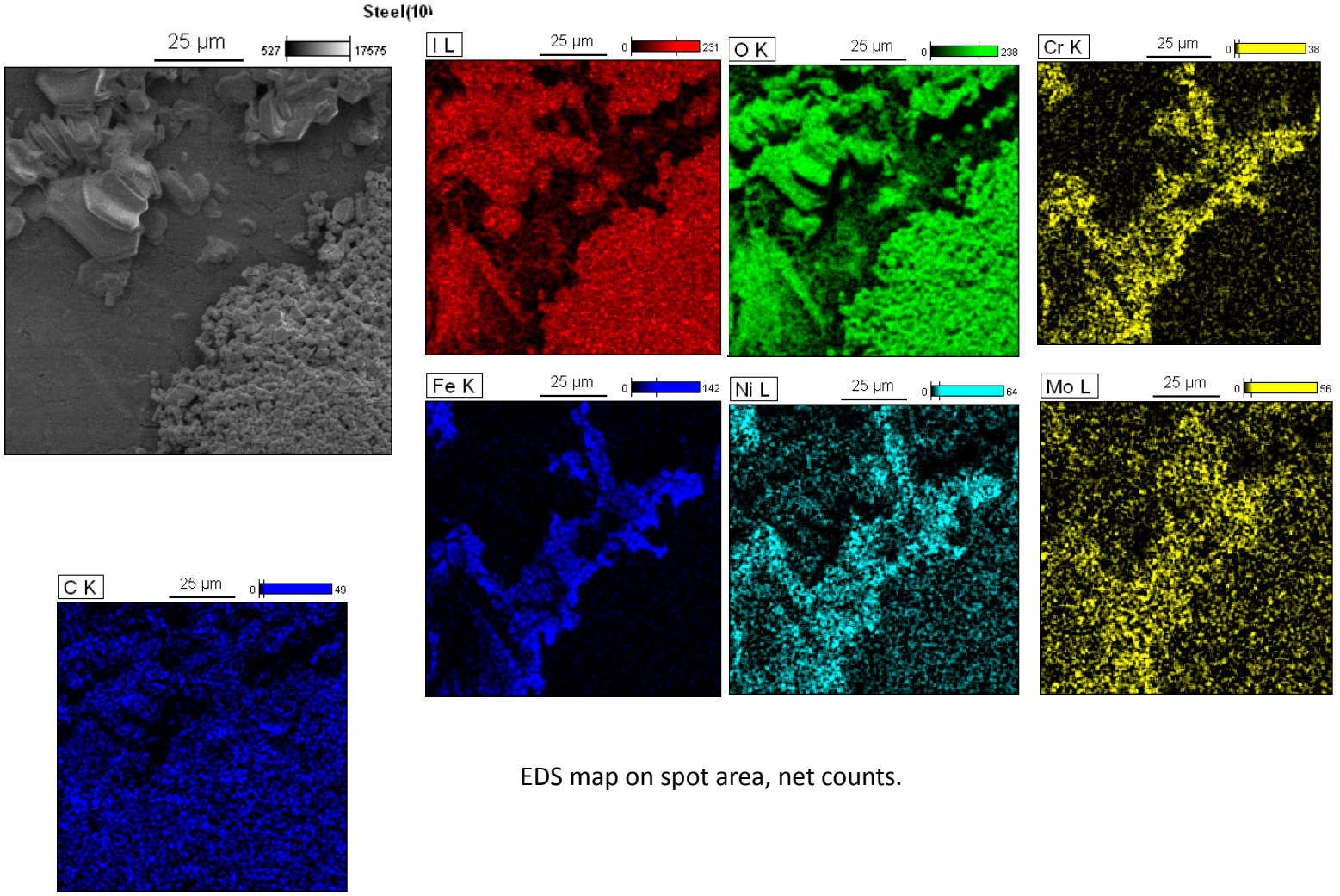

EDS map on spot area, net counts.

Data Type: Net Counts Mag: 1000 Acc. Voltage: 10.0 kV

Appendix E3: EDX map on a stainless steel sample outside of the IOx deposition area

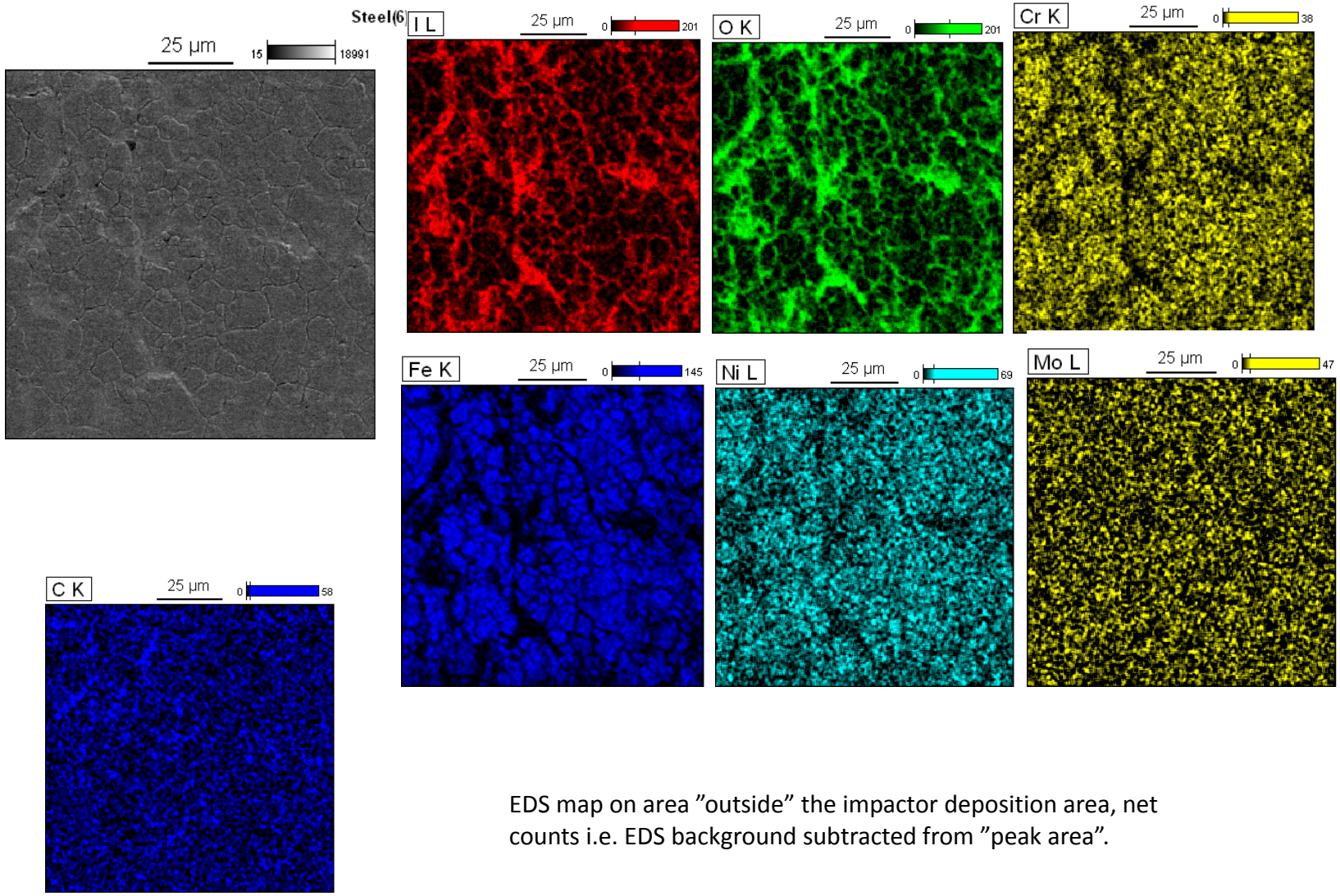

EDS map on area ”outside” the impactor deposition area, net counts i.e. EDS background subtracted from ”peak area”.

Data Type: Net Counts Mag: 1000 Acc. Voltage: 10.0 kV

Appendix E4: EDX spectra of five spots on a stainless steel surface measured on top of the crystalline IOx deposit (spots 2 and 5) or close to it (spots 1, 3 and 4)

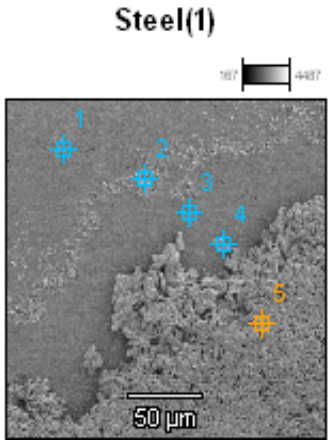

Image Name:	Steel(1)
Image Resolution:	1024 by 1024
Image Pixel Size:	0.21 µm
Acc. Voltage:	8.0 kV
Magnification:	500

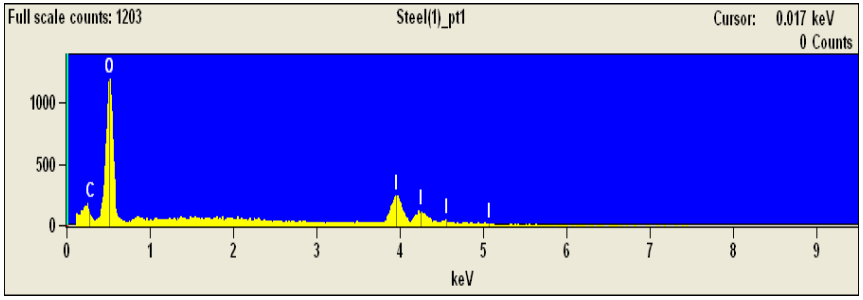

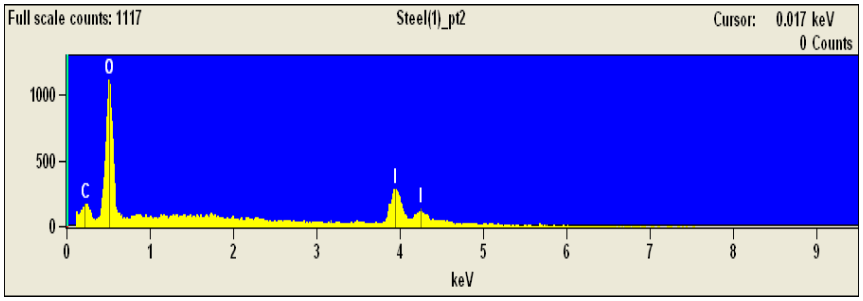

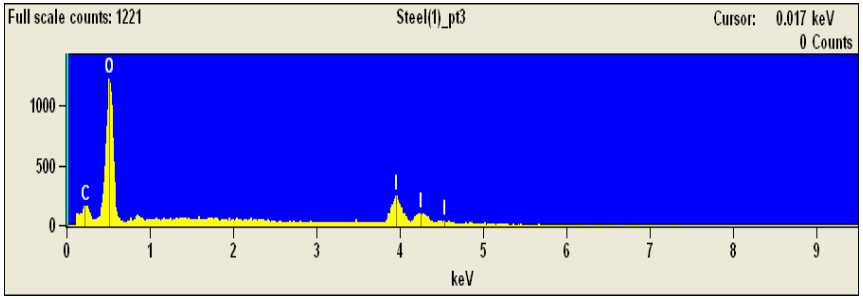

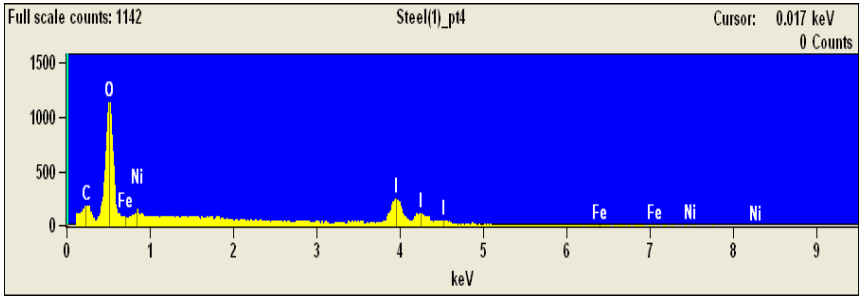

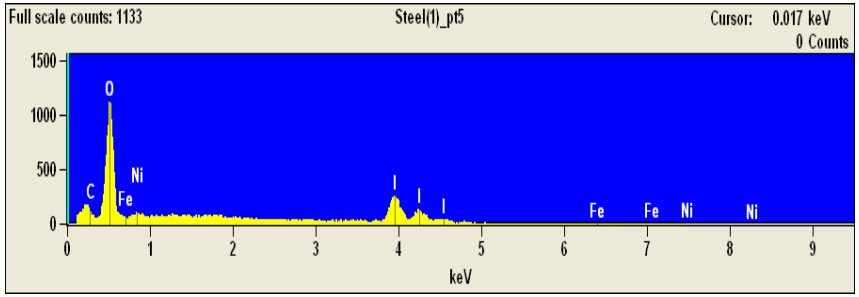

Appendix E5: EDX spectra of two spots on a stainless steel surface measured on top of the crystalline IOx deposit (spot 1) or close to it (spot 2)

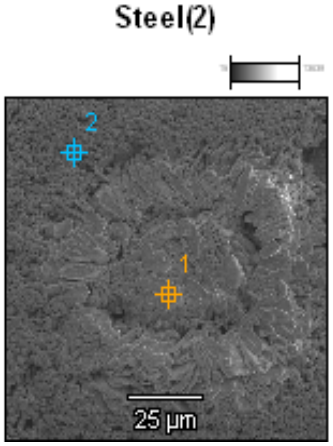

Image Name:	Steel(2)
Image Resolution:	1024 by 1024
Image Pixel Size:	0.11 µm
Acc. Voltage:	8.0 kV
Magnification:	1000

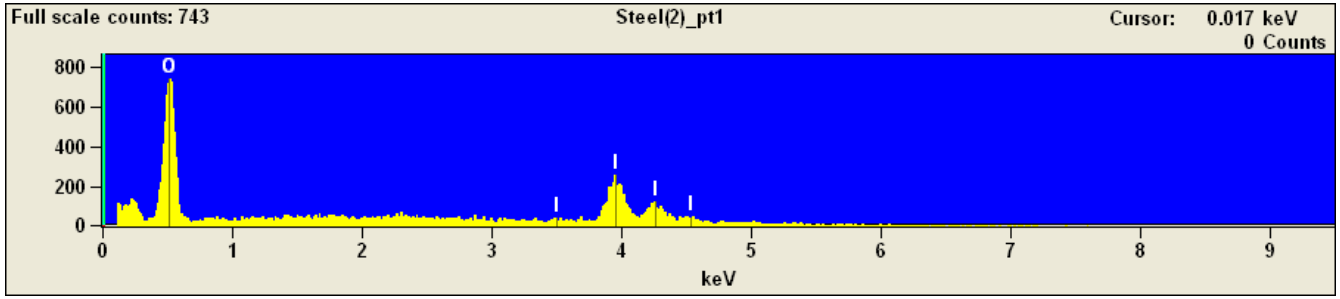

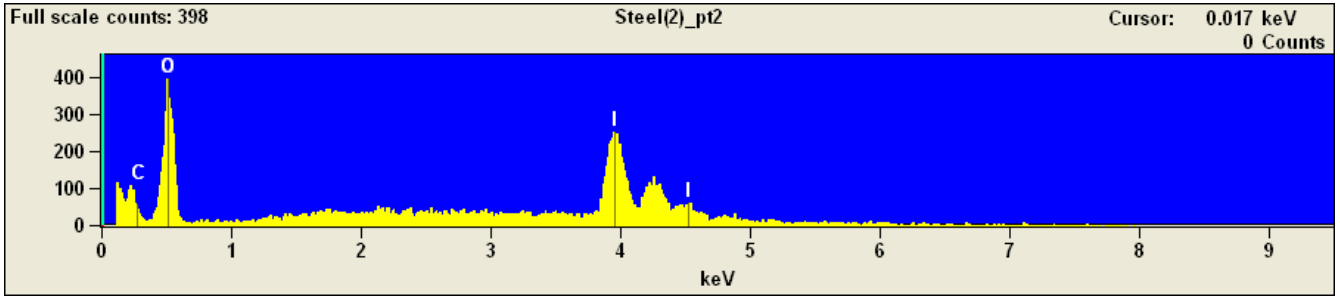
Full scale counts: 398
Steel(2)_pt2
Cursor: 0.017 keV
0 Counts
400
300
200
100
0
O
C
I
I
0
1
2
3
4
5
6
7
8
9
keV

Appendix E6: EDX spectra of two spots on a stainless steel surface measured on top of the crystalline IOx deposit

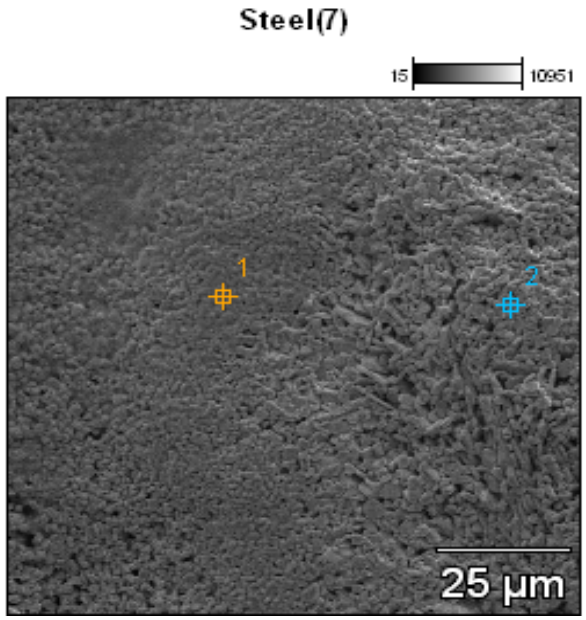

Image Name:	Steel(7)
Image Resolution:	1024 by 1024
Image Pixel Size:	0.11 µm
Acc. Voltage:	10.0 kV
Magnification:	1000

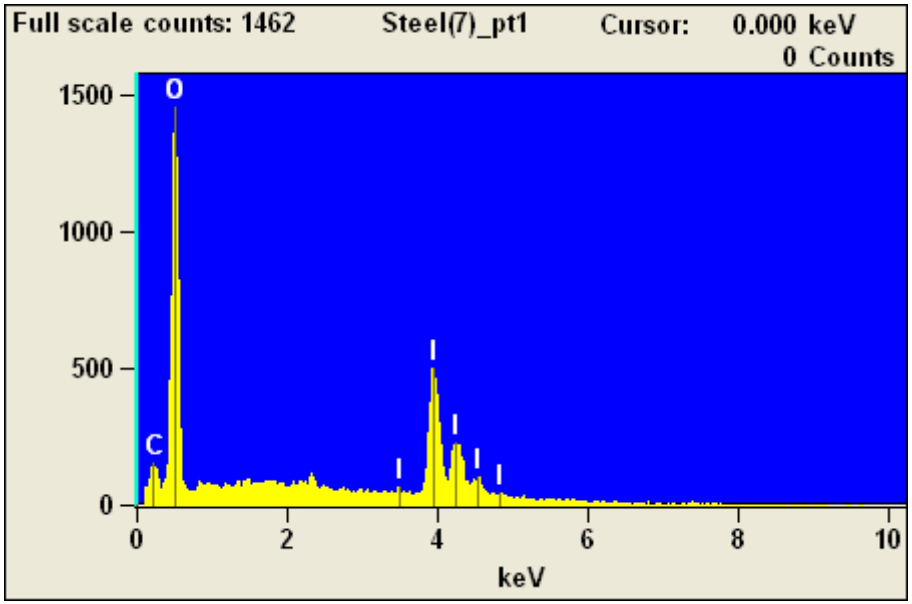

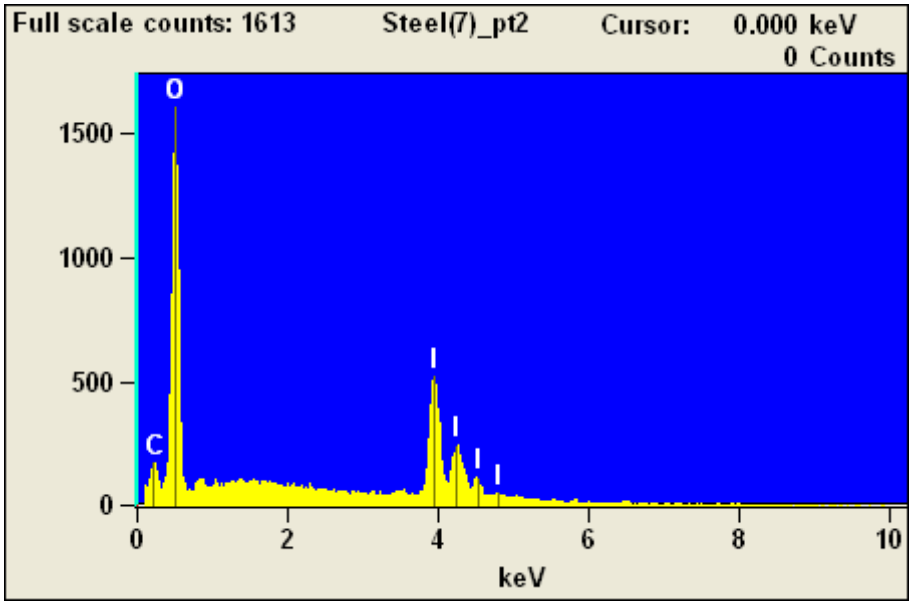

Appendix E7: EDX spectra of three spots on a stainless steel surface measured on the grain boundary of the deposit (spots 1 and 2) or close to it (spot 3)

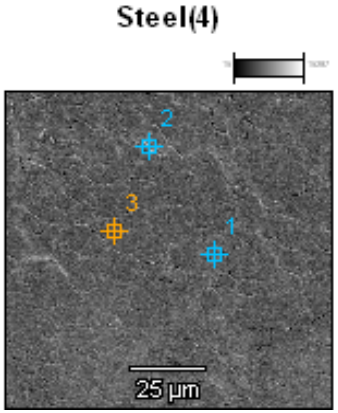

Image Name:	Steel(4)
Image Resolution:	1024 by 1024
Image Pixel Size:	0.11 µm
Acc. Voltage:	8.0 kV
Magnification:	1000

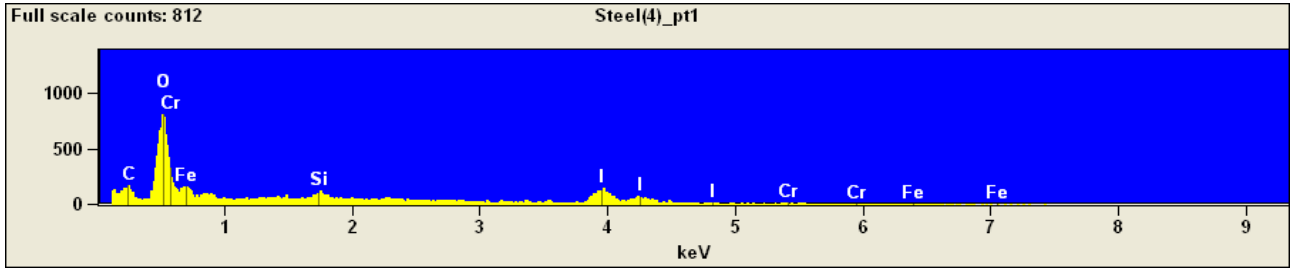

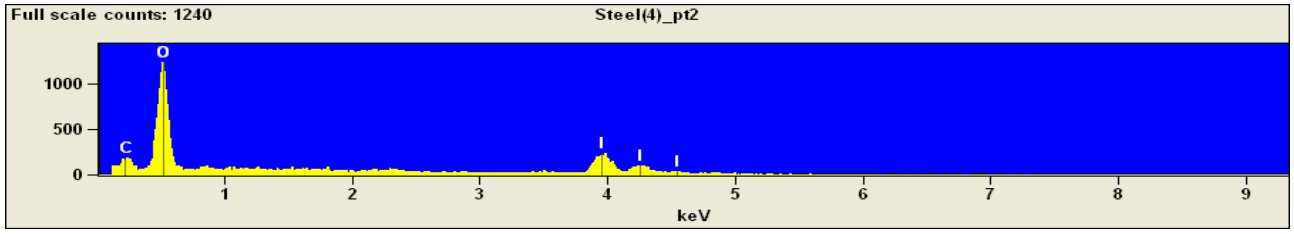

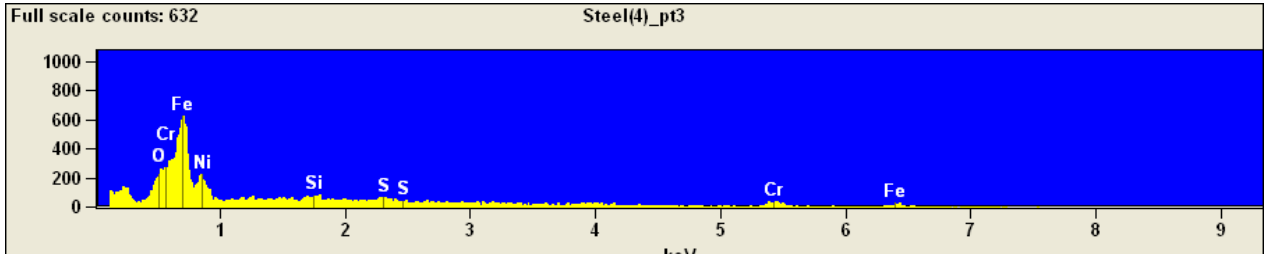

Appendix E8: EDX spectra of two spots on a stainless steel surface measured on the grain boundary of the deposit (spot 2) or close to it (spot 1)

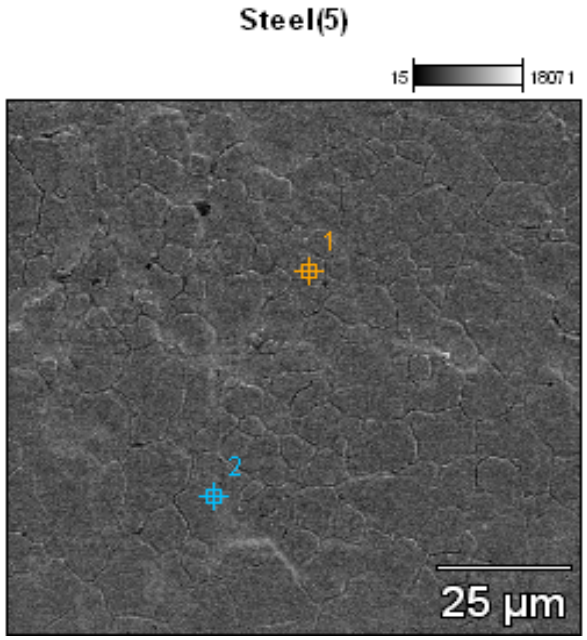

Image Name:	Steel(5)
Image Resolution:	1024 by 1024
Image Pixel Size:	0.11 µm
Acc. Voltage:	10.0 kV
Magnification:	1000

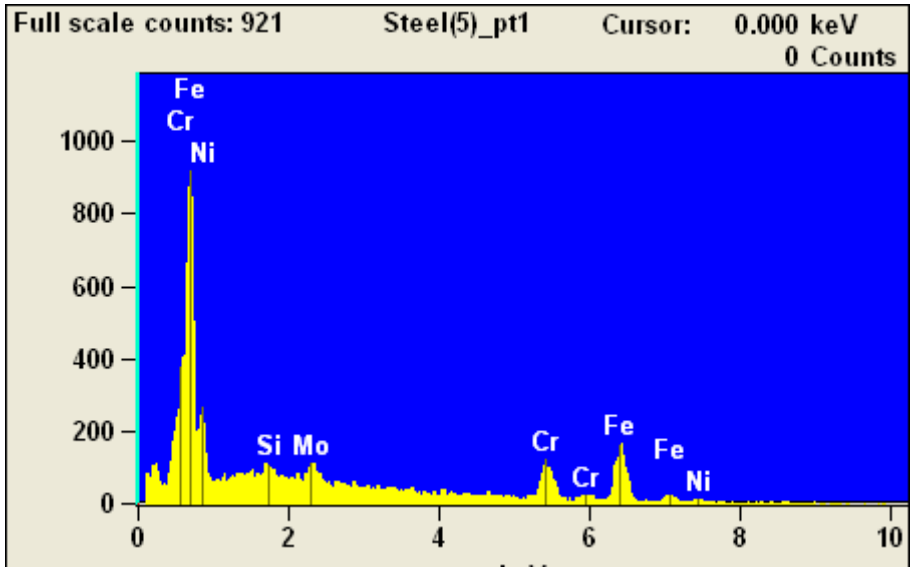

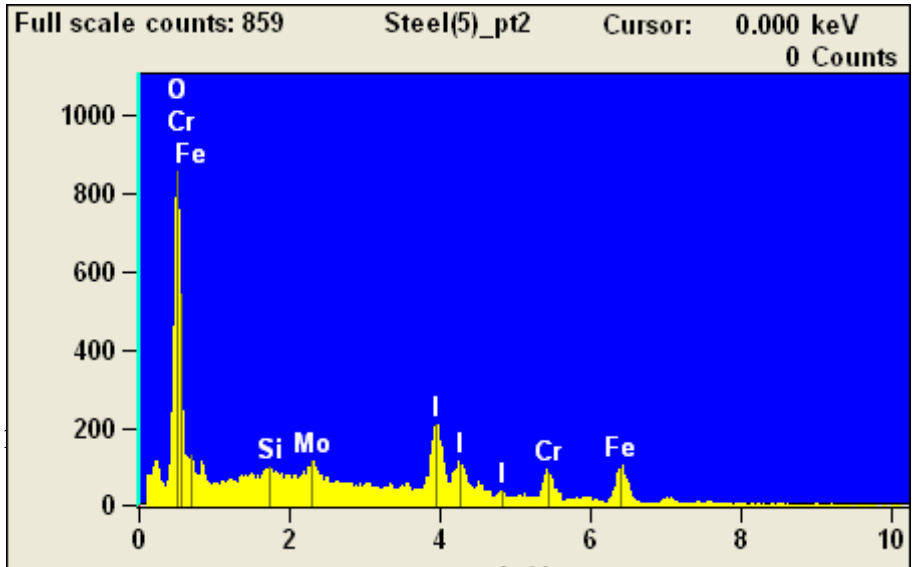

Appendix E9: EDX spectra of two spots on a stainless steel surface measured outside of the deposit area

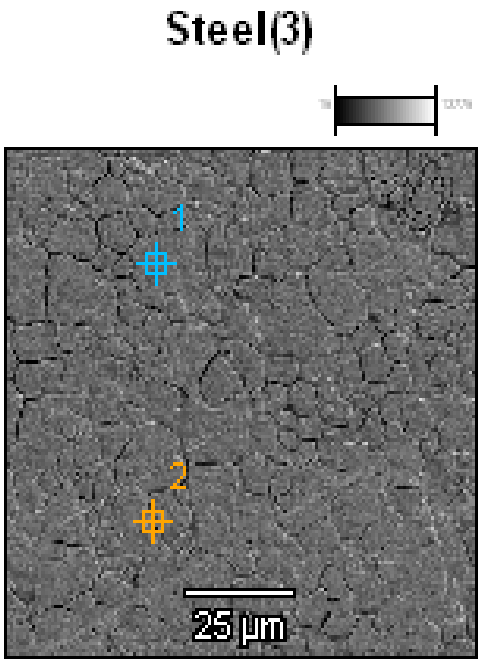

Image Name:	Steel(3)
Image Resolution:	1024 by 1024
Image Pixel Size:	0.11 µm
Acc. Voltage:	8.0 kV
Magnification:	1000

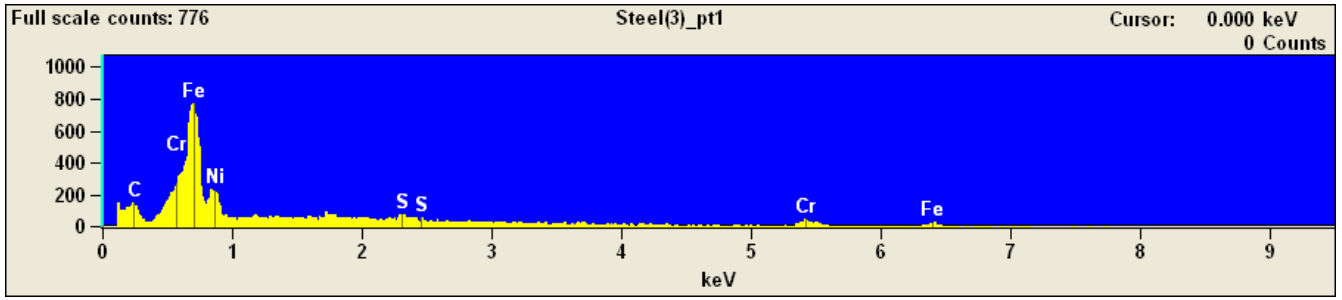

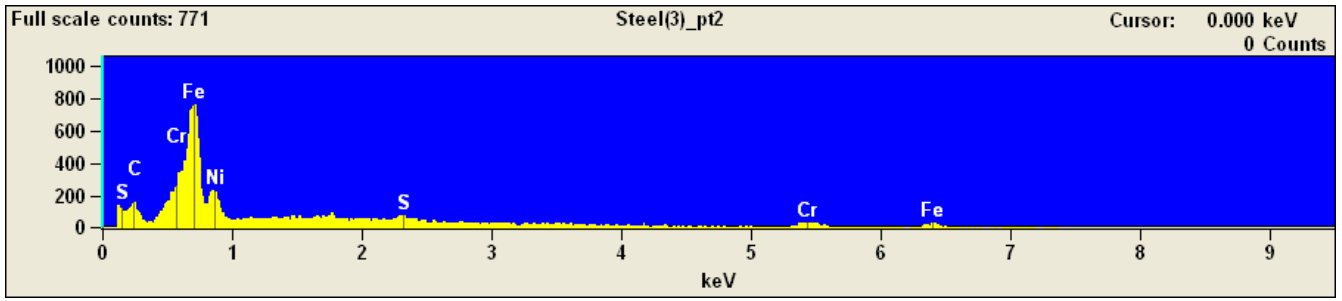

Appendix F1: SEM micrographs of IOx deposits on a copper surface

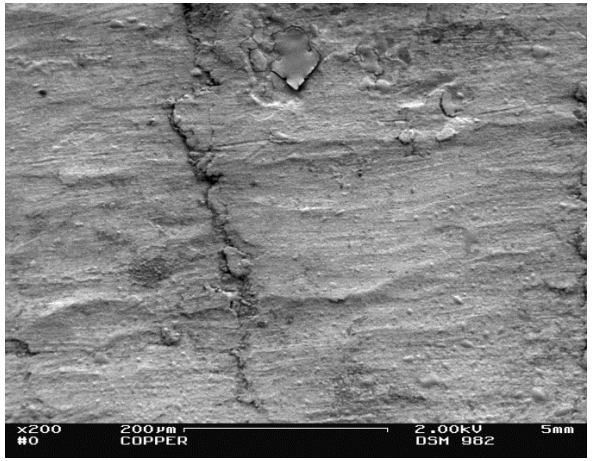

Figure F1. An overview of IO_x deposition on copper surface.

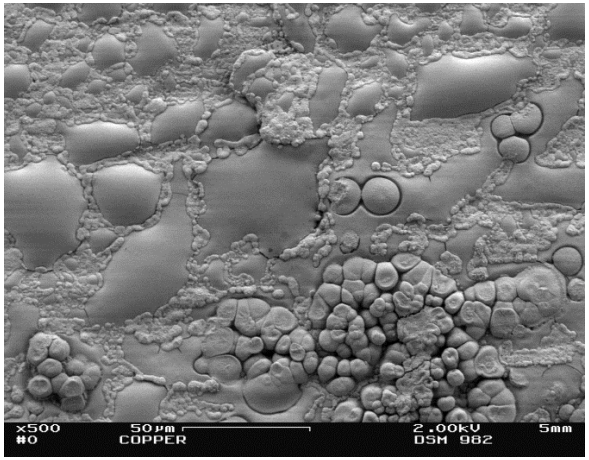

Figure F2. Large pool like structures of dissolved particle deposits had re-solidified on the copper surface. Thick deposits could be observed between the pools.

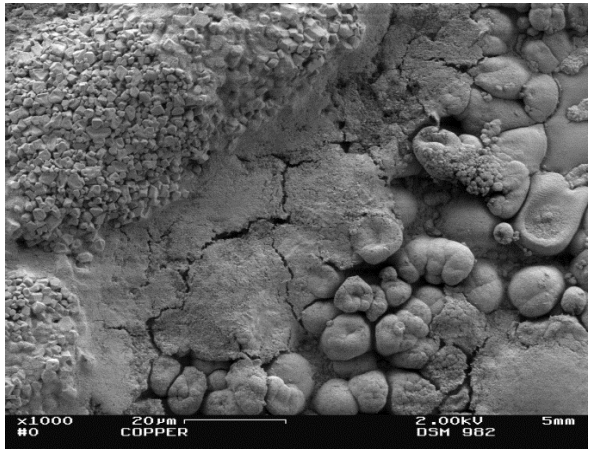

Figure F3. Areas containing small crystals were found among the thick deposits.

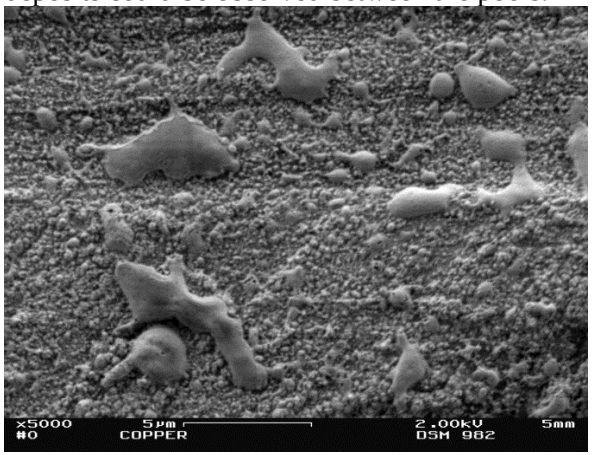

Figure F4. With higher magnification small pool like structures were observed on crystalline areas.

Appendix F2: EDX map of IOx deposit on a copper surface in an area containing small crystals and pool-like structures

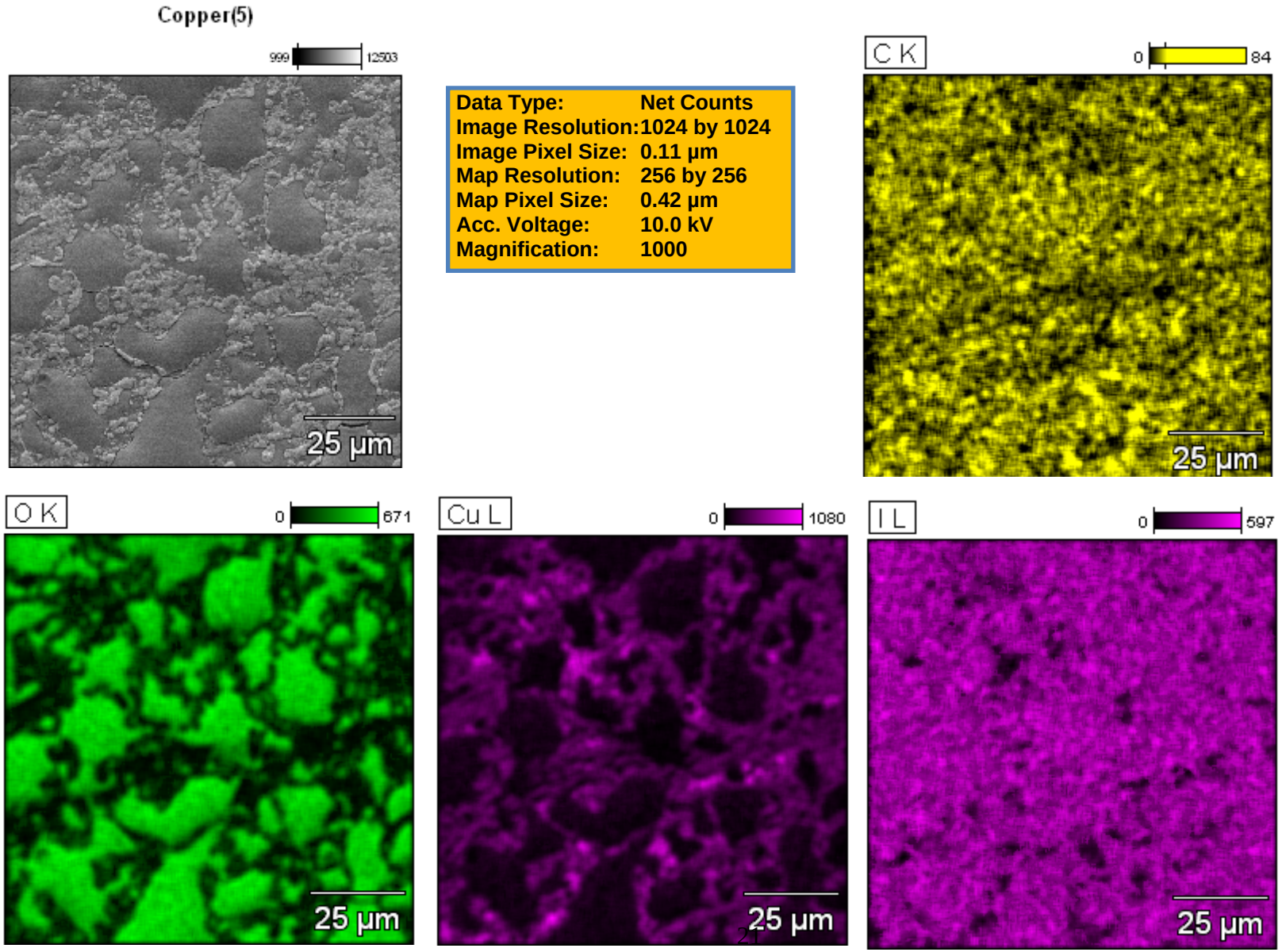

Appendix F3: EDX map of the IOx deposition on a copper surface in an area with thick, uniform deposit with grain-like structures

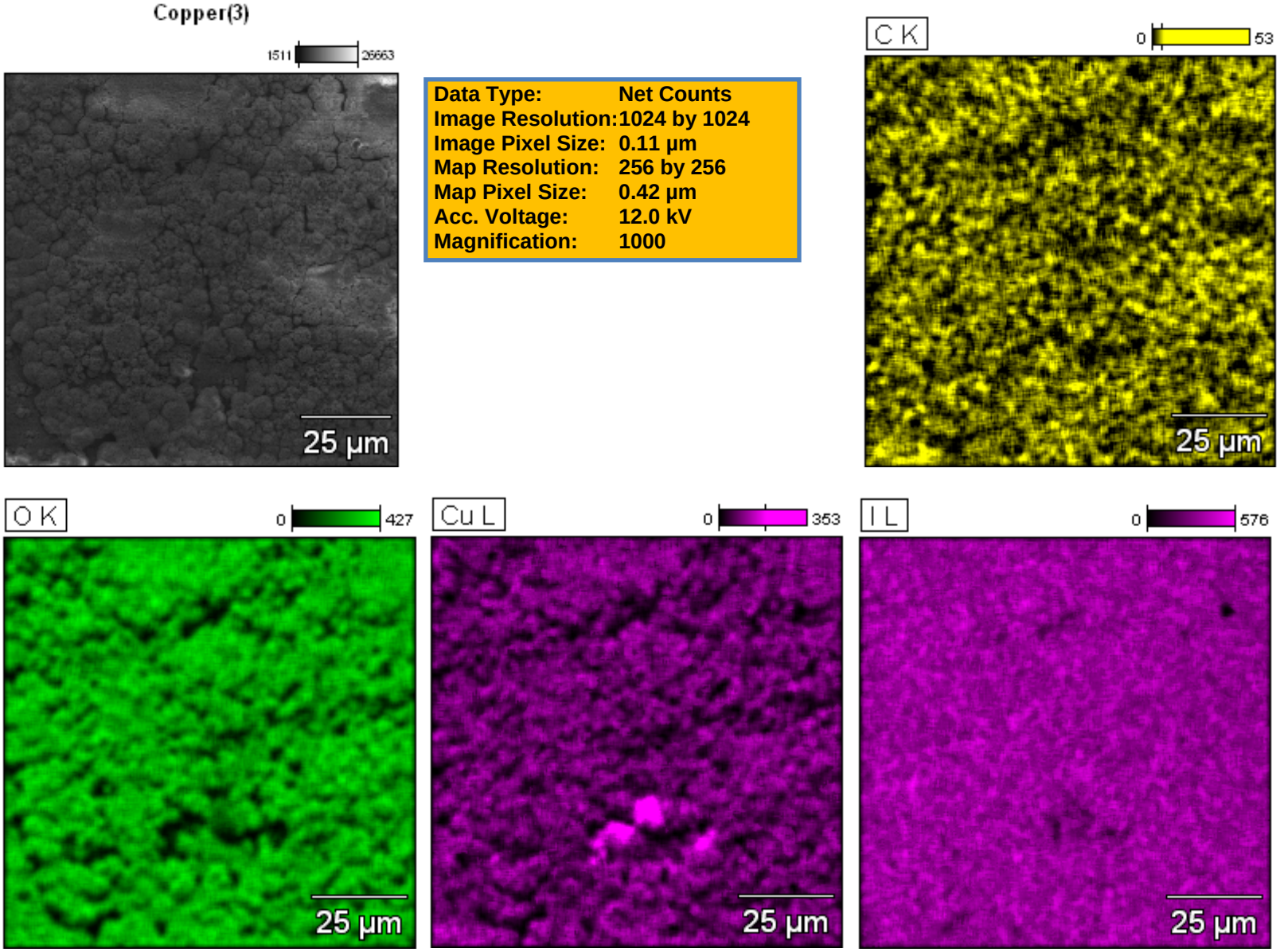

Appendix F4: EDX spectra of two spots on a copper surface measured in an area with pool-like structures (spot 1) and small crystals (spot 2)

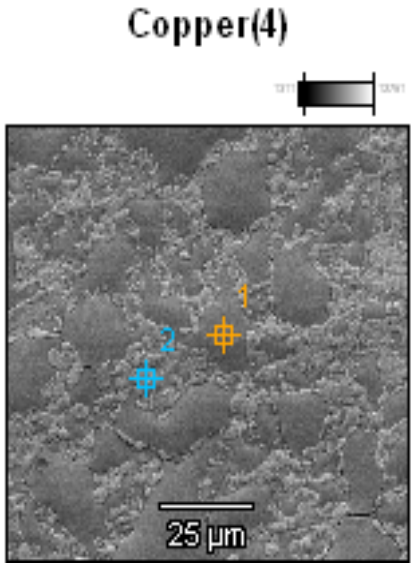

Image Name:	Copper(4)
Image Resolution:	1024 by 1024
Image Pixel Size:	0.11 µm
Acc. Voltage:	10.0 kV
Magnification:	1000

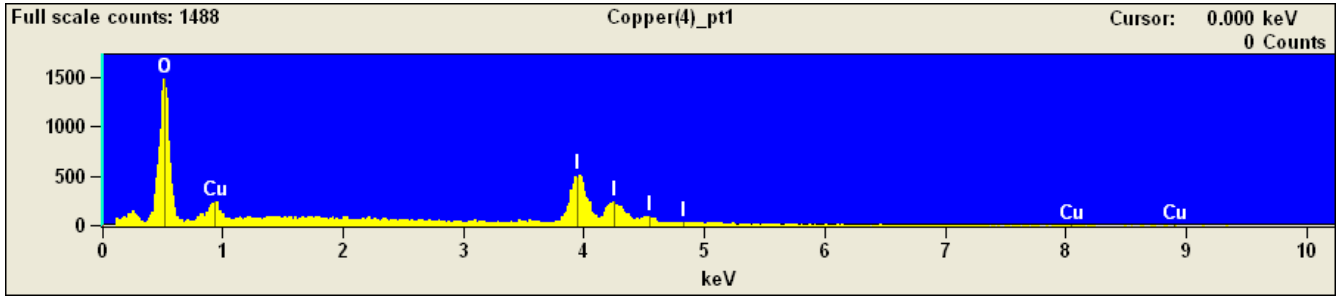

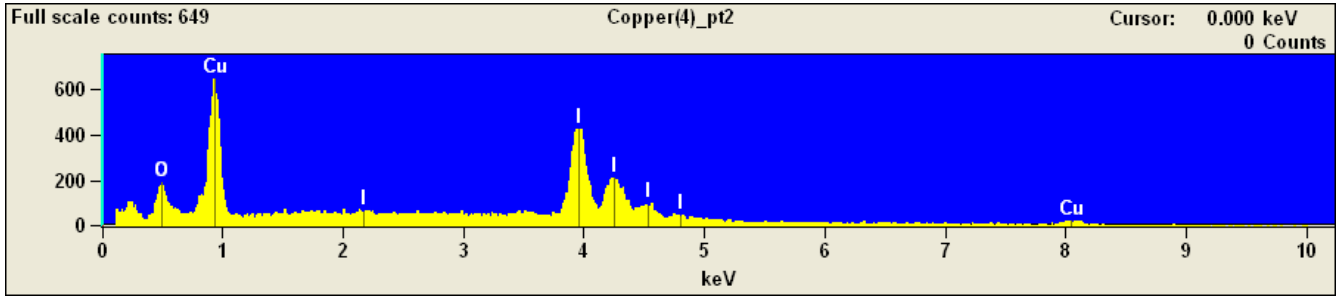

Appendix F5: EDX spectra of two spots on a copper surface measured in an area with uniform IOx deposit

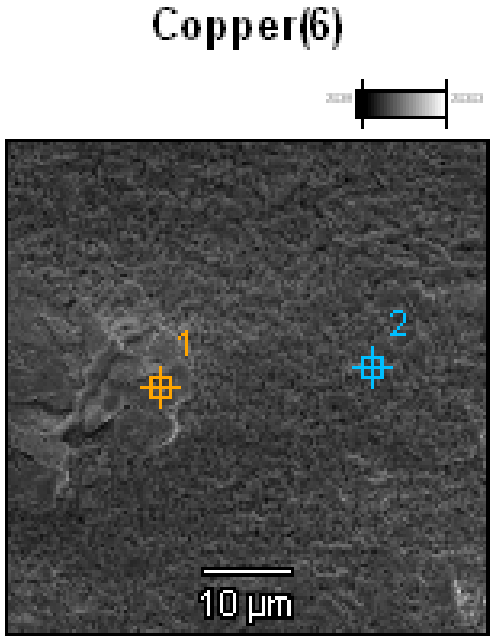

Image Name:	Copper(6)
Image Resolution:	1024 by 1024
Image Pixel Size:	0.05 µm
Acc. Voltage:	10.0 kV
Magnification:	2000

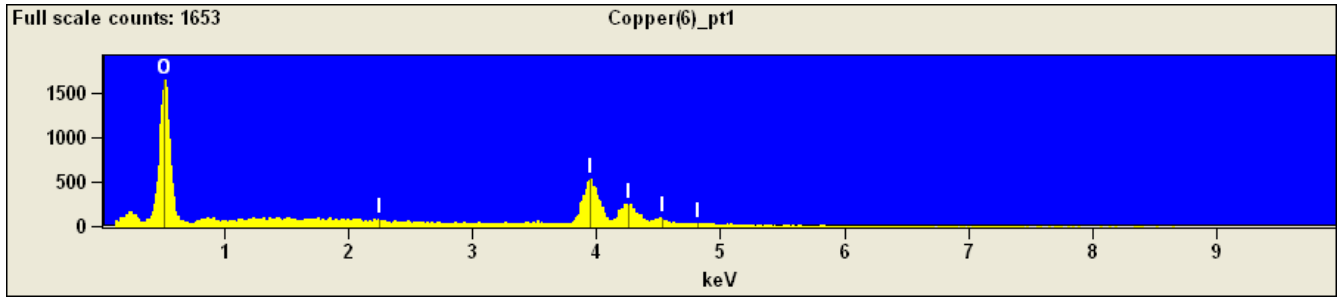

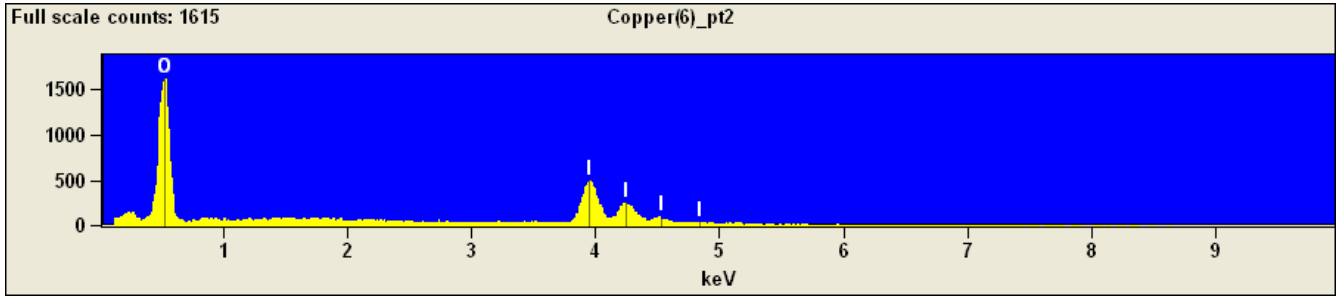

Appendix G1: SEM micrographs of the IO_x deposit on an aluminium surface

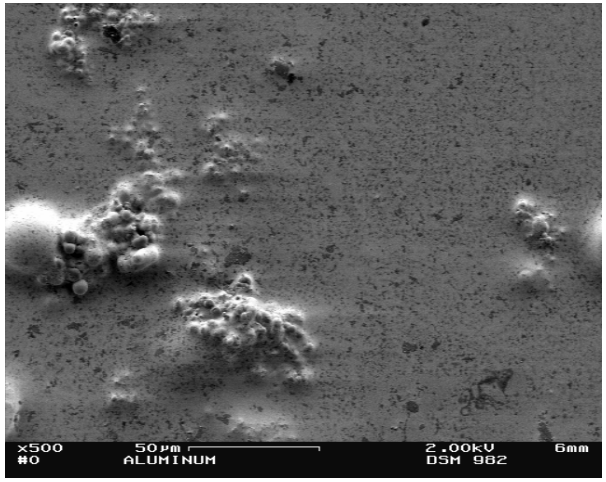

Figure G1. SEM micrograph of the aluminium sample outside of the deposition area revealed some impurities on the surface.

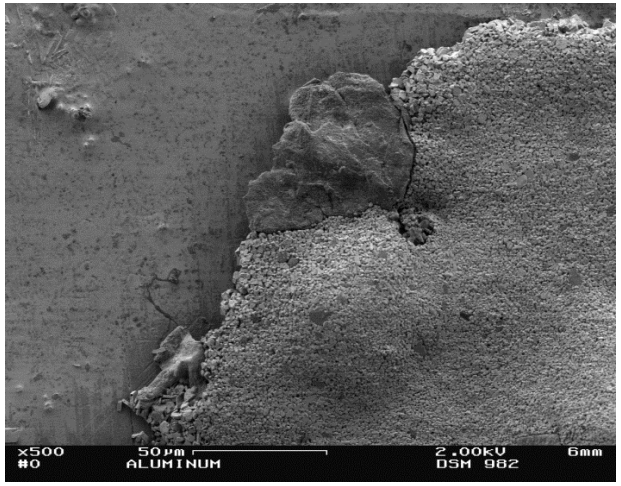

Figure G2. Solid IOx crystals were observed on the edge of the deposition.

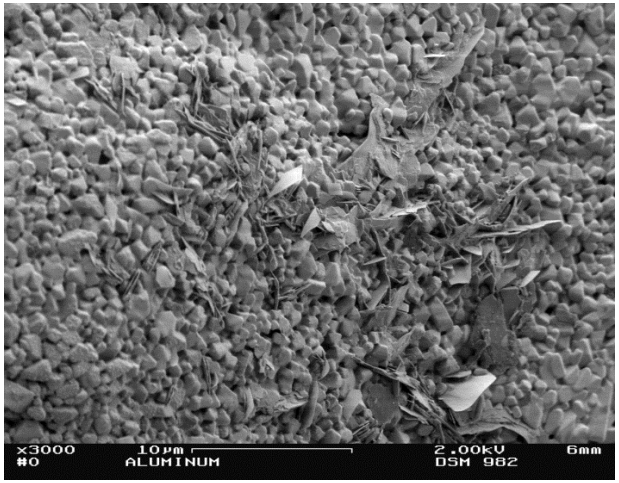

Figure G3. There were leaf like and cubic IO_x crystals on the deposition.

Appendix G2. EDX map of ithe odine oxide deposit on an aluminium surface

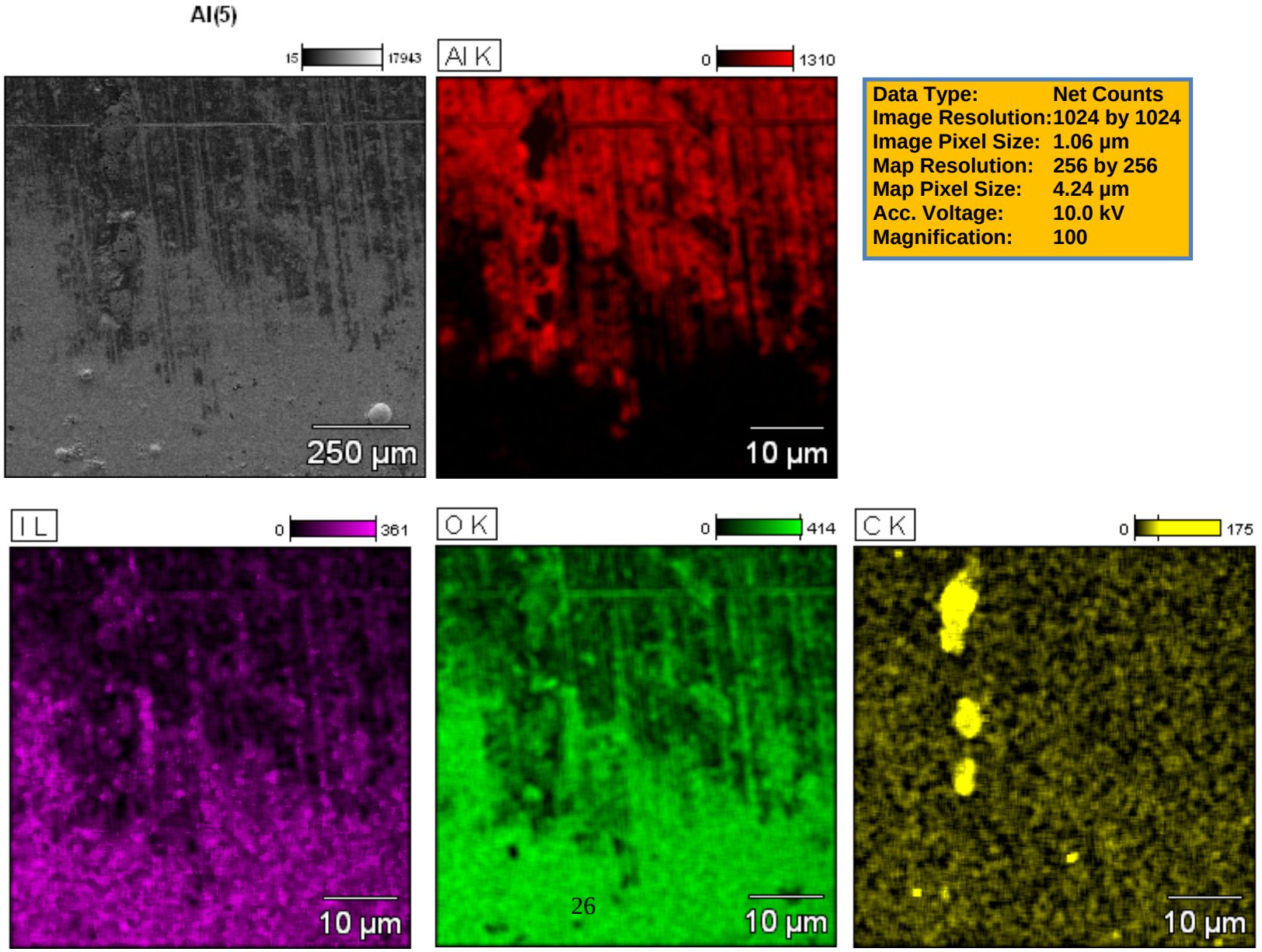

Appendix G3: EDX map of the iodine oxide deposit on an aluminium surface

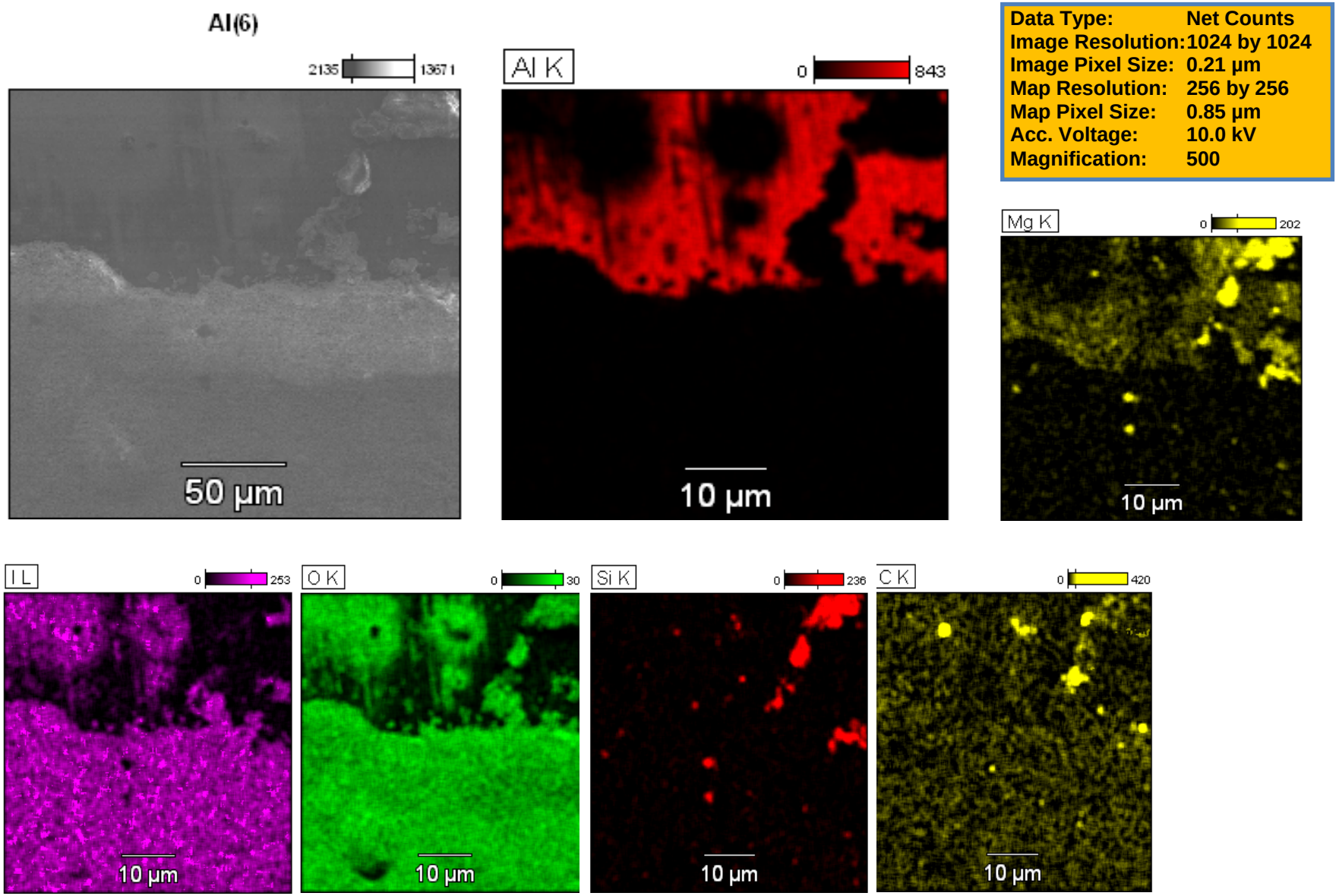

Appendix G4: EDX spectra of two spots on a aluminium surface measured on the edge of the deposit area with and without IO_x deposit.

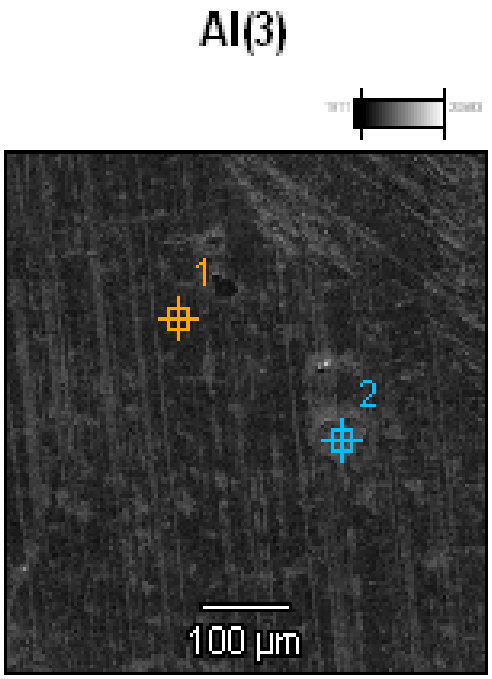

Image Name:	Al(3)
Image Resolution:	1024 by 1024
Image Pixel Size:	0.53 µm
Acc. Voltage:	10.0 kV
Magnification:	200

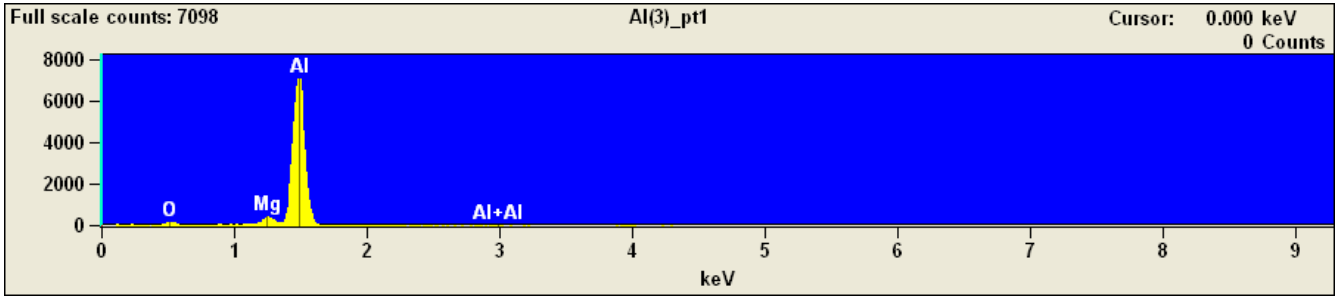

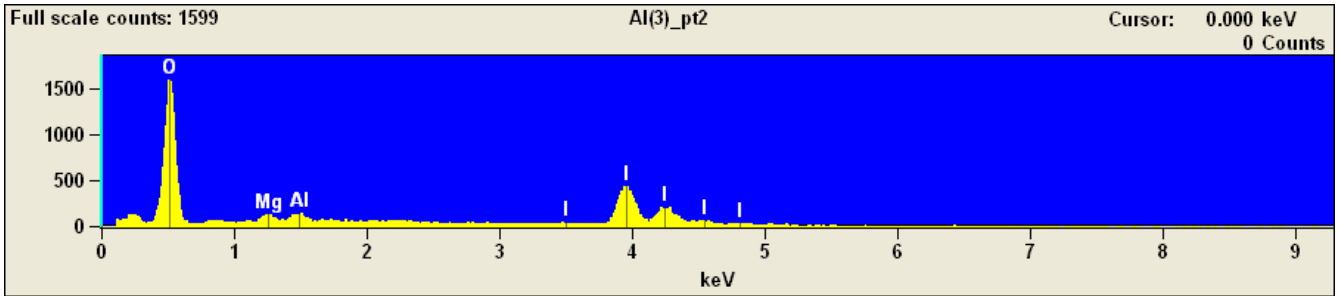

Appendix H1: Details of the EDX analysis on the oxygen and iodine ratios.

The details of the EDX analysis on the oxygen and iodine ratio are presented on the next page. The element line observed, net counts, element weight-% and atom-% are included. The error limits of the results are also presented. The terms used in the analysis are:

Filter Fit: “Filter without standards” was used. It applies a digital top hat filter to remove the background from a spectrum before fitting the spectrum to the reference spectra provided by the software.

Chi-squared value: The lower the calculated Chi-squared value between the sample spectrum and a database spectrum is, the more similar the two spectra are, with a perfect match having a value of 0.0.

Proza (Phi-Ro-Z): Calculates the depth distribution of x-rays emitted from the sample. This method is used in SEM applications, especially for light elements in a heavy matrix.

Acceleration Voltage: The accelerating voltage of a scanning electron microscope is variable, usually in the range 500-30,000 volts. An electron accelerated by a potential of 30Kv has a shorter wavelength than one accelerated by a 5Kv potential. Thus, the 30Kv electron gives better point to point resolution. When it is discussed about the specimen-beam interactions, the difference between point to point resolution and surface resolution will be contrasted.

Take Off Angle: The take-off angle is the angle between the specimen surface (at 0° tilt of specimen) and a line to the center of the detector (detector axis). This angle needs to be optimized so that the count rate of the detector is maximized.

Appendix H2: The details of the EDX analysis on the measured oxygen and iodine ratios

EDX analysis details

correction method Proza (Phi-Rho-Z)

		Element Line	Net Counts	Net Error	Element Wt.%	Wt.% Error	Atom %	Atom % Error
Paint(2), Point 2	Acc.Voltage: 8.0 kV Take Off Angle: 35.0 deg	O K	10814	+/-126	21.91	+/-0.26	69	+/- 0.80
	Chi-squared value: 28.411	I L	4494	+/-211	78.09	+/-3.67	31	+/- 1.46
Paint(4), Point 1	Acc.Voltage: 8.0 kV Take Off Angle: 35.0 deg	O K	10359	+/-125	22.21	+/-0.27	69.37	+/- 0.84
	Chi-squared value: 26.575	I L	4226	+/-218	77.79	+/-4.02	30.63	+/- 1.58
Paint(4), Point 3	Acc.Voltage: 8.0 kV Take Off Angle: 35.0 deg	O K	10447	+/-122	20.94	+/-0.24	67.75	+/- 0.79
	Chi-squared value: 27.434	I L	4615	+/-222	79.06	+/-3.81	32.25	+/- 1.55
Steel(1), Point 1	Acc.Voltage: 8.0 kV Take Off Angle: 35.0 deg	O K	11699	+/-128	27.16	+/-0.30	74.73	+/- 0.82
	Chi-squared value: 30.528	I L	5516	+/-237	72.84	+/-3.14	25.27	+/- 1.09
Steel(1), Point 2	Acc.Voltage: 8.0 kV Take Off Angle: 35.0 deg	O K	10713	+/-131	21.95	+/-0.27	69.05	+/- 0.84
	Chi-squared value: 31.579	I L	6807	+/-258	78.05	+/-2.96	30.95	+/- 1.17
Steel(1), Point 3	Acc.Voltage: 8.0 kV Take Off Angle: 35.0 deg	O K	11906	+/-130	28.28	+/-0.31	75.77	+/- 0.83
	Chi-squared value: 28.236	I L	5289	+/-233	71.72	+/-3.15	24.23	+/- 1.07
Steel(1), Point 4	Acc.Voltage: 8.0 kV Take Off Angle: 35.0 deg	O K	11301	+/-137	24.4	+/-0.30	71.91	+/- 0.87
	Chi-squared value: 32.557	I L	6210	+/-247	75.6	+/-3.01	28.09	+/- 1.12
Steel(1), Point 5	Acc.Voltage: 8.0 kV Take Off Angle: 35.0 deg	O K	10789	+/-132	23.12	+/-0.28	70.46	+/- 0.86
	Chi-squared value: 31.616	I L	6388	+/-247	76.88	+/-2.97	29.54	+/- 1.14
Steel(2), Point 1	Acc.Voltage: 8.0 kV Take Off Angle: 35.0 deg	O K	7595	+/-103	20.27	+/-0.28	66.85	+/- 0.91
	Chi-squared value: 26.467	I L	5368	+/-234	79.73	+/-3.48	33.15	+/- 1.45
Steel(2), Point 2	Acc.Voltage: 8.0 kV Take Off Angle: 35.0 deg	O K	3695	+/-70	10.03	+/-0.19	46.93	+/- 0.89
	Chi-squared value: 23.364	I L	6116	+/-238	89.97	+/-3.50	53.07	+/- 2.07
Steel(4), Point 1	Acc.Voltage: 8.0 kV Take Off Angle: 35.0 deg	O K	7048	+/-121	28.5	+/-0.49	75.97	+/- 1.30
	Chi-squared value: 30.865	I L	3095	+/-197	71.5	+/-4.55	24.03	+/- 1.53

Steel(4), Point 2	Acc.Voltage: 8.0 kV Take Off Angle: 35.0 deg	O K	11534	+/-135	26.62	+/-0.31	74.21 +/- 0.87
	Chi-squared value: 30.949	I L	5600	+/-235	73.38	+/-3.07	25.79 +/- 1.08
Steel(5), Point 2	Acc.Voltage: 10.0 kV Take Off Angle: 35.0 deg	O K	7538	+/-119	26.1	+/-0.41	73.69 +/- 1.16
	Chi-squared value: 26.830	I L	4595	+/-243	73.9	+/-3.91	26.31 +/- 1.39
Steel(7), Point 1	Acc.Voltage: 10.0 kV Take Off Angle: 35.0 deg	O K	13602	+/-140	26.41	+/-0.27	74 +/- 0.76
	Chi-squared value: 25.336	I L	12490	+/-323	73.59	+/-1.90	26 +/- 0.67
Steel(7), Point 2	Acc.Voltage: 10.0 kV Take Off Angle: 35.0 deg	O K	14986	+/-149	28.69	+/-0.28	76.14 +/- 0.76
	Chi-squared value: 28.490	I L	12167	+/-322	71.31	+/-1.89	23.86 +/- 0.63
Copper(2), Point 1	Acc.Voltage: 12.0 kV Take Off Angle: 35.0 deg	O K	2566	+/-56	8.02	+/-0.17	40.89 +/- 0.89
	Chi-squared value: 11.931	I L	15790	+/-361	91.98	+/-2.10	59.11 +/- 1.35
Copper(2), Point 2	Acc.Voltage: 12.0 kV Take Off Angle: 35.0 deg	O K	7939	+/-103	20.17	+/-0.26	66.72 +/- 0.87
	Chi-squared value: 20.566	I L	16225	+/-359	79.83	+/-1.76	33.28 +/- 0.74
Copper(2), Point 3	Acc.Voltage: 12.0 kV Take Off Angle: 35.0 deg	O K	11153	+/-123	22.84	+/-0.25	70.13 +/- 0.77
	Chi-squared value: 23.441	I L	19265	+/-404	77.16	+/-1.62	29.87 +/- 0.63
Copper(4), Point 1	Acc.Voltage: 10.0 kV Take Off Angle: 35.0 deg	O K	14234	+/-143	26.9	+/-0.27	74.48 +/- 0.75
	Chi-squared value: 28.633	I L	12782	+/-332	73.1	+/-1.90	25.52 +/- 0.66
Copper(4), Point 2	Acc.Voltage: 10.0 kV Take Off Angle: 35.0 deg	O K	1844	+/-76	5.93	+/-0.24	33.35 +/- 1.37
	Chi-squared value: 64.606	I L	10231	+/-313	94.07	+/-2.88	66.65 +/- 2.04
Copper(6), Point 1	Acc.Voltage: 10.0 kV Take Off Angle: 35.0 deg	O K	15855	+/-152	20.68	+/-0.20	67.41 +/- 0.65
	Chi-squared value: 27.457	I L	13332	+/-332	79.32	+/-1.98	32.59 +/- 0.81
Copper(6), Point 2	Acc.Voltage: 10.0 kV Take Off Angle: 35.0 deg	O K	15701	+/-151	21.87	+/-0.21	68.95 +/- 0.66
	Chi-squared value: 23.496	I L	12249	+/-318	78.13	+/-2.03	31.05 +/- 0.81
Al(2), Point 1	Acc.Voltage: 10.0 kV Take Off Angle: 35.0 deg	O K	15559	+/-146	20.67	+/-0.19	67.4 +/- 0.63
	Chi-squared value: 21.646	I L	13092	+/-334	79.33	+/-2.02	32.6 +/- 0.83
Al(2), Point 3	Acc.Voltage: 10.0 kV Take Off Angle: 35.0 deg	O K	16243	+/-151	21.78	+/-0.20	68.84 +/- 0.64
	Chi-squared value: 25.404	I L	12743	+/-330	78.22	+/-2.03	31.16 +/- 0.81
Al(3), Point 2	Acc.Voltage: 10.0 kV Take Off Angle: 35.0 deg	O K	15464	+/-146	31.25	+/-0.29	78.28 +/- 0.74
	Chi-squared value: 23.191	I L	11003	+/-304	68.75	+/-1.90	21.72 +/- 0.60

Appendix I. Short review on the Raman analysis of iodine oxides

The Raman analysis of iodine oxide particles has previously been conducted by Ellestad et al. [10]. They presented the measured spectrum of iodine tetroxide, I_2O_4, Figure I1. I_2O_4 was obtained by the sulphuric acid method [11, 12]. The Raman spectra of solid iodine pentoxide, I_2O_5, (bottom curve) and solid I_2O_5 with I_2 molecules adsorbed on it (top curve) were measured by Sunder et al. [7], Figure I2. The band at 192 cm^{-1} in the spectrum of solid I_2O_5 is due to I_2 molecules adsorbed on it. Reference samples for Raman spectroscopy were prepared by heating commercial I_2O_5. The purpose of the heat treatment was to convert commercial grade 'I_2O_5', which was found to be hydrated to HI_3O_8, to I_2O_5.

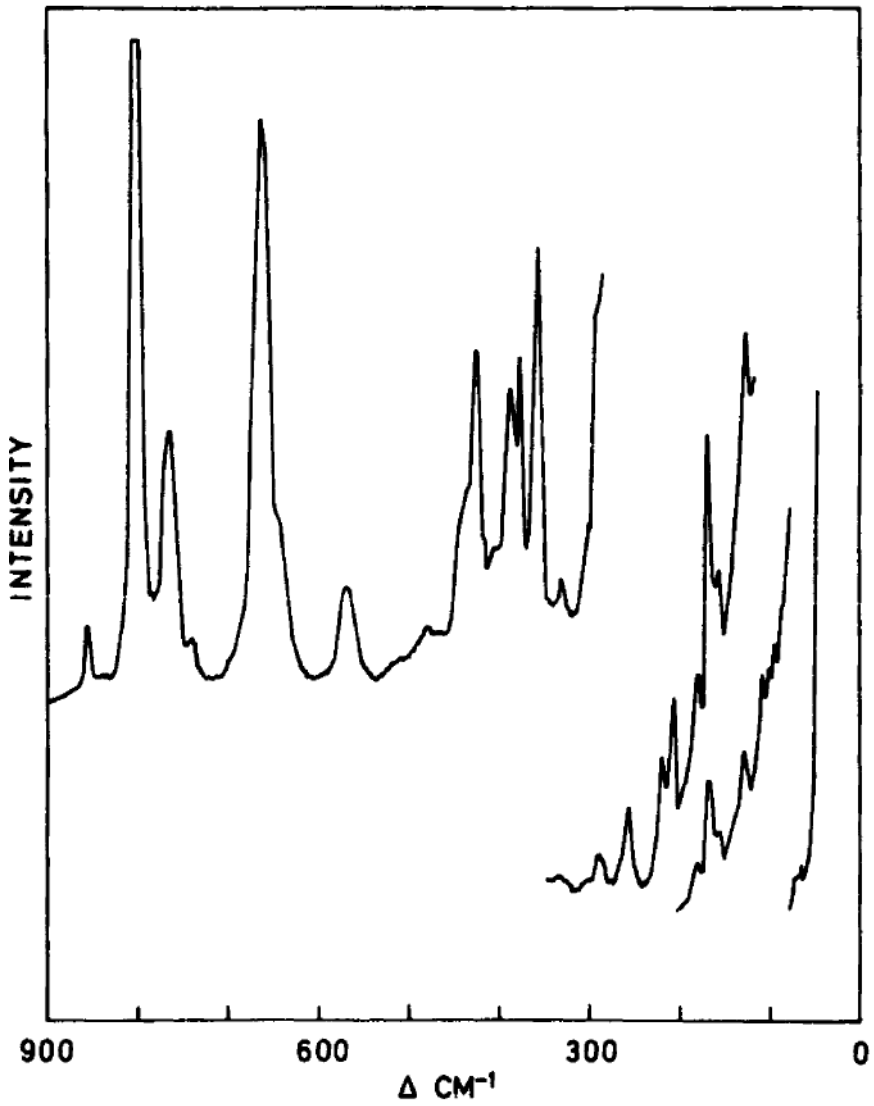

Figure I1. The Raman spectrum of solid I_2O_4. [10]

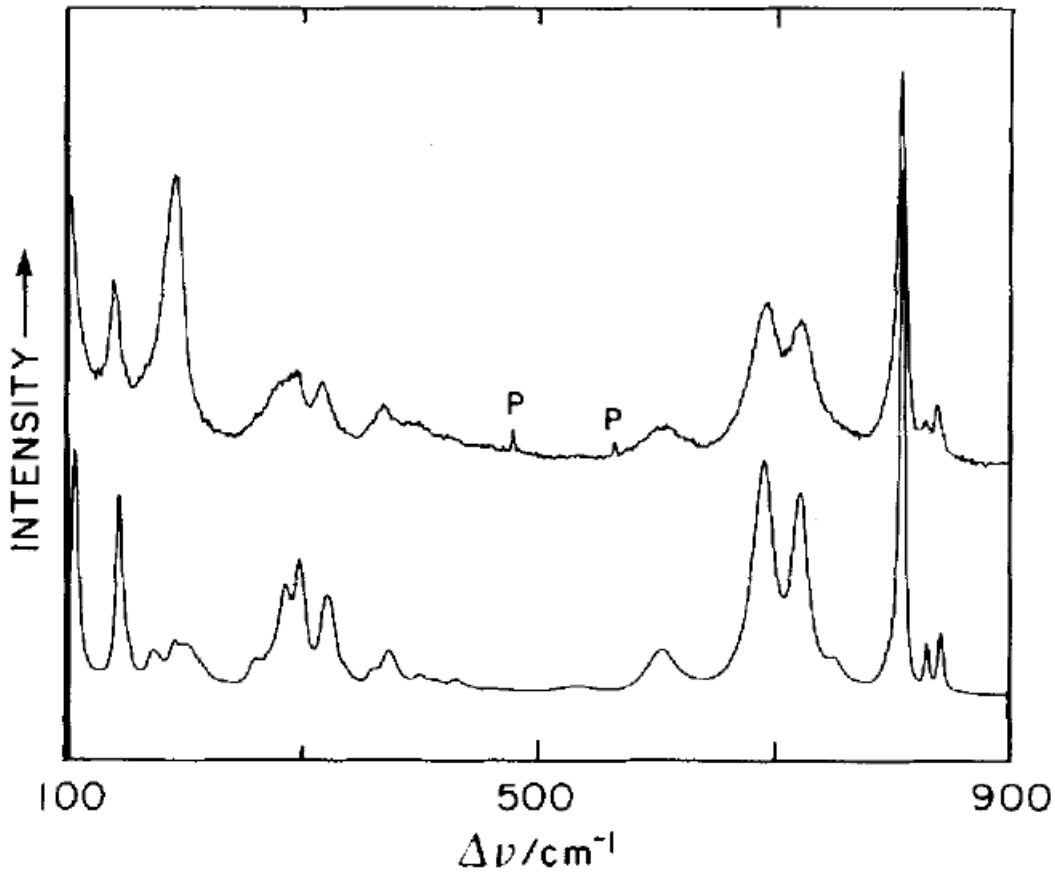

Figure I2. The Raman spectra of solid I_2O_5 (bottom curve) and solid I_2O_5 with I_2 molecules adsorbed on it (top curve). [7]

Sunder at al. [7] measured the Raman spectrum of solid I_4O_9 as well (Figure I3). The I_4O_9 was formed by reaction of gaseous iodine with ozone. The spectrum shown in the figure could not be attributed to I_2O_5, I_2O_4 or a mixture of the two. The following bands seen in the Raman spectrum of I_2O_5 (Figure I2) are absent from the spectrum of the crystalline product shown in Figure I3: (a) doublet at 840 and 830cm^{-1}, (b) strong band at *ca* 723 cm^{-1} and (c) medium intensity bands at 377 and 323 cm^{-1}. Similarly, the following bands seen in the Raman spectrum of I_2O_4 are absent from the spectrum shown in Figure I3: (a) medium intensity bands at 637, 361 and 350 cm^{-1} and (b) strong bands at 230 and 138 cm^{-1}. In addition, the intense peaks seen at *ca* 490 and 401 cm^{-1} in the spectrum of I_4O_9 are not seen in the spectrum of I_2O_5 (see Figure I2). Similarly, the intense peaks at *ca* 805 and 692cm-', seen in the spectrum of I_4O_9, are not reported in the spectrum of I_2O_4. Also, the spectrum of I_4O_9 does not correlate with any of the spectra of the oxyacids HIO_3 or HI_3O_8. [7]

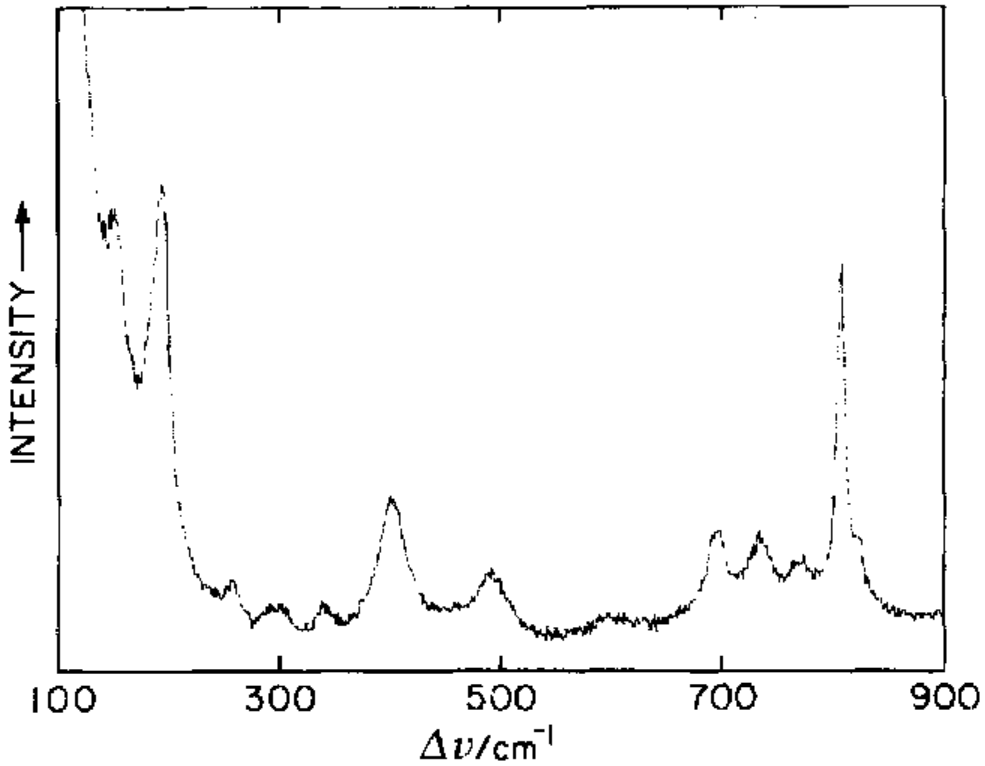

Figure I3. Raman spectrum of solid I_4O_9. [7]

The Raman spectrum of iodic acid has been studied by Durig et al. [13]. They measured the spectrum of solid HIO_3 (commercial product) and 1.054 M aqueous solution of HIO_3, Figures I4 and I5 respectively. Next, they prepared deuterioiodic acid by the addition of commercial iodine pentoxide to heavy water (99.7% isotopic purity). They measured the Raman spectra of solid DIO_3 and its aqueous solution. The spectra corresponded the solid and aqueous spectra of HIO_3, which are presented in Figures I4 and I5. In addition, Durig et al. [13] measured the Raman spectrum of partially dehydrated solid HIO_3, Figure I6. The spectrum is clearly different than the spectra of solid HIO_3.

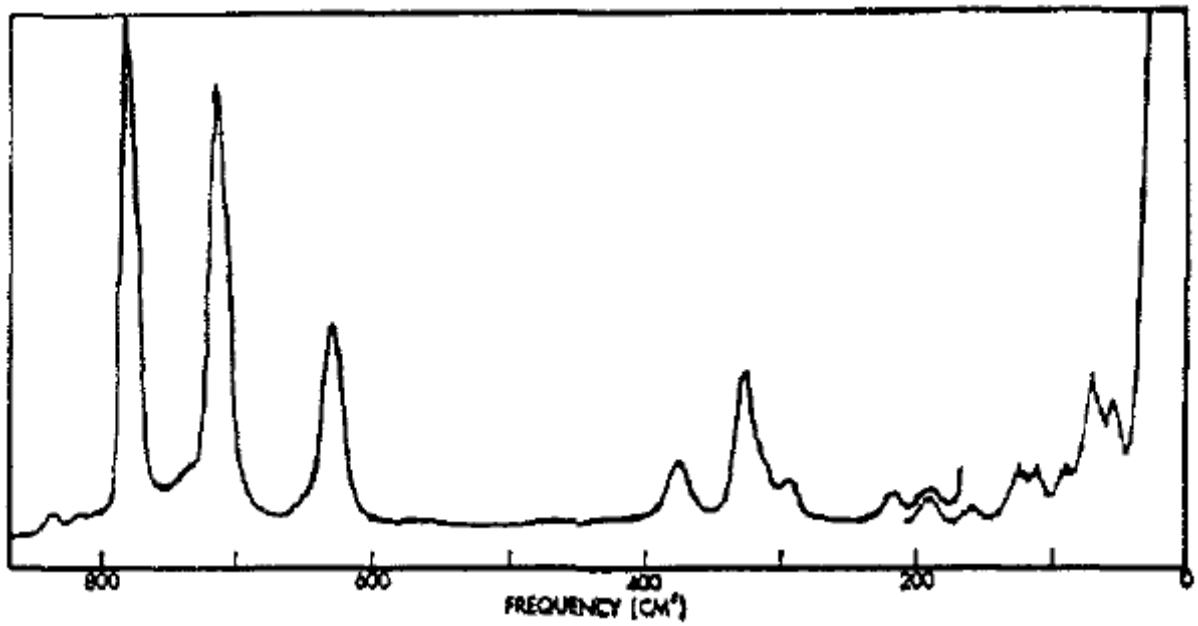

Figure I4. The Raman spectrum of solid HIO_3. [13]

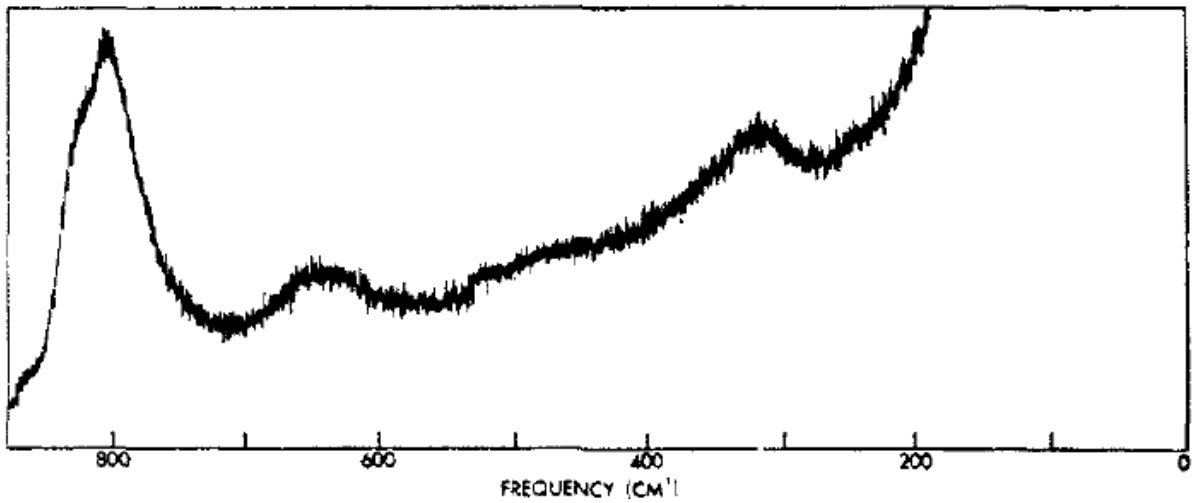

Figure I5. The Raman spectrum of a 1.054 *M* aqueous solution of HIO_3. [13]

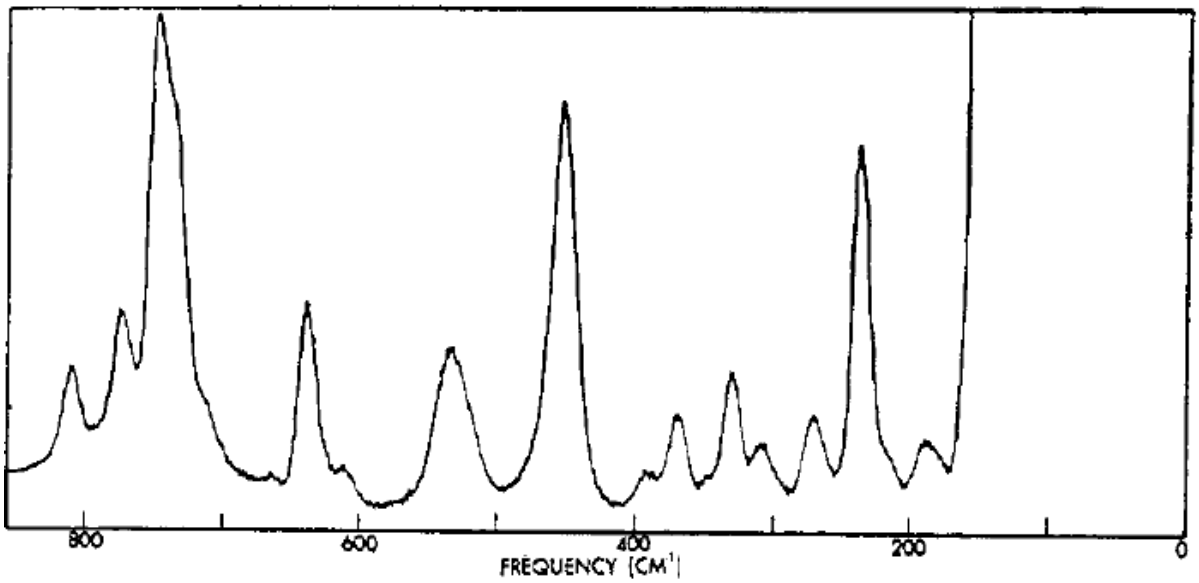

Figure I6. Raman spectrum of partially dehydrated solid HIO_3. [13]

The spectral data of crystalline I_2O_4, I_2O_5, I_4O_9, HIO_3 and aqueous solution (1.05 M) of HIO_3 is presented in Table I1.The intensity of the peaks is presented as well.

Table I1. The spectral data of crystalline I_2O_4, I_2O_5, I_4O_9, HIO_3 and aqueous solution (1.05 M) of HIO_3. The intensity of the peaks is presented as well: s, strong; m, medium, w, weak; v, very, br, broad; sh, shoulder. [7, 10, 13]

I_2O_4		I_2O_5		I_4O_9		HIO_3		HIO_3, 1.05 M solution	
cm^{-1}	Intensity	cm^{-1}	Intensity	cm^{-1}	Intensity	cm^{-1}	Intensity	cm^{-1}	Intensity
830	w	834	w	821	sh	3045	vw	824	sh
775	s	831	w	805	vs	1346	vw	800	s
741	w	810	vs	770	mw	1110	-	645	m
714	vw	748	w	732	m	839	-	319	s
637	m	724	s	692	ms	780	s		
617	vw	693	vs	598	br	741	-		
543	w	607	m	536	vvw	713	s		
490	vw	535	vw	490	ms	631	s		
415	vw	433	w	401	s	378	m		
401	m	412	vw	338	w	328	m		
361	m	401	w	294	w, br	296	m		
350	m	377	m	256	w	220	w		
332	m	361	w	193	vs	192	w		
305	vw	323	m	148	m	158	w		
262	m	300	s			124	w		
230	s	288	m			111	w		
191	s	263	w			91	w		
180	s	202	w			72	m		
161	w	193	w			58	m		
154	s	176	w						
138	s	146	s						
128	m	109	s						
100	m	97	m						
82	w	80	vs						

74	vw	65	m
58	w	59	s
-	-	47	s

Appendix J: The spectral data of the measured Raman spectra

Table J1. The spectral data of IOx particles on filter (analyses 1, 2 and 3). The intensity of the peaks is presented as well: s, strong; m, medium, w, weak; v, very, br, broad; sh, shoulder.

IOx particles on filter (100C)					
Analysis 1		**Analysis 2**		**Analysis 3**	
cm^{-1}	**Intensity**	**cm^{-1}**	**Intensity**	**cm^{-1}**	**Intensity**
826	sh	829	sh	no data	-
804	s	806	s	809	s
-	-	-	-	748	sh
715	s	713	s	719	s
686	s	689	s	689	s
597	m	599	m	601	m
524	w	529	w	-	-
425	w	425	w	425	w
364	m	366	m	368	m
311	m	312	m	316	m
-	-	-	-	293	m
285	m	284	m	281	m
184	m	172	m, br	-	-
142	m	139	m	143	m
no data	-	103	m	105	m
no data	-	83	sh	78	m

Table J2. The spectral data of IOx deposition on paint, stainless steel, copper and zinc. The intensity of the peaks is presented as well: s, strong; m, medium, w, weak; v, very, br, broad; sh, shoulder.

IOx deposit samples							
Paint		**SS**		**Copper**		**Zinc**	
cm^{-1}	**Intensity**	**cm^{-1}**	**Intensity**	**cm^{-1}**	**Intensity**	**cm^{-1}**	**Intensity**
811	m	813	m	-		-	
786	w	794	w	795	s	796	s
775	s	775	s	-		-	
746	s	746	s	-		-	
733	s	733	s	-		-	
-		-		710	s	708	s
661	w	661	w	-		-	
641	m	642	m	645	s	641	s
607	m	608	w	-		-	
533	m	533	m	-		-	
451	s	452	s	-		-	
-		-		403	m	399	m
391	m	390	m	-		-	
369	m	373	m	378	w	379	w
347	m	348	m	355	m	354	m
331	m	332	m	327	w	324	w
309	m	309	m	312	w	309	w
298	sh	301	sh	298	w	295	w
276	m	273	m	-		-	
261	sh	264	sh	-		-	
238	s	238	s	-		-	
-		-		222	w	220	w
215	m	215	m	-		-	
-		-		204	w	202	w
188	s	185	s	185	m	185	m
180	s	180	s	179	s	180	s
150	s	151	s	151	w	155	w
123	w	124	w	128	m	127	m
111	m	112	m	106	m	106	m
93	m	94	m	87	m	86	m

Title	Adsorption and revaporisation studies on iodine oxide aerosols deposited on containment surface materials in LWR
Author(s)	S. Tietze[1], M.R.StJ. Foreman[1], C. Ekberg[1] T. Kärkelä[2], A. Auvinen[2], U. Tapper[2], S. Lamminmäki[2], J. Jokiniemi[2,3]
Affiliation(s)	[1]Chalmers University of Technology, SE-41296 Göteborg, Sweden [2]VTT Technical Research Centre of Finland, FI-02044 Espoo, Finland [3]University of Eastern Finland, FI-70211 Kuopio, Finland
ISBN	978-87-7893-345-4
Date	December 2012
Project	NKS-R / AIAS
No. of pages	49 (+ 36 appendix)
No. of tables	17
No. of illustrations	43
No. of references	15

Abstract

During a hypothetical severe nuclear accident, the radiation field will be very high in the nuclear reactor containment building. As a result gaseous radiolysis products will be formed. Elemental iodine can react in the gaseous phase with ozone to form solid iodine oxide aerosol particles (iodine oxide).

Within the AIAS (Adsorption of Iodine oxide Aerosols on Surfaces) project the interactions of iodine oxide (IOx) aerosols with common containment surface materials were investigated. Common surface materials in Swedish and Finnish LWRs are Teknopox Aqua V A paint films and metal surfaces such as Cu, Zn, Al and SS, as well as Pt and Pd surfaces from hydrogen recombiners. Non-radioactive and ^{131}I labelled iodine oxide aerosols were produced with the EXSI CONT facility from elemental iodine and ozone at VTT Technical Research Centre of Finland. The iodine oxide deposits were analysed with microscopic and spectroscopic measurement techniques to identify the kind of iodine oxide formed and if a chemical conversion on the different surface materials occurs.

The revaporisation behaviour of the deposited iodine oxide aerosol particles from the different surface materials was studied under the influence of heat, humidity and gamma irradiation at Chalmers University of Technology, Sweden. Studies on the effects of humidity were performed using the FOMICAG facility, while heat and irradiation experiments were performed in a thermostated heating block and with a gammacell 22 having a dose rate of 14 kGy/h. The revaporisation losses were measured using a HPGe detector. The revaporisated ^{131}I species from the surfaces were chemically tested for elemental iodine formation. The parameter dominating the degradation of the produced iodine oxide aerosols was humidity.

Cu and Zn surfaces were found to react with iodine from the iodine oxide aerosols to form iodides, while no metal iodides were detected for Al and SS samples. Most of the iodine oxide aerosols are assumed to be degraded or

washed off by containment sprays and steam in the containment. Paint film ingredients were shown to chemically react with the aerosol particles. Pt and Pd surfaces were shown to only weakly physisorb the iodine oxide aerosols which reveals that these aerosols will have a minor effect on the catalytic functionality of the hydrogen recombiners during a severe nuclear accident.

Key words Severe nuclear accidents, LWR, volatile iodine source term, iodine oxide aerosols, adsorption, revaporisation, containment

Available on request from the NKS Secretariat, P.O.Box 49, DK-4000 Roskilde, Denmark.
Phone (+45) 4677 4041, e-mail nks@nks.org, www.nks.org